Titre: Title:	Development of the Piezoelectric Properties of Poly(Vinylidene Fluoride) Based Ferroelectrics and Ferroelectrets Using Fillers and Mechanical Stretching
Auteur: Author:	Nusrat Jahan
Date:	2018
Type:	Mémoire ou thèse / Dissertation or Thesis
Référence: Citation:	Jahan, N. (2018). Development of the Piezoelectric Properties of Poly(Vinylidene Fluoride) Based Ferroelectrics and Ferroelectrets Using Fillers and Mechanical Stretching [Thèse de doctorat, École Polytechnique de Montréal]. PolyPublie. https://publications.polymtl.ca/3060/

UNIVERSITÉ DE MONTRÉAL

DEVELOPMENT OF THE PIEZOELECTRIC PROPERTIES OF POLY(VINYLIDENE FLUORIDE) BASED FERROELECTRICS AND FERROELECTRETS USING FILLERS AND MECHANICAL STRETCHING

NUSRAT JAHAN

DÉPARTEMENT DE GÉNIE CHIMIQUE

ÉCOLE POLYTECHNIQUE DE MONTRÉAL

THÈSE PRÉSENTÉE EN VUE DE L'OBTENTION

DU DIPLÔME DE PHILOSOPHIAE DOCTOR

(GÉNIE CHIMIQUE)

AVRIL 2018

UNIVERSITÉ DE MONTRÉAL

ÉCOLE POLYTECHNIQUE DE MONTRÉAL

Cette thèse intitulée:

DEVELOPMENT OF THE PIEZOELECTRIC PROPERTIES OF POLY(VINYLIDENE FLUORIDE) BASED FERROELECTRICS AND FERROELECTRETS USING FILLERS AND MECHANICAL STRETCHING

présentée par : JAHAN Nusrat

en vue de l'obtention du diplôme de : Philosophiae Doctor

a été dûment acceptée par le jury d'examen constitué de :

M. TAVARES Jason-Robert, Ph. D., président

M. AJJI Abdellah, Ph. D., membre et directeur de recherche

M. MIGHRI Frej, Ph. D., membre et codirecteur de recherche

M. RODRIGUE Denis, Ph. D., membre et codirecteur de recherche

M. CICOIRA Fabio, Ph. D., membre

M. SUNDARARAJ Uttandaraman, Ph. D., membre externe

DEDICATION

To my beloved parents

ACKNOWLEDGEMENTS

I begin by thanking Allah, the most gracious and the most merciful.

First and foremost, I would like to express my heartiest gratitude to my supervisors Prof. Abdellah Ajji, Prof. Frej Mighri and Prof. Denis Rodrigue. I consider myself very fortunate to have such amazing mentors from the very beginning of this journey, who guided and supported my development as a researcher with an extraordinary show of patience and kindness. They are a true inspiration for me to grow.

I am very grateful to Prof. Charles Dubois from Chemical engineering department, polytechnique Montréal for allowing me to use his lab equipements.

I would like to thank Prof. Daniel Therriault and Dr. Sampada bodkhe from Mechanical engineering department of polytechnique Montréal who kindly allowed and helped me to work in their lab.

My heartiest gratitude goes to Prof. Mohamad Sawan and Mr. Laurent Mouden for giving access to their lab and allowing me to use their equipments.

I would like to thank other professors and staff of Chemical engineering department for providing a world-class environment and facilities for graduate research. I would also like to specially thank Mrs. Claire Cerclé, Mr. Richard Silverwood, Mr. Redouane Boutrouka and Mr. Jean Huard. I would like to thank all my friends and colleagues for their support and feedback over the years.

Last but not the least, I am eternally grateful to my parents, who made their lifelong sacrifices to see me happy and successful. My eternal thanks goes to my siblings who were always there with me in spirit. I am very thankful to my mother-in-law who has been a great support for me. I thank my husband Sazzad, who has been on my side with her gracious support and encouragement.

RÉSUMÉ

Les polymères piézoélectriques sont très utiles pour plusieurs applications électrochimiques vu leur forte réponse piézoélectrique, leur flexibilité, leur légèreté ainsi que leur formabilité. En plus des céramiques ferroélectriques, les polymères ferroélectriques (comme le PVDF) et les ferroélectrets sont aussi populaires comme nouveau groupe de piézoélectrique. L'intérêt pour les ferroélectriques basés sur le β-PVDF est dû à la facilite de leur préparation avec une réponse piézoélectrique usable, en plus des avantages de polymères déjà cités. L'incorporation d'une nanocharge (comme le PZT, les nanotubes de carbone, l'argile, les nanoparticules ferrite, la charge pour céramique $BaTiO_3$) dans le PVDF est une des approches faciles pour produire une phase β dans le PVDF souvent suivi par un étirement mécanique. Ces charges aident à la nucléation de la phase β dans la matrice de PVDF tandis que l'étirement mécanique subséquent aide à aligner les dipôles dans une certaine mesure. Par conséquent, le but de la première partie de cette étude est de préparer des films ferroélectriques B-PVDF en incorporant une charge hybride (micro-$CaCO_3$+ nanoargile) suivi par un étirement mécanique. La nanoargile, l'une des charges rentables les plus utilisées, est capable de nucleer le β-PVDF. L'amélioration synergétique dans la formation de la phase β ainsi que les propriétés mécaniques, électriques et piézoélectriques ont été rapportées dans cette partie de l'étude. De plus, l'influence de l'étirement mécanique subséquent (le rapport de tirage, R (longueur finale / longueur initiale)) a également été étudié. FTIR et XRD sont utilisés pour déterminer la teneur en phase β dans les deux échantillons étirés et non étirés. Alors que les propriétés de traction montrent une diminution progressive, la constante diélectrique a augmenté progressivement avec l'augmentation de la teneur en $CaCO_3$ dans la charge hybride. Le coefficient d_{33} piézoélectrique maximum de 30 pC/N est obtenu pour des films composites hybrides étirés. D'autre part, les ferroélectrets sont un autre type de films polymères fonctionnels avec une structure cellulaire hétérogène et des moments dipolaires internes quasi-permanents. La piézoélectricité dans les ferroélectrets provient de la variation des moments dipolaires avec l'application d'une charge mécanique. Au cours des dernières décennies, les films de polypropylène cellulaire (PP) ont été les ferroélectrets les plus populaires et les plus étudiés et ont déjà des applications commerciales. Alors que le coefficient piézoélectrique d_{33} des ferroélectrets PP peut présenter jusqu'à 1000 pC/N ou plus, leur température de fonctionnement est assez faible, inférieure à 60 °C. Les fluoropolymères récemment développés, i.e. les ferroélectrets à base de polytetrafluoroethylene (PTFE) et de

fluoroethylene propylène (FEP), présentent une forte réponse piézoélectrique et une excellente stabilité thermique. Cependant, le traitement de ces ferroélectrets de fluoropolymères en utilisant une technique de fabrication commercialement viable telle qu'une extrusion de film coulé pose quelques défis en raison de leur viscosité très élevée à l'état fondu, de leur haute température de fabrication, de leur tendance à la dégradation et de leur faible élongation à la traction. Par conséquent, dans cette partie de l'étude, un nouveau ferroélectret thermiquement stable a été étudié en utilisant une technique de traitement commerciale avec une forte réponse piézoélectrique. L'extrusion par coulée du mélange polymère / charge suivie d'un étirage mécanique est l'une des techniques prometteuses pour préparer un polymère cellulaire. Les charges à l'échelle micrométrique sont habituellement utilisées pour créer des vides à partir de la délamination interfaciale sous contrainte appliquée. Le fluorure de polyvinylidène (PVDF) est un fluoropolymères qui est facilement transformable à l'état fondu par rapport aux autres fluoropolymères et qui présente d'excellentes propriétés physiques, chimiques et électriques. Un procédé "d'extrusion-étirage-gonflage" a été suivi pour préparer une structure cellulaire dans des films de PVDF. Des films solides de PVDF / charge hybride (micro-$CaCO_3$ + nanoargile) ont été extrudés et ensuite étirés pour créer la structure cellulaire initiale à l'intérieur des films. Tandis que le $CaCO_3$ agit comme centre de nucléation des vides, la nanoargile augmente l'etirabilité des films de PVDF fortement chargés en $CaCO_3$. L'expansion de diffusion de gaz (GDE) ou le gonflage contrôlé est préformé pour ajuster les dimensions des vides à des vides en forme de lentilles conduisant à des modules d'élasticité inférieurs et à une piézoélectricité plus forte. De toute évidence, les caractéristiques de perméation de gaz dans les polymères polaires sont différentes de celles des polymères non polaires en raison de l'interaction polymère / gaz différente et de la forte dépendance des propriétés piézoélectriques finales des ferroélectrets en la morphologie cellulaire comme la taille, la forme et la distribution des vides. Par conséquent, deux gaz de gonflage différents, à savoir le N_2 neutre et le CO_2 polaire, sont utilisés avec différentes stratégies de gonflage. Plusieurs combinaisons de la pression, la température et leur mode d'application (direct ou par paliers) sont examinées pour optimiser le niveau de gonflage. Les films gonflés sont ensuite soumis à une charge corona à température ambiante pour créer les dipôles à l'intérieur des vides. Enfin, les ferroélectrets de PVDF montrent un coefficient piézoélectrique d_{33} atteignant 251 pC/N avec un gonflage N_2 et 327 pC/N pour le traitement au CO_2. Comme prévu, les ferroélectrets de PVDF présentent une meilleure stabilité thermique que le PP, le PETP, le COP et le PEN et aussi

élevés que le Teflon. Les échantillons chargés à température ambiante pourraient avoir leur température de travail jusqu'à 120 °C.

ABSTRACT

Piezoelectric polymers are very useful in various electromechanical applications because of their strong piezoelectric response, flexibility, lightweight and formability. In addition to ferroelectric ceramics, ferroelectric polymers (such as PVDF) and ferroelectrets are also popular as a new group of piezoelectrics. Ferroelectrics based on β-PVDF are interesting due to the ease of preparation with usable piezoelectric response in addition to the above mentioned advantages of polymers. Incorporating nanofillers (e.g. ceramic filler-$BaTiO_3$, PZT, carbon nanotube, clay, ferrite nanoparticles etc.) into PVDF is one of the facile ways to produce β phase in PVDF often followed by mechanical stretching. While fillers nucleate β phase in the PVDF matrix, subsequent mechanical stretching helps in aligning the dipoles to some extent. Therefore, the aim of the first part of this study is to prepare ferroelectric β-PVDF films by incorporating a hybrid filler (micro-$CaCO_3$+ nanoclay) followed by mechanical stretching. While nanoclay is one of the most widely used cost-effective fillers capable of nucleating β-PVDF, synergistic improvement in β phase formation as well as in mechanical, electrical and piezoelectric properties of hybrid composites have been reported in this part of the study. Additionally, the influence of subsequent mechanical stretching e.g. draw ratio, R (final length/initial length), has also been investigated. FTIR and XRD are employed to determine the β phase content in both stretched and unstretched samples. While the tensile properties show a gradual decrease, dielectric constant increased gradually with increasing $CaCO_3$ content in the hybrid filler. The maximum piezoelectric d_{33} coefficient of 30 pC/N is obtained for stretched hybrid composite films. Ferroelectrets, on the other hand, are another type of functional polymer films with heterogeneous cellular structure and internal quasi-permanent dipole moments. The piezoelectricity in ferroelectrets originates from the change in dipole moments under an applied mechanical stress. Over the past few decades, cellular polypropylene (PP) films have been the most popular and widely investigated ferroelectrets and are already in commercial applications. While the piezoelectric d_{33} coefficient of PP ferroelectrets could exhibit up to 1000 pC/N or more, their working temperature is quite low, not higher than 60 °C. Recently developed fluoropolymer i.e. polytetrafluoroethylene (PTFE) and fluoroethylene propylene (FEP) based ferroelectrets exhibit strong piezoelectric response and excellent thermal stability. However, processing these fluoropolymer ferroelectrets using commercially viable manufacturing technique such as cast film extrusion poses few challenges because of their very

high melt viscosity, high manufacturing temperature, degradation tendency and low tensile elongation. Therefore, in this part of the study, a new thermally stable ferroelectret has been investigated using commercial processing technique with strong piezoelectric response. Cast extrusion of the polymer/filler mixture followed by mechanical stretching is one of the promising techniques for preparing a cellular polymer. Micron scale fillers are usually employed for creating voids from interfacial delamination under applied stress. Polyvinylidene fluoride (PVDF) is a fluoropolymer which is easily melt-processable than other fluoropolymers and showing excellent physical, chemical and electrical properties. An "extrusion-stretching-inflation" process has been followed to prepare a cellular structure in PVDF films. Solid PVDF/hybrid filler (micro-$CaCO_3$ + nanoclay) films were extruded and subsequently stretched to create the initial cellular structure inside the films. While $CaCO_3$ acts as void nucleation centers, nanoclay increases the stretchability of the highly $CaCO_3$ filled PVDF films. Gas diffusion expansion (GDE) or controlled inflation is preformed to adjust the voids dimensions to lens-shaped voids leading to lower elastic moduli and stronger piezoelectricity. Obviously, the gas permeation characteristics in polar polymers is different than non-polar polymers because of their different type of polymer/gas interaction and the final piezoelectric properties of the ferroelectrets strongly depend on the cellular morphology such as void size, shape and distribution. Therefore, two different inflation gases i.e. neutral N_2 and polar CO_2 are used with various inflation strategies. Combination of pressure, temperature and their way of application (direct or step-wise) is examined for various times to optimize the inflation level. The inflated films are then subjected to corona charging at room temperature to create the dipoles inside the voids. Finally, PVDF ferroelectrets show piezoelectric d_{33} coefficient as high as 251 pC/N with N_2 inflation and 327 pC/N for CO_2 treatment. As expected, PVDF ferroelectrets exhibit better thermal stability than PP, PETP, COP and PEN and as high as Teflon. Samples charged at room temperature have their working temperature up to 120 °C.

TABLE OF CONTENTS

LIST OF TABLES

LIST OF FIGURES

LIST OF ABBREVIATIONS

AR	Aspect ratio
$BaTiO_3$	Barium titanate
$CaCO_3$	Calcium carbonate
CNT	Carbon nanotube
CO_2	Carbon dioxide
COP	Cyclo-olefin polymer
DC	Direct current
DMA	Dynamic mechanical analysis
DMF	Dimethylformamide
DSC	Differential scanning calorimetry
FEP	Fluoroethylene propylene
FTIR	Fourier transformed infrared spectrocopy
GDE	Gas diffusion expansion
LDPE	Low density polyethylene
Mt	Montmorillonite
MRS	Maxwell-Wagner-Sillars
N_2	Nitrogen
P_c	Critical pressure
PEN	Polyethylene naphthalate
PETP	Polyethylene terephthalate
PLA	Polylactic acid
POSS	Polyhedral oligomeric silsesquioxane
PP	Polypropylene

PTFE	Polytetrafluoroethylene
PVDF	Polyvinylidene fluoride
P(VDF-CTFE)	Poly (vinylidene fluoride- chloride trifluoride ethylene)
P(VDF-TrFE)	Poly (vinylidene fluoride- trifluoroethylene)
PZT	Lead zirconium titanate
SEM	Scanning electron microscopy
T_c	Critical temperature
T_g	Glass transition temperature
T_m	Melting temperature
TSD	Thermally stimulated discharge
TTT	All-trans planar zigzag
TGTG'	Trans-gauche-trans-gauche
XRD	X-ray diffraction
ZnO	Zinc oxide

CHAPTER 1 INTRODUCTION

Piezoelectricity is the word used to define the ability of some materials, especially ceramics and crystals, to generate electrical voltage from an applied mechanical stress and vice versa [1]. Since their discovery, piezoelectric inorganic materials such as quartz and ceramics are used in electromechanical transduction [2]. After the emergence of microelectromechanical systems (MEMS) in 1980, these piezoelectric materials have been considered as an additional functionality in such system and the resultant 'piezoMEMS' have found their applications in the automotive industry, smartphones and in other fields [2, 3]. Because of the difficulty associated with the processing of these piezoelectric inorganic materials at higher temperature, brittleness and high toxicity, polymeric materials had become the material of choice in such applications since 1990s, replacing inorganic materials [2]. After a strong piezoelectric effect discovered by Kawai [4] in β-polyvinylidene fluoride (PVDF) when electrically charged, the interest and use of β-PVDF started to grow fast because they are flexible, lightweight, tough, easy to form and cost-effective [1].

While PVDF could exhibit three primary crystal phases (α, β and γ) based on its chain conformation, the β phase is the main one since only this phase can exhibit a strong piezoelectric response. The α phase is completely non-polar and the γ phase has a very small dipole moment, hence only a weak piezoelectric behavior is observed. Lately, filler incorporation, especially ceramic nanofillers, was found to be an efficient way to improve the ferroelectric properties of PVDF because of their inherently strong dielectric and piezoelectric properties [5, 6]. Among them, barium titanate ($BaTiO_3$) and lead containing perovskites, particularly PZT (lead zirconium titanate), have been most widely studied [5-7], although it is desirable to replace them due to their high cost, as well as environmental and health concerns. Therefore, other nanofillers, such as clay minerals [8-13], are also being used in PVDF because of their additional benefits of being cost-effective and more efficient even at very small content.

Until recently, it has been reported that organically modified clay minerals not only enhances the polar β-PVDF content and improves the PVDF piezoelectric properties [10, 11, 13, 14], but also improves its dielectric and thermomechanical properties [13]. The silicate layers act as nucleation sites stabilizing the β phase chain conformation. However, a maximum d_{33} value of

5.8 pC/N has been reported for poled PVDF/Mt nanocomposite with 2 wt.% clay. Therefore, the complete conversion of α to β phase or hindering the unwanted conversion of α phase to less electroactive γ phase [12] in PVDF/silicate nanocomposites remain as major challenges yet to be explored.

After the concept of ferroelectrets was introduced few decades ago based on non-polar polymers, they have gained constantly increasing attention. These ferroelectrets, electrically charged polymer foams, can be used as sensors and actuators by switching their mechanical and electrical signals [15]. An ideal ferroelectret consists of micron sized voids dispersed in a polymer film which under an applied electric field creates dipoles by separating the positive and negative charges on the internal surfaces of the voids facing each other. The piezoelectricity comes from the internal dipole moment as well as from the anisotropy of the polymer matrix with low elastic stiffness.

For a long time, polypropylene (PP) was the only polymer investigated for ferroelectret properties. Therefore, the basic film preparation, cellular structure control, charging condition optimization and finally the electromechanical properties of PP based ferroelectrets were thoroughly studied [15-22]. After optimized preparation, PP ferroelectrets are able to exhibit strong d_{33} coefficient up to thousand pC/N. Therefore, they are already in commercial applications such as in musical instruments, health care devices and in sensors in touch panels [23].

While the application of ferroelectrets is limited by the working temperature, the poor thermal stability of PP ferroelectret (below 60 °C) has restricted their applications even if they show a strong piezoelectric response. Therefore, polyethylene terephthalate and cyclo-olefin polymer (COP) based ferroelectrets were investigated [24-27] because of their excellent charge retention capability. Because of the elevated thermal and time charge stability, PETP ferroelectrets exhibit working temperature up to 80-100 °C [28]. Moreover, COP based ferroelectrets can even exhibit a higher working temperature up to 110 °C [24]. However, the higher working temperature comes at the price of lower piezoelectric activity (d_{33} value < 100 pC/N) [24, 25].

Lately, non-polar fluoropolymers such as FEP and PTFE have been investigated and strong piezoelectric response (40-220 pC/N in single layer foamed film) along with excellent thermal charge stability (up to 120 °C) has been reported in several studies [28, 29]. However, preparation of this type of ferroelectrets comes with unavoidable difficulties including higher manufacturing

temperature, extremely high melt viscosity, tendency to degrade by releasing hydrofluoric acid and low elongation to break [30].

So the main motivation of this study is to develop the piezoelectric properties of ferroelectric poly(vinylidene fluoride) (PVDF) using hybrid filler (combination of micron- and nano-sized fillers) and introducing a new thermally stable ferroelectret based on PVDF for enhanced performance and prepared using commercially viable techniques. To achieve this goal, cast extruded PVDF films were prepared using different filler concentration to examine their piezoelectric response, as well as to analyze the mechanical and electrical properties of stretched-poled PVDF hybrid composites. Later on, the cast extruded films are stretched-inflated-poled to investigate the piezoelectric response of the cellular PVDF ferroelectret. Moreover, the thermal charge stability of the prepared ferroelectret is examined, helping to determine the maximum working temperature of the system. To this end, the inflation parameters (type of gas, pressure, temperature and the way of application) are varied and the obtained piezoelectric coefficient and the thermal charge stability are discussed as a function of inflation variables. Understanding the inflation procedures in detail is necessary to obtain an optimized cellular structure and thus to get maximum piezoelectricity and charge stability.

This dissertation contains four peer-review articles that have been published or submitted to scientific journals along with the following chapters :

- Chapter 1 gives a brief introduction of the study along with its motivation.
- Chapter 2 provides a literature review to justify the study.
- In Chapter 3, the objectives are explained along with the organization of the articles.
- Chapters 4-7 include four scientific articles, one in each chapter explaining the key outcomes of this study.
- Chapter 8 presents a general discussion about the outcomes of the reported articles included in Chapters 4-7.
- Finally, Chapter 9 includes the conclusions of this dissertation and recommendations for future work.

CHAPTER 2 LITERATURE REVIEW

2.1 Background of Piezoelectricity

The term 'piezoelectricity' is used to describe the ability of a material to generate electrical charges in response to a mechanical stress which is also called the direct piezoelectric effect Figure 2.1(a). Indirect (or converse) piezoelectric effect, on the other hand, arises when a mechanical strain or dimensional change occurs in the material in response to an electrical field Figure 2.1(b) [1, 31]. Therefore, in piezoelectric materials, the induced charges and the mechanical stress have a linear and reversible relationship. The direct piezoelectric effect was first discovered in 1880 by Pierre Curie and Jacques Curie in some crystals including quartz, tourmaline and Rochelle salt. They observed that these crystals could generate electrical polarization under the application of a mechanical stress and the generated voltage changes proportionately with the applied stress [31].

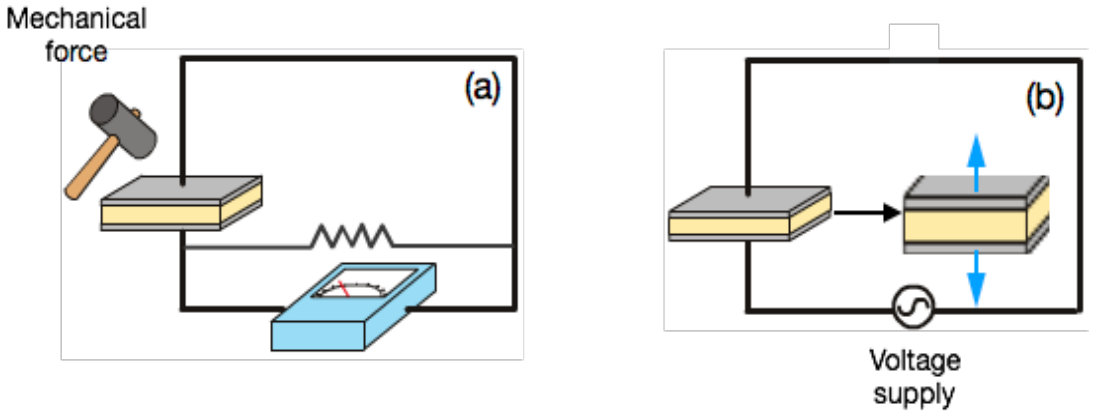

Figure 2.1: Schematic of the piezoelectric effect. (a) direct effect (voltage induced by mechanical force) and (b) indirect effect (strain induced by an electrical field).

However, the indirect effect was first theoretically proposed by Lippmann based on thermodynamic considerations the year after the discover of direct piezoelectric effect and was then experimentally confirmed by Curies in 1884. Thus the complete reversibility of electromechanical deformations was proved quantitatively for piezoelectric crystals [31]. The idea of direct piezoelectric effect is exploited in force, vibration and pressure sensors and the idea of indirect effect is implemented in actuators and displacement devices [32].

In general, piezoelectricity occurs only in nonconductive and polarizable materials (i.e. dielectrics). Although it was discovered in the 1880s, it remained as a mere curiosity until 1940.

Meanwhile, the piezoelectric effect was found to have an intimate connection with ferroelectricity which was discovered in 1921 in Rochelle salt [33]. Ferroelectricity is the property of certain dielectric materials exhibiting nonvolatile spontaneous electric polarization (the event where one side of the crystal becomes positive and the other side negative due to the separation of the center of positive and negative charge) under the application of an external electric field, reorienting the dipoles and leaving a remnant polarization at zero electric field. The remnant polarization varies under applied mechanical stresses and this is where the piezoelectric effect occurs. Therefore, all ferroelectric materials are piezoelectric [2]. Although the ferroelectric effect was firstly observed in a salt, significant application of ferroelectric materials was observed only after the discovery of lead zirconate titanate (PZT), which exhibits a strong piezoelectric effect. Until 1960s, single crystals (quartz) or the polycrystalline ceramics (PZT) were used in all piezoelectric devices. Then, Kawai in 1969 showed that the β-phase polyvinylidene fluoride (PVDF) could exhibit a piezoelectric effect through its internal dipoles reorientation under an electric field. Since then, polymers have emerged as piezoelectric materials because of their additional advantages such as, flexibility, lightweight, easy processing into large scale, cost-effectiveness, formability into complex shape, excellent environmental resistance, and easy use on other substrate compared to inorganic materials [1].

2.2 Definition of Piezoelectric Coefficient

The charge separation and dipole movement of a piezoelectric materials can be explained by parallel-plate capacitors where the plates are separated by a distance h. The capacitance of such system (C) is defined as :

$$C = \varepsilon_r \varepsilon_0 \frac{A}{h} = \varepsilon \frac{A}{h} \qquad (2\text{-}1)$$

where, ε_r and ε_0 are the relative and vacuum dielectric constant, respectively, and A is the area of the plates. The absolute dielectric constant (ε) defines the ability of the dipoles in the material to reorient in response to an external electric field. In other words, ε measures the material polarizability. The applied electric field and the polarization density (P) of a material can be related via :

$$\vec{P} = (\varepsilon_r - 1)\varepsilon_0 \overrightarrow{E_{ext}} \qquad (2\text{-}2)$$

and the electric displacement (D), defined as the displacement effect of the charges in a dielectric material due to the electric field, can be expressed by:

$$\vec{D} = \varepsilon_0 \overrightarrow{E_{ext}} + \vec{P} = \varepsilon \overrightarrow{E_{ext}} \tag{2-3}$$

For piezoelectric materials, both the external electric field and applied mechanical stress can lead to electrical charge displacement. Therefore, Equation (2-3) can be written as :

$$\vec{D} = \varepsilon_0 \overrightarrow{E_{ext}} + d\vec{S} \tag{2-4}$$

where, d is the material piezoelectric coefficient and S is the applied stress.

If $E_{ext} = 0$, the polarization is only generated from the mechanical stress (S). The piezoelectric coefficient d is direction dependent which can be expressed in matrix form. Assuming that the stress can be applied from 6 different directions at $E_{ext} = 0$, Equation (2-4) can be written as :

$$\begin{bmatrix} D_1 \\ D_2 \\ D_3 \end{bmatrix} = \begin{bmatrix} 0 & 0 & 0 & 0 & d_{15} & 0 \\ 0 & 0 & 0 & d_{24} & 0 & 0 \\ d_{31} & d_{32} & d_{33} & 0 & 0 & 0 \end{bmatrix} \begin{bmatrix} S_1 \\ S_2 \\ S_3 \\ S_4 \\ S_5 \\ S_6 \end{bmatrix} \tag{2-5}$$

The 6 different stresses generate 3 axial electrical displacements on the unit cell and 5 different piezoelectric coefficients. Theses piezoelectric coefficients represents different types of piezoelectric coupling mode [32], among which the researchers are mostly interested in d_{33} and d_{31} representing the compression and stretching of a piezoelectric material, respectively. This is because the highest amount of power can be generated from these two modes [34]. The d_{33} coupling mode is known as the longitudinal coefficient in which the force is applied along the poling field direction. Examples include the compression of a piezoelectric material that is poled on its top and bottom surface. The transverse coefficient (d_{31}) represents a coupling mode in which the stress is applied in the direction perpendicular to the poling field to induce an electrical polarization perpendicular to the applied stress. A bending beam poled on its top and bottom surfaces is an example of d_{31} coefficient [34]. An illustration of both modes is shown in Figure 2.2. The direct piezoelectric co-efficient d_{ij} is defined as [15]-

$$d_{ij} = \frac{\delta D_i}{\delta S_j} = \frac{\delta Q_i / A}{\delta F_j / A} = \frac{\delta Q_i}{\delta F_j} \tag{2-6}$$

where, D is the electrical displacement or charge density (=Q/A), S is the applied mechanical stress (= F/A), Q is the accumulated charge and A is the sample area.

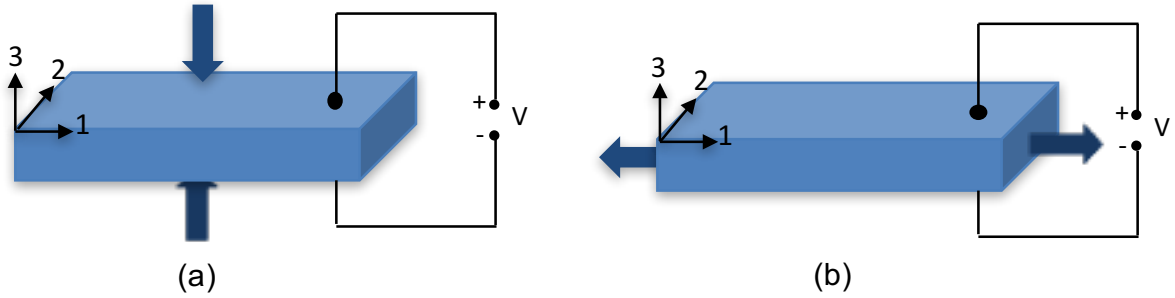

Figure 2.2: Schematic of the transduction mode of piezoelectric materials. (a) -33 mode and (b) -31 mode.

2.3 Typical Piezoelectric Materials

2.3.1 Crystal- Rochelle Salt

The concept of piezoelectricity and ferroelectricity was first discovered in Rochelle salt, $NaKC_4H_4O_6.4H_2O$ and it remained for a long time the only known ferroelectrics [35]. It has a complex crystalline structure : orthorhombic in paraelectric phase and monoclinic in ferroelectric phase. It only exhibits ferroelectric behavior between 255 and 297 K [36]. Its density is about 1.77 g/cm^3 with a melting point around 75 °C. In spite of its poor working temperature, Rochelle salt is used in multiple applications (acoustics) because of its very high piezoelectric coefficients [30]. Santos et al. [36] reported the values of d_{21} = 700 pC/N, d_{22} = 2200 pC/N, d_{23} = 2100 pC/N and d_{25} = 37 pC/N as determined by x-ray multiple diffraction.

2.3.2 Ceramic - Lead Zirconate Titanate (PZT)

PZT ($Pb(Zr_xTi_{1-x})O_3$) is considered as the pioneer material in evolving the piezoelectric effect from a laboratory curiosity to multimillion dollar industrial applications including underwater transducers and medical devices because of its strong piezoelectric coefficients. It is a perovskite crystal structure consisting of a small tetravalent metal ion (titanium or zirconium) in a lattice of large divalent metal ions (lead). With 54% zirconate and 46% titanate, piezoelectric d_{33} coefficients up to 600 pC/N have been reported [30].

Beside these typical materials, ceramic materials such as barium titanate ($BaTiO_3$) and zinc oxide (ZnO) are also used in piezoelectric applications. However, these ceramic based transducers are brittle, non-flexible, hazardous and difficult to manufacture in large quantity [2]. Since in wearable electronic devices, challenges include limited space, shape and geometry, these ceramic based materials are not a suitable choice. However, the piezoelectric effect can be found in polymeric materials and they are an excellent choices for such wearable electronics.

2.4 Ferroelectric Polymer- β-Polyvinylidene Fluoride (β-PVDF)

Among the piezoelectric polymers, PVDF has the best inclusive electroactive properties and therefore, is the polymer of choice for a vast majority of applications [37]. It is a semicrystalline polymer with an amorphous density of 1.74 g/cm^3 and a crystalline density of 2.00 g/cm^3 at room temperature. It has a melting point of 160-165 °C and a glass transition temperature of about -35 °C. The PVDF unit cell contains two hydrogen atoms and two fluorine atoms as shown in Figure 2.3.

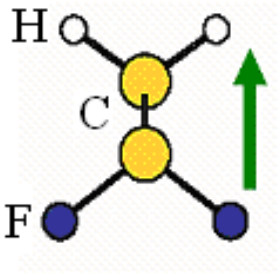

Figure 2.3: PVDF unit cell (-CH_2-CF_2), reprinted from [30].

Based on its chain conformation, PVDF can exhibit five different crystalline phases : all-trans (TTT) planar zigzag conformation for the β phase, TGTG' (trans-gauche-trans-gauche) for the α and δ phases and T_3GT_3G' for the γ and ε phases [37, 38]. From a practical point of view,the α, β and γ phases are the most important and commonly found in PVDF. In general, PVDF has strong electrical dipole moment in the monomer unit because of the higher fluorine atoms electronegativity compared to hydrogen and carbon atoms. Therefore, each polymer chain exhibits a dipole moment perpendicular to its axis. The most stable is the α phase because of the antiparallel packing of the dipoles within the unit cell which is non-polar and has low permittivity. On the other hand, the β phase has a crystal structure with fluorine atoms on one side and hydrogen atoms on

the other side of the polymer chain. Therefore, the dipole moment (8×10^{-30} Cm) is the highest in this crystalline form compared to the other phases because of its parallel dipoles packing [37-39]. The γ phase is also polar and active but, unlike the β phase, it has a g-gauche bond at every fourth C-C repeating unit resulting in a weaker dipole moment compared to the β phase [40]. Figure 2.4 presents the chain conformation for these phases.

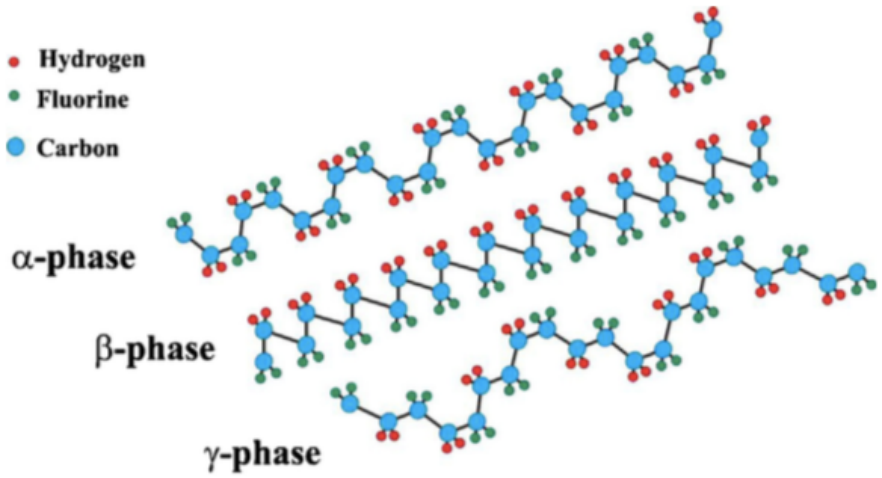

Figure 2.4: Schematic of the chain conformation of PVDF, reprinted form [37].

The piezoelectricity in β-PVDF arises from the electronegativity difference between the fluorine and hydrogen atoms in the molecular chain where the fluorine atoms pull away the shared electron from the hydrogen atom because of its stronger electron affinity. On the other hand, the β phase has a net dipole moment because it is randomly oriented in the film leading to a zero net polarization as shown in Figure 2.5 (a). The crystallites become oriented in response to an applied electrical field and exhibit net polarization even after its removal of the electric field as shown in Figure 2.5 (b). The volume polarization (or surface charge density, P) is given by :

$$P = \left(\frac{N\mu}{V}\right)(\cos\theta)\,,\ \mu = q\times l \qquad (2\text{-}7)$$

where N is the amount of dipoles within a volume V, μ is the dipole moment (a product of the charge q and the distance l between the charges), and θ is the angle between the dipole moment and the polarization direction. The piezoelectricity originates from the volume change in response to the applied force. Under the applied compressive force both the volume V and the distance l

decrease. Since l is in the nanometer scale, its change can be neglected and thus the dipole density can be considered constant. Therefore, the overall volume polarization increases leading to improved compensating charges. Thus a flow of charge occurs in the direction shown in Figure 2.5 (c).

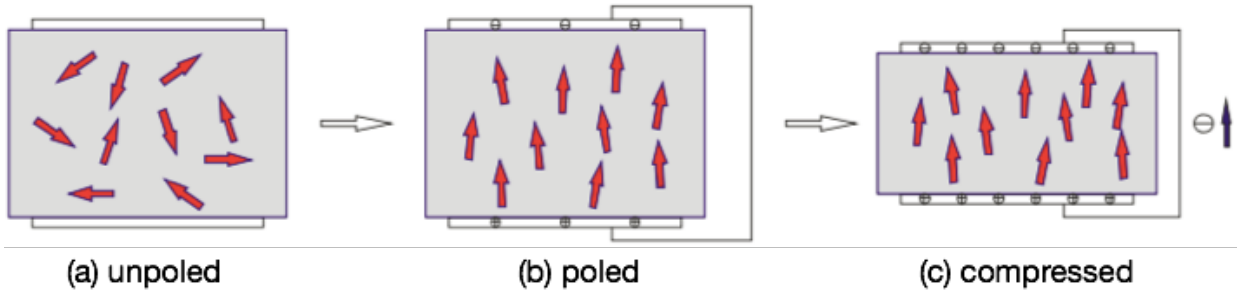

Figure 2.5: Illustration of the evolution of the piezoelectric effect from molecular dipoles in PVDF. (a) molecular dipoles oriented randomly before poling, (b) preferential alignment of the dipoles due to poling, and (c) increased polarization due to decreased thickness, reprinted from [30].

2.4.1 Formation of β-PVDF

Because of the growing interest in β-PVDF, several methods have been proposed and investigated to enhance the amount of β phase : solvent casting [41, 42], mechanical stretching [43], adding a PVDF copolymer [44-46] and nanofiller addition [8, 12, 47-50] as well as their combination.

Solution or solvent casting is one of the most commonly used methods because it is easy to carry out with a yields close to 100% β phase. However, it requires toxic or hazardous solvents like dimethylformamide (DMF) or chloroform [41]. Also, keeping the temperature below 70 °C during evaporation is crucial to maximize the amount of β phase produced since temperatures above 70 °C lead to a mixture of a α and β phases [51, 52]. Moreover, solution casting is not a suitable method for mass production which is a major drawback from an industrial point of view. Therefore, melt mixing like extrusion and injection molding is more acceptable in terms of large scale production.

In contrast to solvent casting, mechanical stretching of melt molded films is considered to be an easier way to obtain β-PVDF. In this process, mechanical stress applied to a PVDF film

resulting in polymer chains orientation with an all-trans planar zigzag (TTT) conformation. During stretching, molecular dipoles orient themselves perpendicular to applied stress direction [53]. Sencadas et al. [54] reported the presence of ~80%(maximum) β phase in PVDF at a temperature of 80°C and a stretching ratio (R) of 5. They also showed that increasing the temperature beyond 80°C significantly deteriorates the β phase formation. Salimi and Yousefi [53] found similar results of maximum β phase of around 75% at a stretching temperature of 75°C and a stretching ratio (R) between 4.5 and 5. They reported that the amount of β phase is more influenced by the stretching ratio than the stretching temperature. Wang et al. [55] found that electrical poling under a strong field could further increase the amount of β-PVDF.

As an attempt to further improve the PVDF properties to meet the increasing demand for modern technological applications, copolymers of PVDF have been introduced and investigated. Poly (vinylidene fluoride-trifluoroethylene) or P(VDF-TrFE) is one of the most popular copolymers where the TrFE monomer with its large steric hindrance forces the polymer to rearrange in an all-trans conformation (TTT) leading to the piezoelectric β phase regardless of the processing techniques: melt or solution casting [1, 37]. The favorable composition for maximum β phase is reported to be 50-80% VDF [56], with a corresponding maximum d_{33} of 38 pC/N. The copolymer of poly(vinylidene fluoride-chloride trifluoride ethylene) or P(VDF-CTFE) is another promising material for piezoelectric applications whose final properties depend on the amount of CTFE [57]. Addition of bulky CTFE makes the polymer structure loose and makes it easier for the molecular dipoles to rotate under an external electric field. A d_{33} coefficient of up to 140 pC/N has been reported [46], which is much higher than PVDF alone (up to 34 pC/N) [58].

The above-mentioned methods to produce the β phase are prone to create structural defects or microstructural restriction which may impede different applications [37, 59]. Hence, alternative methods have been investigated to meet specific technical demands. So, methods of obtaining the β phase by adding different types of fillers such as ferrite [60], organoclay [8, 10, 48, 49, 61], $BaTiO_3$ [62], palladium [63], gold [64], and silver [63] are discussed next.

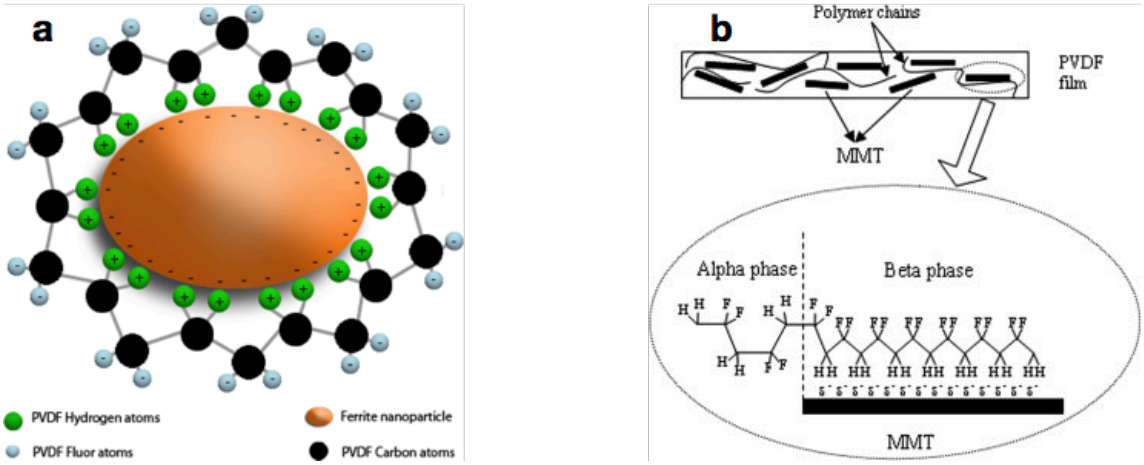

Figure 2.6: Mechanism of PVDF chain conformation change to TTT (β phase) in presence of (a) surface modified ferrite nanoparticle, reprinted from [65] and (b) montmorillonite clay, reprinted from [14].

Although the nucleation mechanism varies from filler to filler, the main driving force for the nucleation of the electroactive phase has been revealed to some extent for various fillers. By varying the surface charge and amount of the fillers, it was found that up to 90% β phase is possible to obtain by adding ferrite nanoparticles [60]. The nucleation of the β phase in such nanocomposites prepared by melt processing has been attributed to the interaction between the positively charged CH_2 groups of PVDF and the negatively charged filler particles as shown in Figure 2.6(a). The d_{33} obtained was up to 33 pC/N in such nanocomposites. Another way to improve the piezoelectric properties of PVDF is adding piezoelectric fillers such as PZT and $BaTiO_3$. The goal is to incorporate the high piezoelectric properties of these fillers in the PVDF matrix. For instance, Ye et al. [62] reported that up to 80% β-PVDF can be nucleated by adding $BaTiO_3$ ceramic filler in PVDF by melt processing depending on the filler size and regardless of the amount of filler. However, the biggest drawbacks of these fillers include cost-intensive and difficulty to manufacture at industrial scales. Therefore, researchers have been inclined to use cheaper and more available fillers such as organoclay serving the purpose of polymer chain conformation in a similar mechanism as ferrite nanoparticles in Figure 2.6(b). Nucleation of the β phase using organically modified nanoclays in melt processed PVDF was first reported by Priya and Jog [8, 10, 49]. Similarly, Sadeghi et al. [61] reported the presence of the polar β phase in melt extruded PVDF/organoclay composites prepared using a twin-screw extruder.

Along with numerous other advantages, the increased interfacial area between the filler and the polymer in nanocomposites is a particularly interesting one. A nanofiller such as TiO_2 has been reported by Nelson et al. [66] to modify the dielectric behavior of the polymer matrix. Interestingly, they found that micro-sized filler is more efficient in increasing the dielectric constant of the polymer because of its higher interfacial polarization compared to nanofillers. This arise from the fact that micro-fillers do not conform to the polymer chain length and enhance the occurrence of Maxwell-Wagner-Sillars (MWS) type of interfacial polarization arising from the difference of dielectric constant between the polymer and filler. Therefore, investigation of micro-sized filler or the combination of the piezoelectric properties of PVDF could be of interest.

2.5 Ferroelectret

An electret is a dielectric material consisting of quasi-permanent electrical charges. The charge is defined as "quasi-permanent" because the time constant characteristics of the charge decay is way much longer than the actual time period over which the studies are carried on these electrets.

Morphologically, a ferroelectret is a cellular polymer film with internally charged cells or voids exhibiting piezoelectric properties as shown in Figure 2.7. Sessler and his team [67] were the first to invent such a polymer structure during developing a charged polymer to be used as a microphone in 1962 and they named such polymer as 'space charge electret'. However, it was not until the late 1980s that researchers accepted this concept and started investigating such systems for their piezoelectric properties [68].

The idea of piezoelectricity in ferroelectrets is illustrated in Figure 2.7. Starting with the polymer film with closed internal voids, the film can be a single layer or multi-layer with a thickness from 20 to 200 μm. The voids are usually lens-shaped but it could also be square or rectangular with a typical dimension of less than a dozen micrometer in the thickness direction and up to few dozens of micrometer in the longitudinal direction. Upon electrical charging, the gas inside the voids breaks down and accumulates on the internal surface of the voids. The piezoelectricity in these films arises from the macroscopic dipoles created from the separated positive and negative charges on the upper and lower surfaces of the voids (Figure 2.7a). The corresponding dipole moment (μ) is defined as:

$$\mu = q \times l \qquad (2\text{-}8)$$

where, q is the amount of charge and l is the dipole distance (void height).

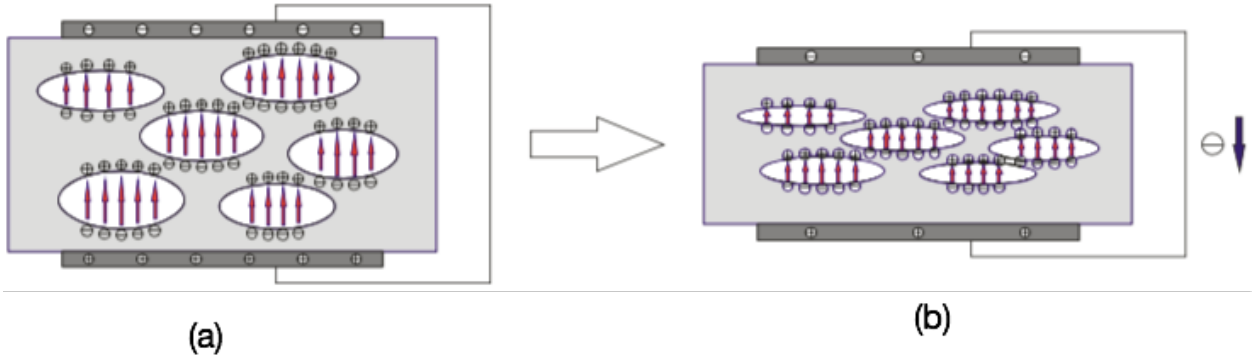

Figure 2.7: Schematic presentation of a ferroelectret. (a) macroscopic dipoles are formed in the voids at the gas/polymer interface after charging and (b) under mechanical stress, change in dipole moment causes the flow of charges, reprinted from [30].

Upon metallization, compensating charges are seen on the electrodes with the polarity opposite of the polarity of the dipoles on that side of the voids as shown in Figure 2.7(a). In this case, under an applied mechanical stress, the ferroelectret volume decreases which is more prominent than that for ferroelectric polymers (β-PVDF) because of the higher compressibility of the voids than the polymer bulk. As a result, the dipole moment (μ) decreases due to the decrease of the dipole distance l (Equation 2-8). On the other hand, the dipole density increases due to the decrease of the whole film volume. However, the extent of the dipole moment reduction is more pronounced than the increase of dipole density [30]. Therefore, the amount of compensating charges on the metal electrode decreases and flow of charges occurs as displayed in Figure 2.7(b).

2.5.1 Piezoelectric Coefficient of Ferroelectret

The piezoelectric coefficient of ferroelectrets is measured using the same principles as ferroelectrics described in section 2.2. Table 2.1 gives the typical d_{33} coefficient for various piezoelectric systems. Apart from the other advantages of ferroelectrets, their excellent piezoelectric d_{33} coefficient compared to traditional piezoelectric materials is the superior one. Despite superior piezoelectric response (d_{33} up to 600 pC/N), ceramics do not have the advantages

of polymers such as lightweight, easy formability, environment friendliness, etc. However, ferroelectric β-PVDF can only exhibit around hundred pC/N of d_{33} value in the form of a copolymer and composites. Ferroelectrets (PP) show a large d_{33} coefficient up to 2000 pC/N as shown in the Table 2.1, which is an added advantage for applications based on the thickness direction. Usually the piezoelectric properties of ferroelectrets are assessed by the d_{33} coefficient.

Table 2.1: Comparison of the piezoelectric d_{33} coefficients for common piezoelectric materials.

Piezoelectric materials	**d_{33} (pC/N)**	**Reference**
Crystal: quartz	2.3	[45]
Ceramic: Lead zirconate titanate (PZT)	170-600	[10]
Ferroelectrics: β-PVDF (homopolymer)	33	[46]
PVDF (copolymer)	72	[47]
PVDF composite	30-87	[19, 48, 49]
Ferroelectrets: Optimized cellular polypropylene (PP) (single)	1400	[50]
Optimized cellular polypropylene (PP) (multi)	2010	[69]
Optimized cellular PETP polyethylene terephthalate	15	[25]
Optimized cellular PTFE	220	[53]
Optimized cellular fluoroethylenepropylene (FEP) (single)	40	[10]

Since the piezoelectric activity (d_{33} coefficient) of polymer films originates from its change in thickness under an applied mechanical stress, the sample compressibility is critical in achieving the maximum piezoelectric response. Therefore, the compressibility, and thus the piezoelectricity, of a polymer foam strongly depends on the cellular structure morphology, its elastic stiffness and also on proper charging conditions. A controlled increase of the void thickness and then proper charging can lead to higher piezoelectric response.

2.5.2 Typical Ferroelectret Materials

2.5.2.1 Polypropylene (PP)

Polypropylene (PP) is a semicrystalline thermoelastic polymer used in a variety of applications like food packaging, automotive industry and medical instruments. Addition polymerization of the monomer propylene yields polypropylene which is chemically resistant (various acids, bases and solvents). The crystalline density of PP is 0.95 g/cm^3 while the amorphous density is 0.85 g/cm^3. The melting point ranges between 167 and 173 °C.

So far, PP foam is the most commonly used and scientifically investigated ferroelectret because of its availability, cost-effectiveness and ease of manufacturing. PP ferroelectret exhibits very high piezoelectric response, up to 1000 pC/N for a single layer [70], but values up to 2000 pC/N for a multilayer system have been reported [71]. However, one major disadvantage of these ferroelectrets is their very poor charge stability above 60 °C.

2.5.2.2 Polyethylene Terephthalate (PETP)

Polyethylene terephthalate (PETP) is a thermoplastic polymer synthesized by the transesterification reaction between ethylene glycol and dimethyl terephthalate. Its crystal density is 1.37 g/cm^3 with a glass transition and melting temperatures of 75 and 260 °C, respectively.

Wegener et al. [25] reported the successful foaming of PETP using supercritical CO_2. They also showed that foamed and stretched PETP films could exhibit a d_{33} of up to 20 pC/N after proper charging. Also, PETP films with density higher than 1 g/cm^3 did not show any piezoelectric response. Later, they found that through optimized adjustment of the cellular structure, the voided-stretched films via inflation had d_{33} coefficients up to 470 pC/N could be obtained [27].

2.5.2.3 Fluoroethylene Propylene (FEP) and Polytetrafluoroethylene (PTFE)

Fluoroethylene propylene (FEP) is a copolymer of hexafluoropropylene (HFP) and tetrafluoroethylene (TFE) with an asymmetrical molecular structure. Unlike FEP, PTFE has a symmetrical structure and is synthesized from the free radical vinyl polymerization of the tetrafluoroethylene monomer. The PTFE chain contains $–CF_2$ groups for every 180° turn in a twisting helix form. FEP has a similar molecular structure as PTFE except that a fluorine atom on each repeating unit is replaced with a perfluromethyl group, $–CF_3$. Both PTFE and FEP were invented by Dupont® and are available on the market by the brand name of Teflon®-PTFE and Teflon®-FEP [30]. The chemical structures of both PTFE and FEP are shown in Figure 2.8.

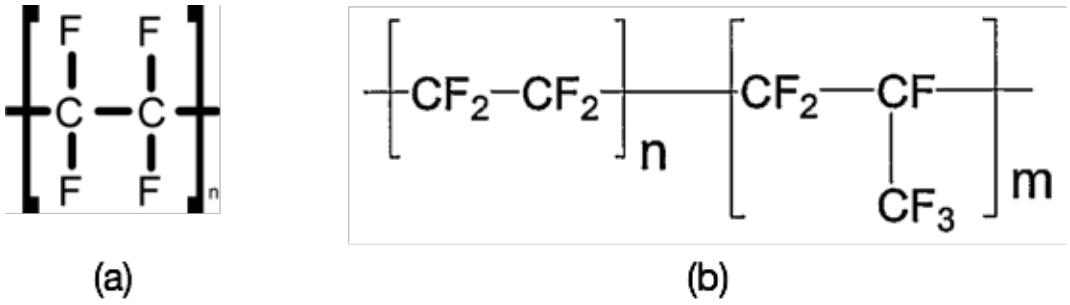

Figure 2.8: Chemical structures of (a) PTFE and (b) FEP.

PTFE and FEP have excellent physical, chemical and electrical properties. In general, PTFE has the highest thermal stability due to its regular packing of $–CF_2$ crystalline unit driven by the mutual repulsion of adjacent fluorine atoms. Because of its extremely high molecular weight and consequently virtually infinite melt viscosity, PTFE is not melt-processable. Because of its fibrillar structure, it is not even suitable as ferroelectret. On the other hand, the bulky side group $-CF_3$ in FEP disturbs the crystalline packing of the main chain and increases the amorphous fraction. Additionally, $-CF_3$ group can be considered as defects in the crystallites. Therefore, FEP has a lower melting point than PTFE and is melt processable using conventional methods. Table 2.2 summarizes the useful properties of FEP and PTFE.

Table 2.2: Properties of PTFE and FEP [10].

Properties	**PTFE**	**FEP**
Density (kg/m^3)	2200	2150
Elastic modulus (MPa)	500	480
Tensile strength (MPa)	23	23
Elongation at break (%)	250	325
Melting point (°C)	327	260
Maximum operating temperature (°C)	260	204
Dielectric constant at 1 MHz	2.1	2.1

2.5.3 Ferroelectret Formation

A lot of work has been devoted to cellular polymer systems to obtain an optimized piezoelectric response. In this regard, the formation of a cellular electret using fillers requires the following steps : (a) formation of voids by stretching the films filled with micron size particles or

by physical foaming, (b) improving the void geometry via gas inflation and heat treatment, and (c) formation of dipoles inside the voids by electrical charging and their stabilization. The process is schematically presented in Figure 2.9.

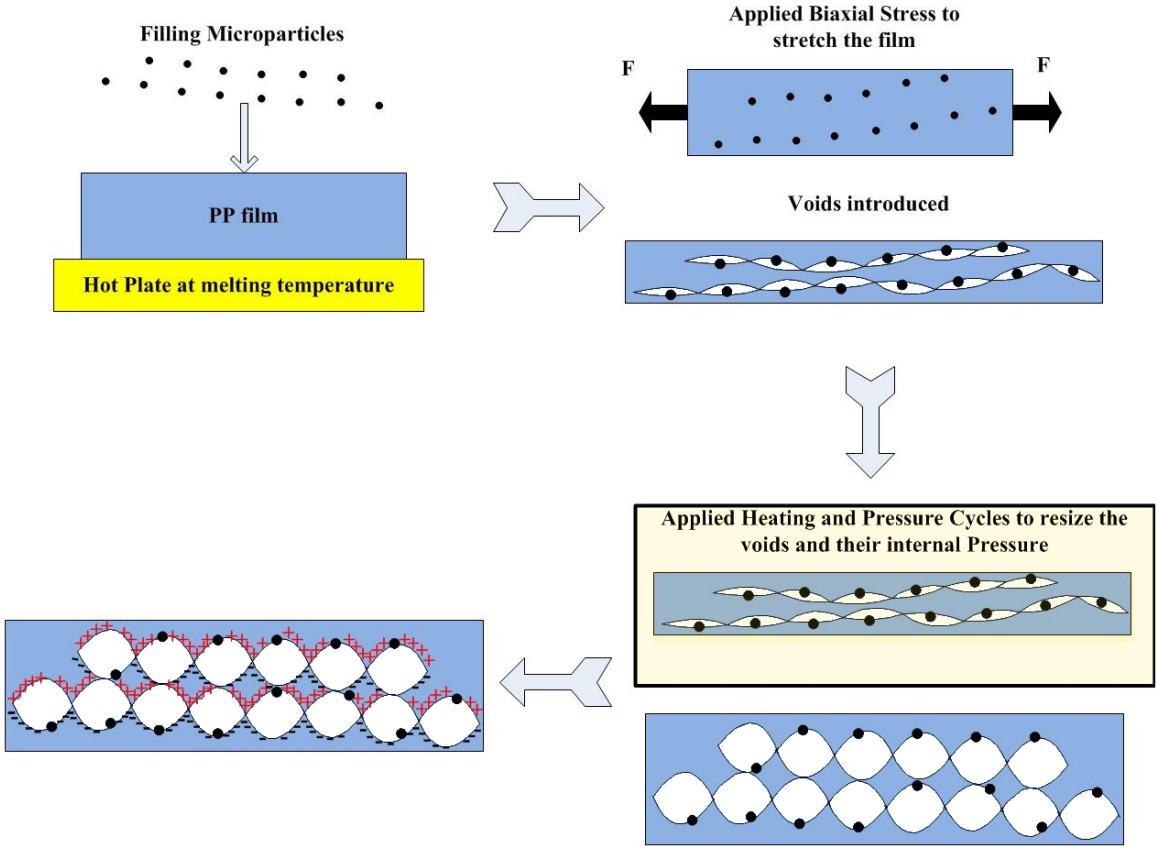

Figure 2.9: Schematic presentation of the fabrication process of ferroelectret using filler particles, reprinted from [2].

2.5.3.1 Cellular Structure Formation via Stretching or Foaming

There are few main routes to form voids in polymer systems. One of them involves modified extrusion process where gas injection into the molten polymer results in spherical voids. The resulting film is then reheated and biaxially stretched to reshape the spherical voids into lens-shape. The process was first introduced in the late 1980s for PP, but one of the main drawbacks of this technique is precise control of the blowing gas [30]. Therefore, another technique was proposed and investigated in the late 1990s by Raukola and Paajanen [21, 22, 69] where micron sized inorganic fillers such as titanium dioxide and calcium carbonate were melt mixed with PP via

extrusion. The mixture was extruded into films which was then stretched either uniaxially or biaxially using various stretching parameters including drawing ratio, temperature and others. During stretching, voids are formed around the filler particles through interfacial delamination of the partially molten polymer and the filler particles. A similar technique was successfully applied to cyclo-olefin polymers [24]. Since the resulting cellular structure is strongly dependent on the melt viscosity, fluoropolymers such as FEP and PTFE are not suitable for this technique because of their higher melt viscosity [30]. Another commonly used technique involves void formation by penetration of supercritical CO_2 inside the polymer film under high pressure (up to 150 bar) followed by a heat treatment above 31 °C (T_c of CO_2) of the CO_2 saturated samples to transform CO_2 into a gaseous state inside the films. PP [72], PETP [27] and FEP [28] have been investigated using these physical foaming processes. Sometimes, filler addition in the polymer matrix was made where the fillers acted as void nucleation sites [72]. Often, the void formation step is followed by high pressure gas inflation to adjust the void geometry as described in the next section.

2.5.3.2 Gas Diffusion Expansion (GDE) or Inflation

Stiffness, which is inversely related to the piezoelectric response of the polymer [73], is highly dependent on the size, shape and amount of voids of the cellular structure. There is a typical inversely-U shaped behavior as shown in Figure 2.10 (a-c). Films with small amount of voids with limited thickness (or flat) have relatively higher stiffness and therefore exhibit only low piezoelectricity (condition a). However, the controlled expansion of the void thickness by gas treatment lowers the overall film stiffness and increases the piezoelectric coefficient until a highly compressible, lens-shaped cellular structure is obtained (condition b). With continuous gas treatment, the lens-shaped, highly compressible voids in the film become more spherical in shape (with very low compressibility) leading to a strong stiffness increase. The increased stiffness ultimately results in a corresponding decrease in the piezoelectric response [17, 25]. Therefore, to adjust the cellular morphology in terms of amount of voids, void size, shape and aspect ratio inside the polymer films, gas diffusion expansion (GDE) or inflation treatment is performed. The overall dependence of the elastic stiffness, cellular morphology and piezoelectric response (Figure 2.10) has also been confirmed for PP foams via numerical simulations [74].

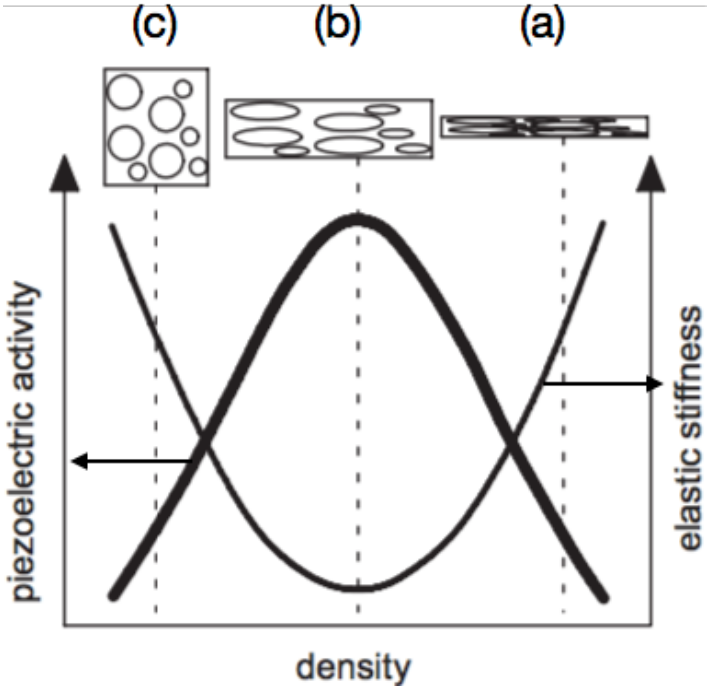

Figure 2.10: Schematic presentation of the correlation between the piezoelectric activity and elastic stiffness of a cellular film as a function of sample density and cellular morphology, reprinted from [26].

In a typical inflation treatment, the stretched or foamed polymer films are subjected to high pressure treatment for a certain period of time to ensure the saturation of voids with the high pressure gas. Once the applied pressure is reduced to atmospheric, the voids inside the film expands and the overall film thickness increases. If these films are left at rest, they return to their initial thickness in few hours. However, an elevated temperature treatment can stabilize the cellular structure and help retaining the increased sample thickness by increasing the crystallinity level and stiffening the foamed film to some extent [17, 75]. The temperature treatment could be done simultaneously or after the pressure treatment.

Furthermore, the way of applying pressure and heat treatment during inflation plays an important role on the ultimate film morphology. In an inflation experiment, Qaiss et al. [76] reported that an abrupt increase of pressure to higher value, 5 MPa for example, does not allow a progressive diffusion of the gases into the various cavities of the stretched PP-$CaCO_3$ films. Rather, such high pressure can collapse part of the voids due to a high compression effect related to the highly pressurized advancing gas. They found that pressure treatment in a stepwise manner at

higher temperature (close to the melting PP temperature) could create a progressive path for gas diffusion and push the inflation gas even in the small voids as well as preventing the collapse of cavities [76]. Mohebbi et al. [72] obtained similar results for PP foams prepared using supercritical CO_2. In a separate experiment, Wegener et al. [18] performed an inflation experiment on foamed PP where the pressure was applied from 0.2 MPa to 5 MPa followed by a heat treatment from 60 to 160 °C. They found that the inflation level saturates at a pressure around 5 MPa followed by a heat treatment at a temperature above 100 °C. They reported a 165% improvement in sample thickness over the non-inflated sample with an evenly distributed cellular structure (Figure 2.11). In a similar experiment, Sborikas et al. [17] obtained a maximum thickness increase of 257% for PP foam with an inflation pressure of 5 MPa and at a heat treatment temperature of 120 °C. However, Zhang et al. [70] suggested an additional inflation step followed by corona charging and metallization. They found that the obtained cellular structure after the first expansion of the PP foams at 2.5 MPa and an annealing treatment at 100 °C returned to its initial thickness after metallization. But a higher inflation level is obtained after the second expansion and after metallization at an annealing temperature of 45 °C with a stable cellular structure and reduced density.

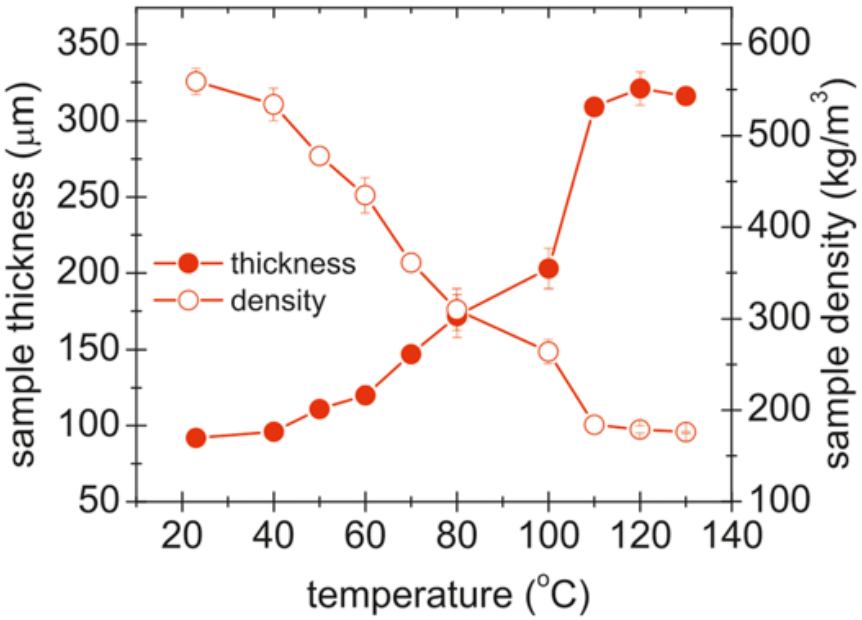

Figure 2.11: Change in thickness and density of cellular PP film as a function of heat treatment temperature after inflation at 50 bar in N_2 gas, reprinted from [17].

Apart from pressure and temperature, the type of inflation gas is another parameter that can potentially affect the overall film expansion. Not only that, the gas plays a major role in the next step of corona charging where the gas breakdown creates the space charge electrets. The interaction between the penetrating gas with polymer chains, gas viscosity, and its molecular size play a very important role in their permeation [77]. The most commonly investigated inflation gas is relatively–neutral nitrogen (N_2) [17, 78, 79]. However, polar gases such as CO_2 [30] and SF_6 [16] are seldom investigated.

Heat treatment of the film plays an important role with respect to the density and stabilization of cell morphology. Cellular polymer films can be annealed to change the crystallinity of the matrix and thus change the cellular geometry and the overall film elasticity. The annealing process can change the film thickness, but does not destroy the cell structure if appropriate annealing temperature is selected [17, 23, 80]. The heat treatment of the inflated samples is performed either simultaneously [72, 76, 81, 82] or after the inflation treatment [17, 19, 70]. However, the end result in both cases is a stable cellular structure with increased sample thickness and reduced density as shown in Figure 2.12.

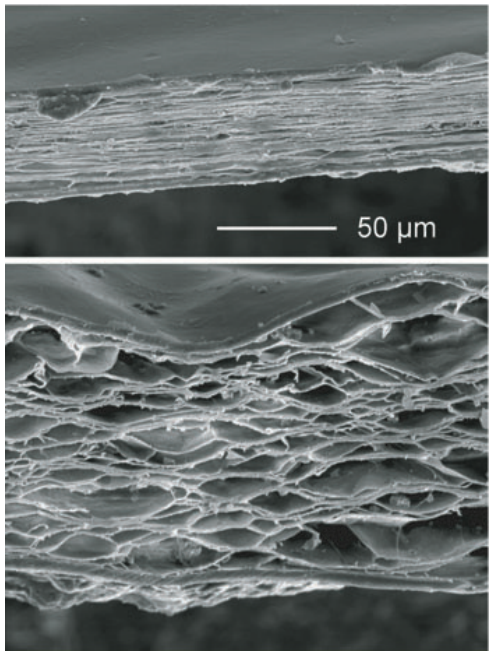

Figure 2.12: Scanning electron micrographs of the cross-section of cellular PP. Top image: film without inflation, and bottom image: film inflated at 5 MPa followed by a heat treatment at 100 °C, reprinted from [18].

2.5.3.3 Thermal Stability of Ferroelectrets

The two important aspects of the piezoelectricity of ferroelectrets are : the charges which constitutes the dipoles and the cellular structure (i.e. void height) which regulates the change in dipole moment (by changing the distance between the positive and negative charges in the voids) under an applied stress. Therefore, the ferroelectrets level is influenced by the stability of both cellular structure and of the charges. The application of a polymer in general is limited by temperature. Certainly, the cellular polymer cannot be used at a temperature higher than its melting temperature which in general, is much higher than the temperature for charge de-trapping. Therefore, the working temperature range of ferroelectrets is determined based on the temperature of charge stability [30].

Charge storage in polymers takes place in traps dispersed both on the surface and in the volume of the polymer in the electrets [83]. However, it is quite difficult to determine the molecular origin of this trapping. While the chemical impurities, specific surface defects, broken chains or adsorbed molecules make up the surface traps according to Sessler et al. [84], volume trapping takes place at three structural trapping levels. The primary levels are atomic sites on the molecular chains; the secondary levels consist of interaction between groups of atoms in neighboring molecules, and the tertiary levels are at the crystalline-amorphous interfaces. Some of these defects or anomalies have been found to be responsible for deep trapping of the electrons and also for longer period trapping [83]. However, these charges are not stable and will decay as a function of time, temperature, humidity or radiation. Despite the charges being characterized as quasi-stable for most ferroelectrets, the decay of charges with time still happens. This decay is faster in a humid environment due to the increased number of charge carriers. The decay is even faster at high temperature and in radiation. Both of them activate the charges in the trap levels and charge de-trapping occurs when the charges achieve enough energy [30]. As a consequence, various attempts have been made to improve the charge stability of ferroelectrets, especially at higher temperature as discussed later in this section.

So far, excellent piezoelectric d_{33} coefficient has been reported in PP and other non-polar electrets. However, the challenge remained in the lifetime of charges trapped in the voids as well as the thermal stability of the polymer films for high temperature applications. Typically, the d_{33} coefficient of the most popular and widely investigated cellular polymer (polypropylene) is up to

60 °C due to its poor charge retention capability [80, 85-87] and the value could go down to zero at 120 °C [88]. Therefore, investigations are performed to improve the working temperature range of typical ferroelectrets through structural modification as well as surface property changes. These structural modifications can be accomplished by stretching [89], increasing crystallinity or by adding nucleating agents like triphenylamine based trisamide derivatives [90, 91]. Addition of certain fillers to the polymer matrix also improves the charge retention capability by acting as charge traps [92]. Moreover, the structural changes occuring in the polymer matrix due to filler addition can also act as traps for the carriers, i.e. interface boundary [93, 94]. Additionally, Maxwell-Wagner-Sillar (MRS) polarization might occur at the interface between the fillers and polymer due to the conductivity difference in the system components [95]. The physical adsorption of polymer on solid filler surface reduces its mobility and results in stable electromechanical response via lower relaxation process rate [96]. Finally, a large number of voids generated by the filler hinder the drift/depolarization process by increasing the travelling distance of the carrier across the film [92, 97-99].

The other approach is to chemically modify the surfaces of the polymer film to thermally stabilize the charges at high temperature. Paajanen et al. [86] reported that after the modification of the PP surface by polyhedral oligomeric silsesquioxane (POSS), the cellular PP electret is more thermally stable at 85 °C than the reference PP. Similar result was reported by An et al. [100] where thermally stable ferroelectrets were obtained through direct fluorination of the PP film compared to the untreated counterpart up to 90 °C. However, the mechanism behind the improved thermal stability due to surface modification is still unclear. One possible explanation is that the space charges are stored on POSS acting as deeper charge traps [30]. Similarly, in a multilayer PDMS system with various void geometries internally coated with PTFE layer, the space charge density could maintain its stability for years [2].

In a completely different approach to obtain thermally stable electrets, fluorinated polymers such as FEP and PTFE have been proposed and investigated over the years. The thermal stability of the d_{33} coefficient for both single and multilayer based FEP and PTFE has been reported to be up to 120 °C because of their excellent charge retention capability [29, 87, 97, 101-103]. A comparison between the thermal stability of PP and PTFE has been reported in [87] as shown in Figure 2.13. Recently, Xia et al. [97] investigated PTFE films with porosities ranging from 50 to

80%. They observed that charge stability increases with increasing degree of porosity due to the corresponding increase of crystallinity and trap levels at the void/polymer interface. However, higher porosity beyond 80% has a negative effect on the piezoelectricity because of the increased leakage current. They also reported only 10% decay of the d_{33} coefficient for 70% porous samples annealed at 100 °C for 25 hrs. However, manufacturing FEP or PTFE films is a challenge using conventional methods like cast extrusion as mentioned in section 2.5.3.1.

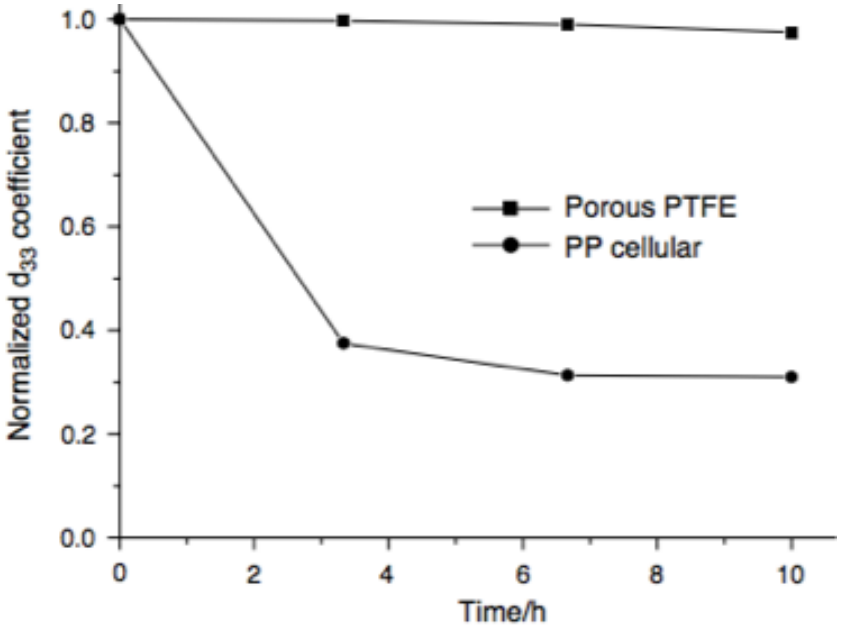

Figure 2.13: Isothermal d_{33} decay curve of cellular PP and porous PTFE aged at 80 °C, reprinted from [87].

2.6 Summary

Several efforts have been made to improve the piezoelectric activity of ferroelectric β-PVDF. However, some inherent drawbacks of these studies have been outlined earlier in this chapter. One promising approach is using nanofillers in the PVDF matrix to nucleate the polar β-PVDF. In general, ceramic based piezoelectric fillers yield better piezoelectric response in PVDF due to their own contribution. However, their application is limited because of their high cost and toxicity. On the other hand, easily available and cost effective fillers such as organoclay also lead to β-PVDF, but not enough to compete with ceramic based fillers. Moreover, the most common approach of

preparing the PVDF nanocomposite films is solution casting which is not a commercially viable method. Therefore, cost-effective ferroelectric PVDF composites prepared via commercially adaptable technique such as extrusion with strong piezoelectric response has been discussed in the first part of this work. For this purpose, a hybrid filler was been used in this study which is composed of industrially available and cost-effective micro-$CaCO_3$ and montmorillonite nanoclay. The effect of the hybrid filler composition on the electrical, mechanical and piezoelectric properties of the composite system has been investigated in detail.

While the ferroelectric PVDF film is easy to prepare, it requires less processing facilities and is easier to electrically pole. Nevertheless, its low piezoelectric coefficient is its main drawback limiting its application. Therefore, various ferroelectrets have gained attention and have been widely investigated because of their enhanced piezoelectric properties. The most popular is PP ferroelectret exhibiting very strong piezoelectric response but limited by its poor thermal stability. While fluoropolymer (i.e. FEP or PTFE) based ferroelectrets have the combined advantages of strong piezoelectric coefficient and excellent thermal charge stability, their processing into films using industrially viable techniques is quite difficult because of their high manufacturing temperature, tendency to degrade and poor deformability. Therefore, in the last part of this dissertation a new thermally stable ferroelectret based on PVDF is investigated. Moreover, a conventional cast extrusion process is used for film preparation.

CHAPTER 3 : OBJECTIVES AND ORGANIZATION OF THE ARTICLES

Piezoelectric polymers offer excellent possibilities in the field of advanced electromechanical systems. According to the literature review presented in Chapter 2, various ferroelectric and ferroelectret polymers have been developed with a range of piezoelectric sensitivity offering a degree of charge stability. Nevertheless, there is a gap between the advanced ones and those that are cost effective and industrially viable. Thus, a sufficiently high piezoelectric and thermally stable material must be developed and processed in a cost-effective way.

3.1.1 Objectives

3.1.2 General Objective

The main objective of this study is:

To develop and characterize new PVDF based ferroelectric and ferroelectret with enhanced piezoelectric response.

3.1.3 Specific Objectives

To meet the main objective, the specific objectives were defined:

1. To optimize the polar β-PVDF content in a PVDF matrix using various concentrations of hybrid fillers and through subsequent stretching.
2. To determine the combined effect of the hybrid filler concentration and stretching ratio on the electrical, mechanical and piezoelectric properties of PVDF hybrid composites.
3. To optimize the cellular structure through various inflation procedures and to investigate their effect on the piezoelectric response of cellular PVDF ferroelectret prepared from cast extruded film.
4. To analyze the effect of two different types of inflation gases (N_2 and CO_2) combined with multiple inflation procedures on the piezoelectric activity and thermal and temporal charge stability of PVDF ferroelectret.

3.1.4 Organization of the Articles

This section describes the scientific contribution of this thesis in the form of four original articles presented in Chapter 4 to 7. The following paragraphs are brief descriptions of each chapter along with co-dependence.

The first part of the study presented in chapters 4 and 5 involves the preparation and characterization of the piezoelectric response of ferroelectric β-PVDF. In Chapter 4, the combined effect of the hybrid filler (micro- $CaCO_3$ + Mt-clay) concentration and drawing ratio (R) on the polar β phase content of PVDF is investigated. To this end, the hybrid filler concentration was chosen by varying the $CaCO_3$ content from 30-40 parts with a constant 3 parts of Mt-clay. It was found that increasing the $CaCO_3$ content in the hybrid filler gives higher β-PVDF amount reaching almost 100% after stretching regardless of the drawing ratio. Chapter 5 describes the effect of the hybrid filler and the drawing ratio on the electrical, mechanical and piezoelectric properties of PVDF hybrid composites. The results confirm that using a hybrid filler has a synergistic effect on the volume resistivity, dielectric and piezoelectric properties of PVDF. Subsequent stretching results in further properties improvement as a function of the drawing ratio (R).

The 2nd part of the study is presented in Chapters 6 and 7 investigating the piezoelectric response of PVDF ferroelectrets. In this case, the inflation parameters are investigated to determine their effect on the final piezoelectric coefficient of cellular PVDF. Chapter 6 presents the effect of various inflation procedures on the piezoelectric response of PVDF ferroelectret. The inflation procedures are chosen by combining the associated parameters (pressure, temperature and the way of application) in nitrogen gas. After a systematic study, it is found that the optimized inflation procedures involve the stepwise application of pressure up to 5 MPa at a constant temperature of 130 °C yielding a maximum piezoelectric coefficient. Chapter 7 discusses the effect of CO_2 as the inflation gas on the d_{33} coefficient of PVDF ferroelectret and compares the result with the ones from Chapter 6 using N_2 as the inflation gas. The results reveal that due to the polar nature of CO_2, it has better interaction and hence better permeation in polar PVDF than N_2. Corresponding improved charge stability is also obtained in CO_2-inflated samples because of their improved crystallinity and more important charge trapping levels

CHAPTER 4 ARTICLE 1 : ENHANCED ELECTROACTIVE β PHASE IN THREE PHASE PVDF/$CACO_3$/NANOCLAY COMPOSITES: EFFECT OF MICRO-$CACO_3$ AND UNIAXIAL STRETCHING

Nusrat Jahan[1,2], Frej Mighri,[1,3], Denis Rodrigue[1,3], Abdellah Ajji[1,2*]

[1]CREPEC, Research center for high performance polymer and composite systems

[2]Department of Chemical Engineering, Polytechnique Montréal,
C.P. 6079, Montreal, QC, H3C 3A7, Canada

[3]Department of Chemical Engineering
Université Laval, Quebec, QC, G1V 0A6, Canada

Published in: Journal of Applied Polymer Science, 2017, Vol. 134, Page 44194

DOI: 10.1002/app.44940

4.1 Abstract

In this study, electroactive polar phase transformation and crystallinity of Poly(vinylidene fluoride) (PVDF) based composites, such as PVDF/$CaCO_3$/nanoclay, is explored as a function of micro-$CaCO_3$ fraction and draw ratio (R) of uniaxial stretching. Composites including PVDF/clay, PVDF/$CaCO_3$ and most importantly PVDF/$CaCO_3$/clay with varying fraction of micro-$CaCO_3$ were extruded into homogenous and flexible cast films. Characterization via Fourier transform infrared spectroscopy (FTIR), X-ray diffraction (XRD) and Differential scanning calorimetry (DSC) confirmed the presence of β phase in all the composites incorporated with micro-$CaCO_3$ and nanoclay either individually (i.e., PVDF/$CaCO_3$ and PVDF/clay films, respectively) or together (i.e. PVDF/$CaCO_3$/nanoclay composites). Interestingly, a gradual but significant improvement in this electroactive phase (β phase) was obtained with successive increment in $CaCO_3$ content into a fixed composition of PVDF and nanoclay (PVDF/$CaCO_3$/clay composites). Further increment in β phase content was obtained via uniaxial stretching to different draw ratios and at a temperature of 90°C, where for PVDF/$CaCO_3$/clay (especially, 100-35-3 and 100-40-3) samples almost no α phase was observed irrespective of R. On the other hand, the crystallinity of melt extruded samples decreased gradually all the way with $CaCO_3$ concentration in PVDF/$CaCO_3$/clay composites compared to the neat PVDF while increased gradually with increasing draw ratio.

4.2 Introduction

Since its discovery, the field of piezoelectric polymers has been dominated by poly(vinylidene fluoride) (PVDF) and its copolymers because of their excellent physical and thermal properties as well as their enhanced chemical stability [38]. Among the polymers exhibiting piezo and ferroelectric characteristics, such as Nylon [104] and polylactic acid (PLA) [105], PVDF family has the most versatile electroactive properties, which paved its way to numerous applications including sensors, actuators, energy harvesting and as biomaterials in medical field where its nonreactive nature has been credited [37, 38, 106-108]. This semi-crystalline polymer has a complex structure with the constitutional repeating unit [–CH_2-CF_2-]. Based on the chain conformation, PVDF can exhibit five different crystalline phases, among which β phase with all trans (TTT) planar zigzag, α phase with TGTG' (trans-gauche-trans-gauche) and

γ phase with T_3GT_3G' are the important phases from the practical point of view ([37, 38], Biswas, et al. [109].

The non-polar α phase is the most stable one with the antiparallel packing of the dipoles within the unit cell. On the other hand, β phase with the crystal structure of fluorine atoms on one side and hydrogen atoms on the other side of the polymer chain forming a parallel packing of dipoles, has the highest dipole moment (8×10^{-30} Cm) compared to the other phases [37-39]. The γ phase is also polar and active but, unlike β phase, it has a g-gauche bond at every fourth repeat unit of C-C band which results in a weaker dipole moment compared to the β phase [40]. Hence, the pursuit of enhancing the β phase in PVDF has yield significant interest to the researchers.

Therefore, over the years, different strategies have been developed to form β phase in pure PVDF and its composites. Mechanical stretching is one of the techniques to transform the originally formed α phase into β phase by transferring the applied tension to the crystals to rearrange the polymer chain conformation [43, 110]. Sencadas et al. [54] reported the presence of ~80% (maximum) β phase in pure PVDF stretched at a temperature of 80 °C and a draw ratio (initial length/final length) of 5. According to Salimi and Yousefi [43], a maximum of 75% β phase could be achieved at a temperature of 75 °C and a draw ratio between 4.5 and 5 in pristine PVDF. However, the tendency of stretched β phase to depolarize far below the curie temperature because of the smaller crystal size and conformational defects [111] has made the technique thermally vulnerable to higher temperature applications [112]. Also, since it is almost impossible to stretch a film deposited directly on devices or substrates, melt crystallization at higher pressure or solution casting at temperatures below 70 °C emerged as a popular way to achieve β-PVDF [47] although their poor electrical and mechanical performances due to porous and fragile nature of the final crystallized film have been recently reported [113].

Lately, incorporation of fillers, especially nanofillers such as nanoclay [8, 49, 61, 114], $BaTiO_3$ [62], gold [115], silver [116], TiO_2 [117], $CaCO_3$ [106] and carbon nanotubes [118] have been proven to be an easy way to introduce β phase in PVDF because of their high interfacial area. Although no universal nucleation mechanism exists for these fillers, numerous studies have unveiled the interaction of specific fillers with the polymers compelling the nucleation of crystalline phases. Until recently, PVDF/clay nanocomposites have achieved significant attention because of the capability of the nanoclay to enhance the electroactive phases remarkably even when

added at very small amounts [61]. Priya and Jog [8, 49] were the first to prepare the PVDF/clay nanocomposites where they observed that organically modified nanoclays can potentially introduce β phase upon melt processing because of the similarity in the crystal lattice of clay and β phase of PVDF. In another study, the effect of different surface modified nanoclays on the electroactive β phase formation of cast extruded PVDF/clay nanocomposites was observed by Sadeghi et al. [61]. They showed that branched PVDF incorporated with nanoclay exhibits a maximum amount of β phase.

Although numerous research has been performed on PVDF/clay nanocomposites, only a few have been reported on the effect of $CaCO_3$ on PVDF in spite of its abundance, low cost, suitability for industrial application and biocompatibility. Campos et al. [106] studied PVDF/$CaCO_3$ nanocomposite up to the fraction 70/30 in weight. They found that $CaCO_3$ acts like an anti-nucleating agent in PVDF, therefore, has no effect in phase transformation (α to β) and gradually reduces the crystallinity of the composite samples. On the other hand, Ma et al. [107] showed that nano-$CaCO_3$ is an effective filler to form β phase in PVDF and also increases the crystallinity of PVDF/$CaCO_3$ nanocomposite over neat PVDF. Therefore, further study is required to explore the full potential of $CaCO_3$.

While majority of the studies in the field of piezoelectric composite thus far have been focused on various nanocomposites, extent of investigation regarding the role played by micro-level filler geometry on the formation of electroactive phase in PVDF remains insufficient. Dependence of such formation process on filler geometry has indeed been predicted in literature [62]. On this basis, we explored the role of micro $CaCO_3$ particles introduced in various fractions on the electroactive phase formation and crystallinity in PVDF, especially in PVDF/$CaCO_3$/clay based composite structures. Synergistic effects of micro-$CaCO_3$ and nanoclay has been examined in both melt-extruded and simultaneously stretched PVDF/$CaCO_3$/clay composites. Also, the crystallinity of pure and composite materials was investigated by DSC. While nanoparticles are typically employed to obtain high interfacial area and good flexibility of final composites, the large percentage of micro $CaCO_3$ used in this work to achieve the equivalent interfacial exposure in the cast samples seems to retain a very good flexibility.

4.3 Experimental

4.3.1 Materials

PVDF (Kynar 720) (M_w = 265 kDa, T_m = 165 to 172 °C, density = 1.77 to 1.79 g/cm^3, PDI (Poly dispersity index) = 2.3, MFR = 5-29 g/10 min (at 450 °C under 3.8 kg load) is an extrusion grade polymer supplied by Arkema, USA. Nanomer I44P (dimethyl hydrogenated tallow quaternary ammonium ion exchanged montmorillonite ; density 1.4 g/cm^3) was purchased from Nanomer Inc. and was used as filler to prepare the nanocomposites of PVDF. The untreated calcium carbonate ($CaCO_3$), micro filler (particle size: 3-13 μm, density: 2.7 g/cm^3) was supplied by Univar, Canada. It is an industrial grade filler and was used without further purification.

4.3.2 Film Preparation

Three different types of composite films along with neat PVDF were prepared using a tightly intermeshing co-rotating twin screw extruder equipped with a typical compounding screw provided with two kneading block zones fitted with a slit die (20 cm × 1.8 mm). The composites were- PVDF/$CaCO_3$ (100-40-0), PVDF/clay (100-0-3) and PVDF/$CaCO_3$/clay (100-30-3, 100-35-3 and 100-40-3). The numbers in each system indicate the weight content of each constituent in the indicated order, e.g. PVDF/$CaCO_3$/Clay, 100-30-3 is 100 part PVDF, 30 parts $CaCO_3$ and 3 parts clay. A fixed fraction of 3 parts clay was chosen for the study because experiments showed that higher fractions hardly improve the β-PVDF in the composites compared to 3 parts clay. In the compounding process, first, weighted amount of PVDF and fillers (nanoclay, $CaCO_3$ or nanoclay/$CaCO_3$) were mixed in the extruder to prepare the small pellets and then the pellets were passed through the extruder again, pulled by the calendar to prepare the composite cast film with a thickness in the range of 80-100 μm. Since the extrudate velocity at the die exit was constant, the draw ratio or the film thickness was controlled by the pulling speed of the calendar. Besides natural air cooling, a controllable air knife was installed right at the exit of the die to supply sufficient air to the film surface. All composite films were prepared using a constant extrusion speed of 100 rpm with the temperature of compounding zone of 185 °C and die temperature of 195 °C. Pure PVDF, $CaCO_3$ and nanoclay were vacuum dried overnight at 70 °C before compounding. The polymer (PVDF) was fed from the main hopper using a volumetric feeder and the fillers ($CaCO_3$ and nanoclay) were introduced to the extruder using a high precision powder feeder (side feeder) at the

main feeder. The materials were fed into the extruder at a constant rate to maintain the specific composition for each composite film. Details of nanocomposite samples used in this study are shown in Table 4.1.

Table 4.1: Detail of sample composition used in this study.

Elements	**Fraction of $CaCO_3$**	**Fraction of nanoclay**	**Sample ID**
PVDF	0	0	100-0-0
PVDF/clay	0	3	100-0-3
PVDF/$CaCO_3$	40	0	100-40-0
PVDF/$CaCO_3$/clay	30	3	100-30-3
PVDF/$CaCO_3$/clay	35	3	100-35-3
PVDF/$CaCO_3$/clay	40	3	100-40-3

4.3.3 Uniaxial Stretching

Since PVDF shows a shear thinning behavior during stretching, it can be stretched using regular processing equipment with a precision temperature control chamber. All the samples, including pure PVDF, PVDF/clay, PVDF/$CaCO_3$ and PVDF/$CaCO_3$/clay composite films, were stretched uniaxially using Instron (ElectroPlus^{TM} E3000) instrument equipped with an environmental (heating) chamber. The samples were cut in rectangular shape with width of 4.5 cm and length of 1 cm (gage length). The temperature of the chamber was set to 90 °C and the drawing speed was fixed at 2.5 mm/min, only the draw ratio (R=final length/initial length) was varied from 4 to 5 (4, 4.5 and 5). In order to maintain the thermal equilibrium between the surface and the inside of the samples, each sample was held inside the chamber at 90 °C for 5 mins before stretching. After the stretching was done, the stretched samples were cooled down to room temperature in natural air.

4.3.4 Characterization Techniques

Fourier transform infrared spectroscopy (FTIR : Nicolet 6700, Thermoscientific, USA) measurements were performed to determine and analyze the crystalline phases of both stretched and unstretched PVDF and its composites. Infrared spectra were recorded in the range of 600-4000 cm^{-1} in the transmission mode for 32 scans with a resolution of $4cm^{-1}$.

X-ray diffraction (XRD: Philips X'PERT diffractometer) measurements were carried out by using Cu-Kα radiation for X-ray of wavelength 1.54 Å. The generator was set to 50 kV and 30 mA. The test was performed in θ/2θ reflection mode using a step scan interval of 0.0158 with 2 s/step.

The melting and crystallization behaviors as well as electroactive phases of neat PVDF and its composites with varying fraction of $CaCO_3$ and nanoclay were analyzed using a differential scanning calorimeter, DSC Q1000, TA Instruments under nitrogen atmosphere. The samples were heated to 220 °C at a ramp rate of 15 °C/min.

4.4 Results and Discussion

4.4.1 Infrared Spectroscopy : Analysis of the Crystalline Structure

In order to identify the crystalline structures, FTIR was performed on PVDF composite films with nanoclay and varied fractions of $CaCO_3$. Figure 4.1 presents the FTIR spectra of cast extruded neat PVDF and its composite films at room temperature. According to literature, the characteristic peaks at 612 and 764 cm^{-1} (CF_2 bending and skeletal bending), 795 (CH_2 rocking) and 975 cm^{-1} (CH_2 twisting) represent the α-phase. On the other hand, absorption peaks at 1234, 811 and 833 cm^{-1} correspond to the γ-phase and the peaks at 840 (CH_2 rocking) and 1274 cm^{-1} correspond to the β phase. As shown in the figure, relatively intense absorption peaks of α-phase at 612, 764, 795 and 976 cm^{-1} are present in neat PVDF, PVDF/clay (100-0-3) and PVDF/$CaCO_3$ (100-40-0) composite films, although the peaks corresponding to β-PVDF are absent in neat PVDF. However, the β-phase peak at 840 cm^{-1} is prominently visible in PVDF/clay (100-0-3) and PVDF/$CaCO_3$ (100-40-0) samples. According to Buckley et al. [12], β phase does not usually form in the melt cast pure PVDF films as found in our results. In case of three phase composites (PVDF/$CaCO_3$/clay), with the increasing fraction of $CaCO_3$ at a constant fraction of PVDF and clay, the α peaks seem to be diminished gradually and β-peaks appear prominently at 840 cm^{-1} and a tiny one shows up at 1274 cm^{-1}. Specially, in 100-35-3 and 100-40-3 composite films, the α peaks are almost invisible and the β-phase peak is the strongest one.

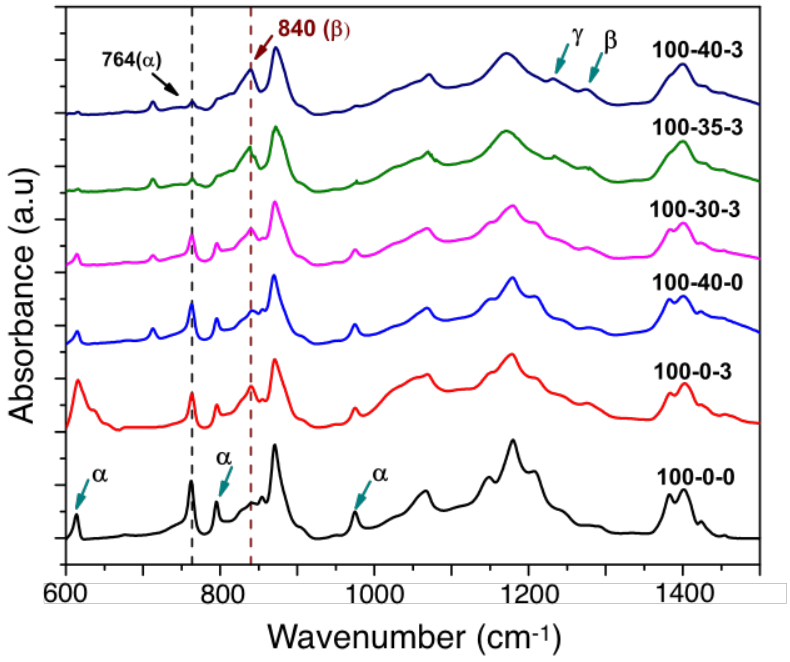

Figure 4.1: FTIR spectra of extruded neat PVDF and its various composites.

Also, the absorption band at 706 cm^{-1} represents the calcite structure [106] and is also typical of the interaction of $CaCO_3$ with PVDF, therefore, the composite formation is confirmed (top four spectra in Figure 4.1). Since the intensity of this peak (706 cm^{-1}) increased with the increasing fraction of $CaCO_3$, as shown in Figure 4.1, the composition of $CaCO_3$ is quantitatively confirmed for the three phase composites (PVDF/$CaCO_3$/clay).

The characteristic peak for β and γ-phases at 840 and 833 cm^{-1} respectively, is very close to each other in the FTIR spectra, even sometimes the peak at 833 cm^{-1} appears as a shoulder of the peak at 840 cm^{-1}, hence is difficult to distinguish between them. Therefore, it has been proposed by various authors to use the peak at 1234 cm^{-1} as a way to distinguish the γ-phase from the β phase [119]. Yet, no absorption peak at 1234 cm^{-1} was found in any sample, except the 100-40-3 film where only a very tiny band was observed but, as it will be shown in the next sections, the XRD and DSC results did not support this γ-PVDF formation in the 100-40-3 sample.

FTIR spectrums are commonly used to quantify the electroactive phases of PVDF and its composites. In order to determine the relative percentage of β-phase evident in PVDF based composites, including the two phase composites (PVDF/clay and PVDF/$CaCO_3$) and the three phase composites (PVDF/$CaCO_3$/clay with varying fraction of $CaCO_3$), the absorption coefficients

K_α and K_β corresponding to the peaks at 764 and 840 cm^{-1}, respectively, were compared as follows according to the Lambert-Beer law:

$$A_\alpha = \log\frac{I_\alpha^o}{I_\alpha} = K_\alpha C X_\alpha L \tag{4-1}$$

$$A_\beta = \log\frac{I_\beta^o}{I_\beta} = K_\beta C X_\beta L \tag{4-2}$$

Where,

A_α and A_β are the absorption bands at 764 and 840 cm^{-1}, respectively.

K_α and K_β are the absorption coefficients of the respective bands ($K_\alpha = 6.1\times10^4$ and $K_\beta = 7.7\times10^4$ $cm^2\,mol^{-1}$)

X_α and X_β are the percentage (%) crystallinity of the respective phases.

C, L are the average monomer concentration in the crystal phase and the thickness of the sample, respectively.

Using eqn (4-1) and (4-2), the relative amount of β phase with respect to the total crystalline phase in the sample is quantified as:

$$F(\beta) = \frac{A_\beta}{(K_\beta/K_\alpha)A_\alpha + A_\beta} \tag{4-3}$$

Where, F(β) is the relative amount of β phase. The calculated F(β) using eqn (4-3) is listed in Table 4.2 (2nd column). As mentioned earlier in this section, pure PVDF did not contain any β phase. Apparently, the addition of nanoclay (sample:100-0-3) transformed the relative β content to 50% whereas $CaCO_3$ (sample:100-40-0) increased it to around 58%. In the case of three phase (PVDF/$CaCO_3$/clay) composites, with increasing amount of $CaCO_3$ incorporated in a constant fraction of PVDF and nanoclay, F(β) increased gradually to around 58% for the 100-30-3 composite film and up to around 80% for both 100-35-3 and 100-40-3 composites, which corresponds to around 60% improvement over the PVDF/clay sample (100-0-3) and around 38% over the PVDF/$CaCO_3$(100-40-0) sample. This improvement in β phase content due to $CaCO_3$ can

be attributed to the enhanced nucleation of β phase due to the increased filler density or the capability of $CaCO_3$ to hinder the polymer chain mobility during melt crystallization, leading to the formation of more extended chain β crystals [12]. The appearance of the weak γ-PVDF signal in the 100-40-3 sample could not be further verified by any of the XRD (section 4.4.2) or DSC (section 4.4.3) measurements, which allowed us to proceed with our calculation without taking this phase into account. Although noticeable improvement in β phase content is confirmed by FTIR due to the addition of $CaCO_3$ in PVDF in presence of nanoclay, β phase content was reported by [106] to be unaffected in PVDF/ $CaCO_3$ composites.

On the other hand, FTIR spectra of samples including PVDF/clay(100-0-3) and PVDF/$CaCO_3$/clay (100-40-3) stretched at three different draw ratios (4, 4.5 and 5) at a temperature of 90 °C are shown in Figure 4.2(a-b). F(β) calculated using eqn (4-3) for all the samples is listed in Table 4.2 (3rd, 4th and 5th column) and the effect of $CaCO_3$ under various draw ratios is shown in Figure 4.2(c) by comparing 100-40-3 sample with 100-0-0, 100-0-3 and 100-40-3 samples. During stretching, a necking region was formed along with the occurrence of film whitening and the thickness of the sample was reduced on both sides of that region, which continued throughout the stretching process. According to Matsushige et al. [120], α to β transformation initiates simultaneously with the initiation of this necking region. Necking indicates the transformation from spherulites (α) to micro-fibrils (β) structure indicating how the β phase forms during stretching.

Table 4.2: Effect of fillers and draw ratio on the F(β) of neat PVDF and its composites.

	F(β)			
Draw Ratio	**R0***	**R4**	**R4.5**	**R5**
Sample	0	0	100-0-0	
Neat PVDF (100-0-0)	No β peak, 0	59±1.5	55±2	62±2
100-0-3	50±1	70±2	72±1.5	70±2
100-40-0	58±1	63±1	66±1.8	76±1
100-30-3	58±2	67±1.5	73±0.5	73±1
100-35-3	80±3	No α peak, 100	No α peak, 100	93±2
100-40-3	80±2	No α peak, 100	No α peak, 100	No α peak, 100

*R0 refers to unstretched samples.

As shown in Table 4.2, F(β) increased in all the stretched samples including neat PVDF and PVDF composites compared to their respective melt cast (unstretched) counterparts. A

maximum F(β) value of 62% was estimated for neat PVDF stretched @ R=5 at 90 °C, which is close to that reported by salimi and Yousefi [42] (67%). The stretched samples presented enhanced β phase over the melt cast samples due to the transformation of α to β phase (i.e., spherulites to micro-fibrils) by the tension applied during stretching. In the case of PVDF/clay (100-0-3) sample, the amount of β phase was almost constant, close to 70% regardless to draw ratios.

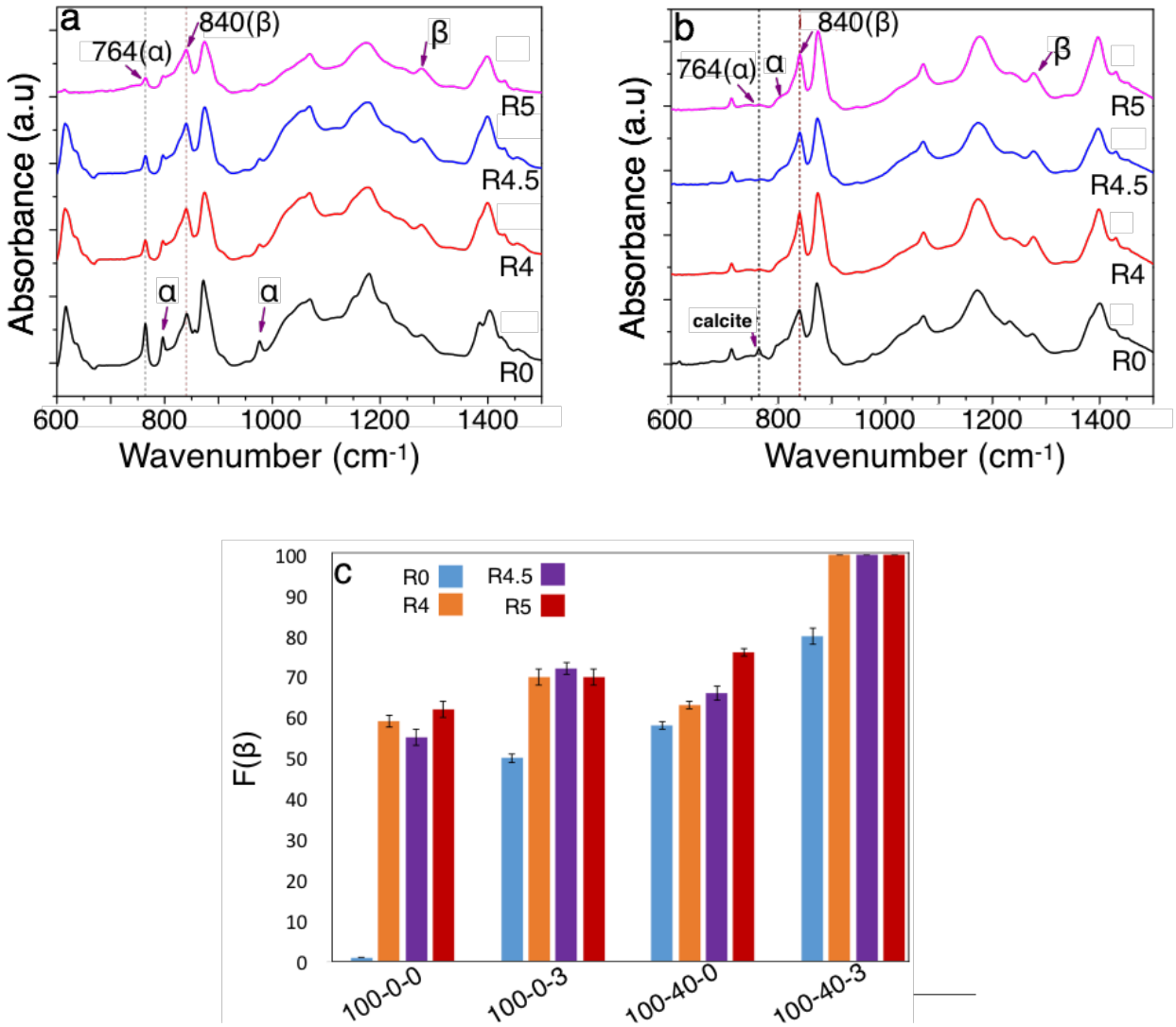

Figure 4.2: FTIR spectra of stretched (a) 100-0-3, (b) 100-40-3 samples and (c) Comparison of β phase content of three phase 100-40-3 composite with pristine PVDF and two phase composites drawn at different ratios.

However, for PVDF/$CaCO_3$(100-40-0) films, F(β) increased gradually with draw ratio up to 76%. Further, for the three phase (PVDF/$CaCO_3$/clay) composites, with increasing draw ratio, a significant transformation of α to β phase was observed with $CaCO_3$. Even for 100-35-3 (except at R5) and 100-40-3 (Figure 4.2(b)), no α-peaks were observed and only β peaks were evident. Hence, in presence of nanoclay, $CaCO_3$ can efficiently transform the α phase to electroactive β phase in PVDF composites under uniaxial stretching which might be attributed to the increased local stress compared to the critical stress during stretching due to the presence of higher fraction of $CaCO_3$. In such case, it is likely for these $CaCO_3$ fillers to transfer this excess stress to the matrix and an efficient transition of α to β phase at the interfacial region between the fillers (nanoclay and $CaCO_3$) and PVDF might be anticipated [47]. Since the interfacial area increases with the fraction of $CaCO_3$, the composite with higher amount of $CaCO_3$ exhibits higher F(β) value.

4.4.2 X-ray Diffraction : Analysis of Crystalline Structure

To further investigate the crystalline phases of samples including neat PVDF and PVDF composites, X-ray diffraction was carried out at room temperature. Figure 4.3 presents the diffraction patterns of melt cast samples, i.e., pristine PVDF, PVDF/clay, PVDF/$CaCO_3$ and PVDF/$CaCO_3$/clay composites. The XRD patterns for the crystalline phases (i.e., α, β or γ) of PVDF are easily distinguishable because of their respective characteristic peaks. The characteristic peaks at 17.5° (100), 18.2° (020) and 19.8° (021) are assigned to α-PVDF while the bands at 20.2° (combination of (110) and (200) planes) and 20.9° represent the β phase [11, 12, 37]. The XRD pattern of all the samples (including PVDF/clay (100-0-3), PVDF/$CaCO_3$ (100-40-0) and PVDF/$CaCO_3$/clay (100-30-3, 100-35-3 and 100-40-3)) in Figure 4.3 exhibited the presence of either only α-PVDF or a mixture of both α and β-PVDF.

Furthermore, no characteristic β phase peaks were observed for neat PVDF rather multiple α peaks were visible in the spectra, therefore, the neat PVDF is completely α-phase dominated, which supports our FTIR results (section 4.4.1) where no traces of β absorption band was found. Then, addition of nanoclay and $CaCO_3$ separately in PVDF (samples: 100-0-3 and 100-40-0, respectively) resulted in a strong crystalline β peak at $2\theta = 20.2°$ and a relatively weaker α peak at $2\theta = 18.5°$ and 17.9°. Under the same preparation conditions, in case of three phase (PVDF/$CaCO_3$/clay) composites, with increasing fraction of $CaCO_3$ (while PVDF and nanoclay

amounts were maintained constant), α peaks got weaker and β-PVDF band appeared stronger as well as broader. Even the α peaks were almost indistinguishable in PVDF/$CaCO_3$/clay (both 100-35-3 and100-40-3) samples while β peak was the strongest one, which again supports our FTIR result in section 4.4.1. Therefore, the enhancement in β-PVDF can be attributed to the α to β transformation due to the higher amount of $CaCO_3$ in presence of nanoclay in the PVDF matrix.

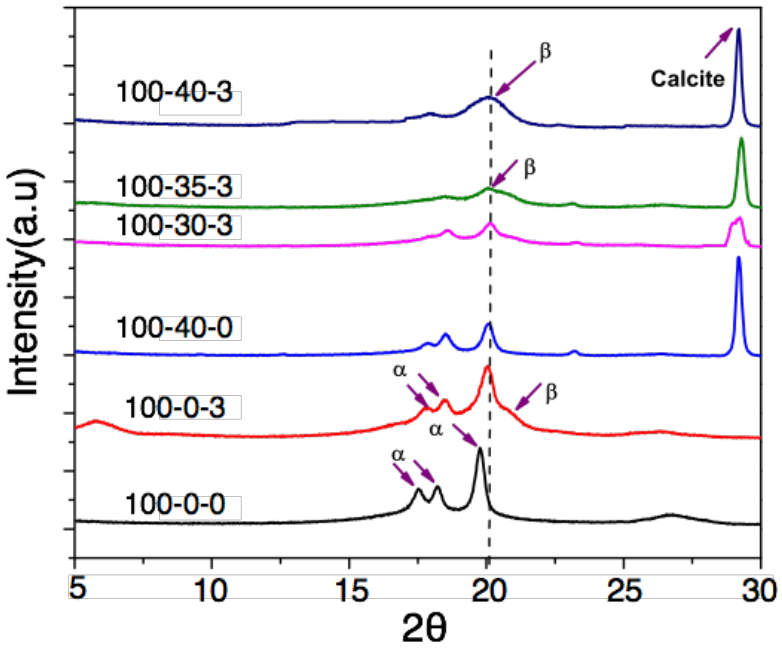

Figure 4.3: XRD patterns for pristine PVDF and its composite films for phase detection.

In other words, the addition of nanoclay and $CaCO_3$ simultaneously had a synergistic effect on introducing significant β-PVDF. The peak broadening for PVDF/$CaCO_3$/clay samples (especially 100-35-3 and 100-40-3) could be attributed to the presence of higher fraction of fillers ($CaCO_3$) in PVDF. With increasing $CaCO_3$ concentration, the density of nucleation sites available for crystallization is consequently increased, leading to finer crystals (see Table 4.3). The broader peaks were also reported by Buckley et al. [12] where they showed that nanocomposites with more β phase exhibit broader band than the one with α phase.

Also, the peak at around $2\theta = 30°$ is the characteristics of the presence of $CaCO_3$ in calcite structure [106] which, became more and more prominent with increasing fraction of $CaCO_3$. This confirms the presence of $CaCO_3$ in the matrix and a small shift in the peak position represents the interaction

of $CaCO_3$ with the PVDF matrix in the composite Sui, et al. [121].

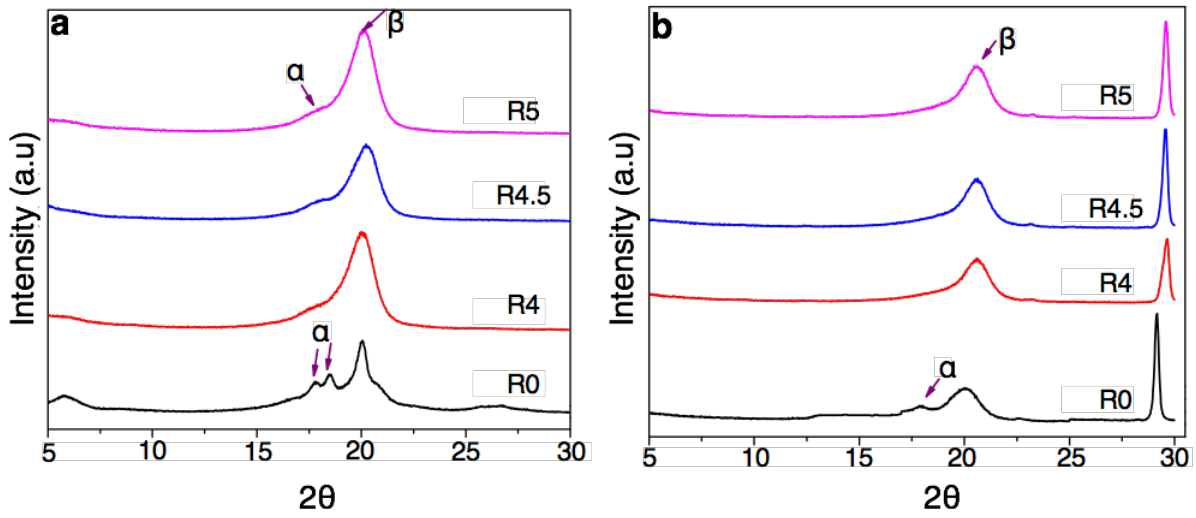

Figure 4.4: XRD spectra of stretched samples (a)100-0-3 and (b) 100-40-3.

Table 4.3: Coherence length and amount of α and β phase of neat PVDF and its composites.

Sample name	**L_α (nm)**	**L_β (nm)**	**α (wt.%)**	**β(wt.%)**	**Relative β % in crystalline content (%)**
100-0-0	31.7	0	47.3	0	0
100-0-3	23.2	16.1	17.7	23	56.5
100-40-0	21.8	15.2	16.4	17.1	51.04
100-30-3	19.0	15.3	28.6	28.5	49.9
100-35-3	11.5	6.2	10.1	39.7	79.7
100-40-3	10.1	4.1	10.5	46.2	81.48

The crystallite size or the coherence length of phases (α and β) was measured using Debbie Scherrer equation: $L = \frac{0.9\lambda}{B\cos\theta}$ where, λ is wavelength of X-ray, B is the full width at half maximum (FWHM, in 2θ), θ is the diffraction angle [44, 122]. Although each diffraction pattern consists of several peaks associated to α and β only the ones at 18.2° and 20.2° for α and β respectively, were used for the calculation. The data has been recorded in Table 4.3. As seen from the table, fillers have a significant effect on reducing the coherence lengths of both α and β. The neat PVDF has

the largest crystallites among all the samples because of the minimum possibilities of nucleation in the given processing condition. For two phase composites (100-0-3 and 100-40-0), the crystallite size decreased substantially because of the presence of fillers and the trend continued for three phase composites. With increasing filler content (in this case $CaCO_3$) The coherence length for both α and β kept decreasing.

The actual content of α and β was calculated by their respective crystallinity measured by deconvolution of the peak followed by peak fitting of the XRD patterns as described in ref [122] and then the relative amount (Table 4.3, last column) was calculated as a percentage with respect to the total crystalline content measured in the earlier step (see Table 4.3). By comparing the last column of Table 4.3 with the FTIR result in Table 4.2, first column, the relative β phase content is very comparable measured by two different methods. In both case, the β phase increased with $CaCO_3$ concentration in presence of clay and only a small amount of α phase was observed for 100-35-3 and 100-40-3 samples.

Figure 4.4 displays the XRD pattern of uniaxially stretched PVDF/clay (100-0-3) and PVDF/$CaCO_3$/clay (100-40-3) composite films stretched at draw ratios of 4, 4.5 and 5 under the temperature of 90 °C. In both cases, the stretched sample showed a strong β-PVDF peak, at 2θ = 20.1° for PVDF/clay (100-0-3) and 2θ = 20.9° for PVDF/$CaCO_3$/clay (100-40-3) sample, which proves their β domination. In Figure 4.4(a), PVDF/clay (100-0-3) nanocomposite was still showing the presence of α peak at 2θ = 17.6° as a shoulder of strong β peak which implies that even stretching at highest ratio (R=5) was not adequate for complete transformation of α to β phase. This supports our FTIR results presented in section 4.4.1 where maximum of 72% for F(β) was calculated at R4.5. On the other hand, for PVDF/clay/$CaCO_3$ films (100-40-3) presented in Figure 4.4(b), stretching seemed to transform all the α phase to electroactive β phase because of the favorable alignment of the PVDF chain segments and therefore, showing a single β peak. No traces of α or γ peaks were found in the diffraction pattern. Therefore, the XRD result shows a completely β dominated PVDF , which is in well agreement with the FTIR result.

4.4.3 Differential Scanning Calorimetry

Differential Scanning Calorimetry (DSC) is one of the most popular thermos-analytical techniques that has been used complementarily with other techniques, such as FTIR and XRD, to

detect the crystalline phases in polar polymers like PVDF and its composites [12, 37]. Each crystalline phase has its characteristic peaks on the thermogram. However, the thermal behavior of PVDF and its composites not only depends on the crystalline phases but also on the morphology, like defects, lamellae thickness, crystal size etc. [37]. Therefore, instead of using DSC as a way to estimate crystalline phases, it is mainly used to quantify the percentage of crystallinity in PVDF composites.

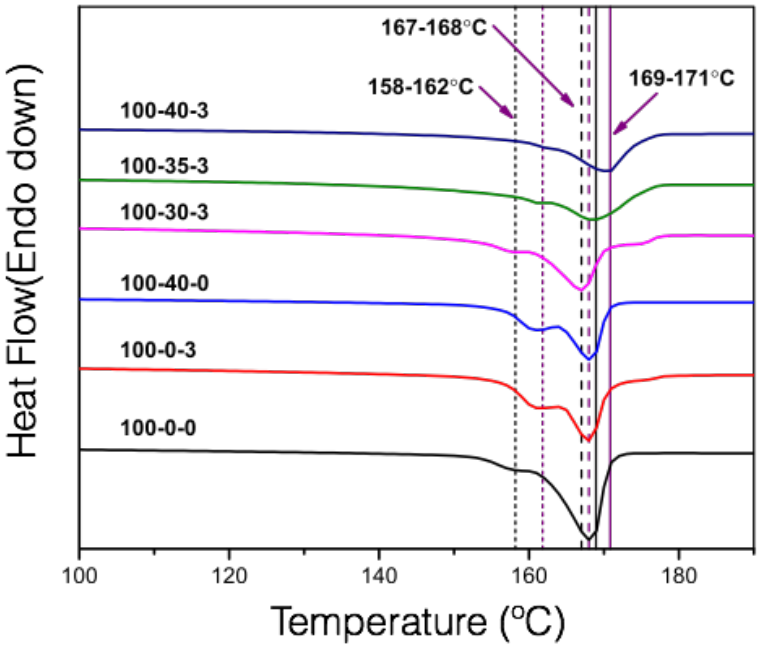

Figure 4.5: DSC thermograms of pure PVDF and its composites with various fraction of fillers.

DSC thermograms of neat PVDF, PVDF/clay, PVDF/$CaCO_3$ and PVDF/Clay/$CaCO_3$ composites (with varying percentage of $CaCO_3$) are presented in Figure 4.5. As seen from the thermograms, samples showing predominantly α phase, including neat PVDF, two phase composites (100-0-3 and 100-40-0) and three phase composite 100-30-3 (evident from FTIR and XRD results), exhibited a major melting endotherm at 167-168 °C. On the other hand, samples exhibiting predominantly β-PVDF, including 100-35-3 and 100-40-3 composites had their major melting peak at 169-171 °C. This increment in the melting temperature due to the presence of predominant β phase is supported by the literature [37, 38, 61, 119] since in β-PVDF, the coherence energy in the crystal is higher due to the larger dipole interaction.

On the basis of these facts, it can be postulated that in PVDF/$CaCO_3$/clay composites, with

increasing concentration of $CaCO_3$, not only the lamellae thickness increased but also the physical interaction between $CaCO_3$ and PVDF/clay matrix enhanced, which eventually improved the thermal stability as proven by the higher melting temperature [47, 110]. Higher melting temperature endotherm that could be attributed to the γ-PVDF [42, 114] was not evident in the samples. Therefore, the absence of γ phase was further confirmed by DSC thermograms. A low temperature shoulder in the range of 158-162 °C was observed for all the samples, including neat PVDF and its composites. According to Yang et al. [47, 110], this low temperature shoulder reflects the different crystallite size present in the sample. Ma et al. [107] explained this double endotherm as the occurrence of melting-crystallization where the lower peak indicates the onset of melting of characteristics crystals; in between the two peaks, all the molecules experience a continuous melting and recrystallization process and at the peak endotherm, the ultimate difference between melting and recrystallization is maximum. They also attributed this phenomenon to the imperfect crystal and varying lamellae thickness due to the addition of different size, shapes and concentrations of fillers.

Therefore, the low temperature shoulder endotherm in Figure 4.5 can be attributed to the imperfect crystal or defects, lamellae thickness or melting–recrystallization technique. This shoulder endotherm is almost indistinguishable with increasing concentration of $CaCO_3$ added in presence of nanoclay in PVDF (samples-100-30-3, 100-35-3 and 100-40-3), which could be explained by the fact that a small amount of nanoclay alone might be working as defect sites or creating imperfect crystals in PVDF/clay (100-0-3) composite. Therefore, an intense shoulder endotherm was observed in PVDF/clay nanocomposite but when $CaCO_3$ was added to the PVDF/$CaCO_3$/clay composite, a relatively continuous network of fillers was formed in the matrix and the clay particles were no longer working as defects. Also, higher amount of fillers might be worked as nucleation sites, as mentioned earlier in section 4.4.1 and 4.4.2 and created more homogenous crystal distribution and thicker lamellae.

The melting enthalpy (ΔH_m) calculated as the area under the endotherm in the range of temperature 140-200 °C is proportional to the crystallinity of the respective polymer sample. The crystallinity (χ_c) of neat PVDF and its composites was estimated according to the following equation (4-4) [47]:

$$\chi_c = \frac{\Delta H_{\beta m} \times 100}{x\Delta H_\alpha + y\Delta H_\beta (1-P))} \quad (4\text{-}4)$$

Where,

ΔH_m = melting enthalpy (J/g)

ΔH_α= melting enthalpy for 100% α-PVDF (93.07 J/g) [47]

ΔH_β= melting enthalpy for 100% β-PVDF (103.4 J/g) [47]

x, y= fraction of α and β phase respectively (calculated from FTIR)

P= weight fraction of fillers added

The areas of endotherm (ΔH_m) and calculated crystallinity are listed in Table 4.4. Addition of nanoclay or $CaCO_3$ separately (samples : 100-0-3 and 100-40-0) did not change the crystallinity of neat PVDF. In other words, nanoclay or $CaCO_3$ separately could not transform the amorphous PVDF to crystalline PVDF. However, when both $CaCO_3$ and clay were added together to PVDF (samples-100-30-3), the crystalline percentage increased significantly by around 31% over PVDF/clay (100-0-3) composite. With further increase of $CaCO_3$ concentration (samples-100-35-3 and 100-40-3), the crystallinity decreased gradually.

Generally, the presence of fillers (both micro and nano) can affect the crystallization behavior of a semi-crystalline polymer by enhancing the nucleation while interrupting the crystallization [47]. Since these two phenomena happen at the same time, it is hard to predict their individual contribution to the crystallization process. Therefore, from the obtained data, it can be concluded that for 100-30-3 sample, the nucleation effect prevailed over the crystallization process since the crystallinity increased significantly over PVDF/clay composite. For higher $CaCO_3$ concentrations, (100-35-3 and 100-40-3 composites) the crystallization process prevailed since the crystallinity decreased gradually. At this point this drop in crystallinity could be attributed to the confinement of polymer chains ; the dispersion of higher amount of $CaCO_3$ resulted in low inter-particle distance along with smaller effective particle size and therefore, higher number of effective particles, as compared to the other cases. Hence, the arrangement of the polymer chains in the matrix was hindered leading to lower crystallinity [123, 124].

Table 4.4: Melting enthalpy and crystallinity data for both as extruded and stretched samples.

Draw ratio	R0		R4		R4.5		R5	
Sample	ΔH_m (J/g)	χ_C (%)	ΔH_m (J/g)	χ_C (%)	ΔH_m (J/g)	χ_C (%)	ΔH_m (J/g)	χ_C (%)
100-0-0	41	42.5	52	52	51	52	68	68
100-0-3	41	43	48	49	49	50	52	53
100-40-0	30	42	32	44	34	48	36	51
100-30-3	43	56	--	--	--	--	--	--
100-35-3	39	53	--	--	--	--	--	--
100-40-3	28	39	34.76	49	35.31	50	38.74	55

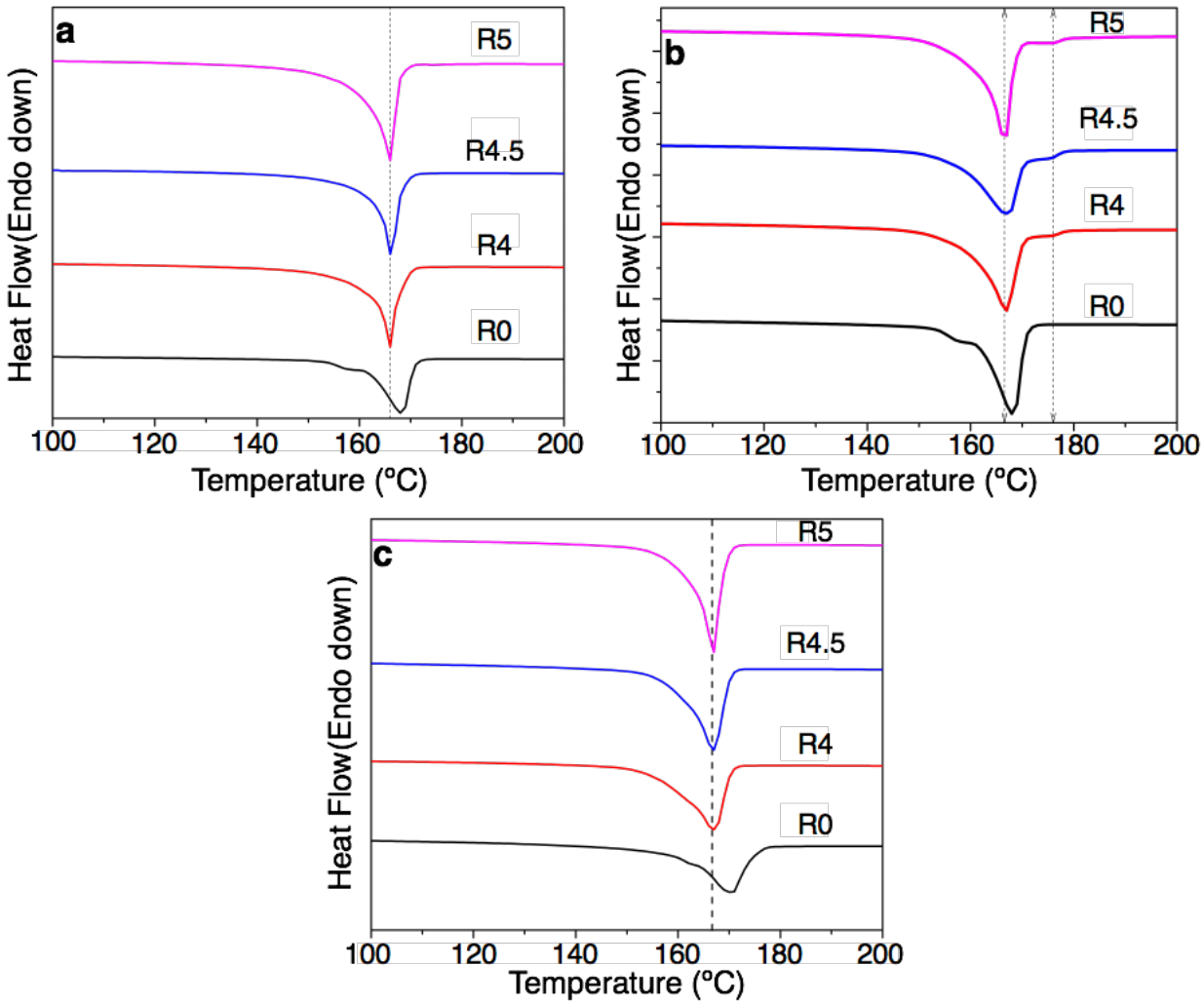

Figure 4.6: DSC thermograms of stretched samples (a)100-0-0, (b) 100-0-3 and (c) 100-40-3.

Compared to the melt extruded samples, the stretched samples showed relatively simpler pattern in the melting behavior. As shown in Figure 4.6, all the stretched samples showed a single melting peak unlike unstretched samples as shown in Figure 4.6(a-c). The peak melting temperature of all the uniaxially stretched samples fell at 167-168 °C, which is 2 to 3 degrees below the unstretched melt cast sample. According to FTIR result, the stretched samples had a significantly higher amount of β phase compared to the melt cast sample and due to the all-trans zigzag conformation of β phase, it had the highest crystal density compared to other phases. Therefore, the stretched samples were expected to show higher melting temperature than the unstretched samples [123], which did not happen as seen from Figure 4.6(a-c). This can be attributed to the fact that not only the electroactive phases of PVDF influence its thermal behavior, but also crystal defects, lamellae thickness, fillers etc., affect the phenomena significantly. During stretching, the lamellae thickness is reduced significantly, which eventually reduced the melting temperature of PVDF and its composites. A high melting temperature endotherm at 176 °C was observed in 100-0-3 sample regardless of stretching ratios (Figure 4.6(b)). According to Martins et al. [37], this high temperature peak might be attributed to γ-PVDF, which is not supported by our FTIR and XRD results. Therefore, further study is required in this regard.

As shown in the Table 4.4, the melting enthalpy and the crystallinity increase noticeably with stretching ratio compared to their as cast counterpart, suggesting that part of the amorphous area might have been converted into crystalline area (preferably into β crystalline phase) due to the stretching as mentioned in ref [47, 125].

4.4.4 Flexibility Test

Figure 4.7 exhibits the digital image of films of neat PVDF (100-0-0), PVDF/clay (100-0-3), PVDF/$CaCO_3$(100-40-0) and PVDF/$CaCO_3$/clay (100-40-3) before and after rolling which depicts the flexible nature of PVDF and its filled composites.

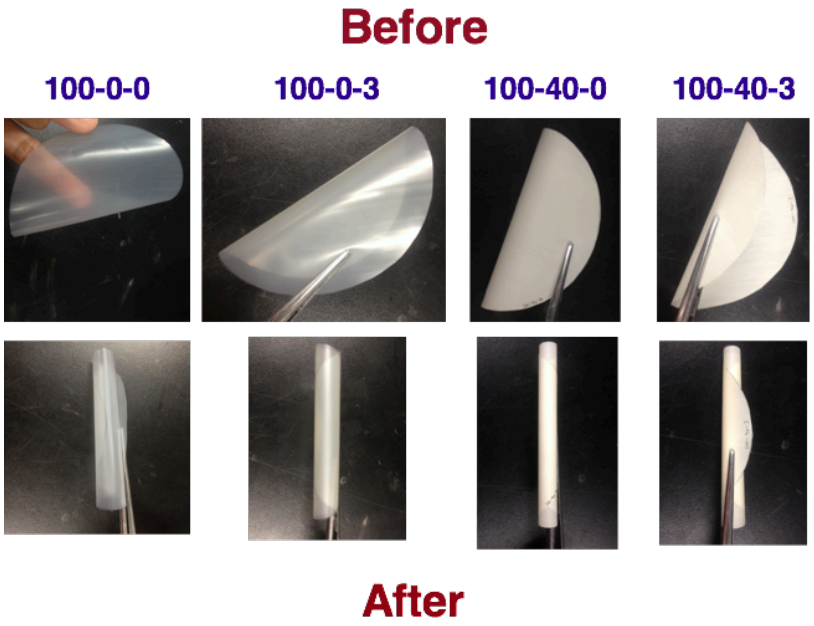

Figure 4.7: Digital photographs showing the flexible nature of 100-0-0, 100-0-3, 100-40-0 and 100-40-3 samples.

4.5 Conclusion

This study shows that the low cost, industrial grade and poorly explored (in the field of electroactive polymers) micro-$CaCO_3$ fillers could exhibit synergistic effect along with nanoclay in terms of introducing electroactive β crystalline phases in PVDF based composites. Although higher concentration of $CaCO_3$ was required to introduce maximum β phase in PVDF composites, viable flexibility (or mechanical properties) of the PVDF composites were maintained which is the key in many applications. Stretching of composite films at 90 °C to a draw ratio of 4 to 5 was proved to be an effective way to maximize the β phase in PVDF/$CaCO_3$/clay samples. Amount of β phase gradually increased in both un-stretched and stretched samples with increasing $CaCO_3$ content in PVDF/$CaCO_3$/clay samples. A maximum of 80% and almost 100% β phase was observed in unstretched (as extruded) and stretched 100-40-3 samples, respectively. On the other hand, crystallinity decreased with increasing concentration of $CaCO_3$ in PVDF/clay/$CaCO_3$ composites whereas increased gradually with increasing draw ratio (R) for the same samples. Therefore, the crystallinity and F(β) have an inverse relationship in un-stretched samples whereas having a relatively direct relationship in stretched samples in terms of $CaCO_3$ content in

PVDF/clay/$CaCO_3$ composites. The mechanism of the interaction of micro-$CaCO_3$ with PVDF chain to form the β crystalline phase is still unknown and needs to be resolved via future studies. Further study is required to confirm the crystallization behavior of such filled systems, specifically PVDF composite comprised with both nano (clay-surface treated) and micro ($CaCO_3$-untreated) fillers. Also, investigation of the thermal, mechanical and electrical properties of these three-phase composites could be an interesting study.

4.6 Acknowledgement

The authors acknowledge the technical support from Mr. Richard Silverwood and Ms. Claire Cerclé and the financial support from FRQNT (Fond de Recherche du Quebec en Nature et Technologie).

CHAPTER 5 ARTICLE 2: SYNERGISTIC IMPROVEMENT OF PIEZOELECTRIC PROPERTIES OF PVDF/ $CACO_3$/MONTMORILLONITE HYBRID NANOCOMPOSITES

Nusrat Jahan[1,2], Frej Mighri,[1,3], Denis Rodrigue[1,3], Abdellah Ajji[1,2*]

[1]CREPEC, Research center for high performance polymer and composite systems

[2]Department of Chemical Engineering, Polytechnique Montréal,
C.P. 6079, Montreal, QC, H3C 3A7, Canada

[3]Department of Chemical Engineering
Université Laval, Quebec, QC, G1V 0A6, Canada

Published in: Applied Clay Science, 2018, Vol. 152, Page 93-100

DOI: 10.1016/j.clay.2017.10.036

5.1 Abstract

Poly (vinylidene fluoride), PVDF, based hybrid nanocomposites (micro-$CaCO_3$ + nanoclay) containing varying amounts of $CaCO_3$ (30-40 parts) were developed via co-rotating twin-screw extrusion and were subjected to uniaxial stretching. A systematic study was performed to investigate the effect of micro-$CaCO_3$ content of the hybrid filler and subsequent uniaxial stretching at various draw ratios, R (4-5), on the mechanical, dielectric, electrical and piezoelectric properties of hybrid nanocomposites. For the as-extruded hybrid nanocomposites (without post-extrusion stretching), both dielectric properties and DC volume resistivity improved significantly, probably due to the enhanced charge trapping capability of nanoclay in the presence of $CaCO_3$ micro-filler. Similarly, hybrid nanocomposite containing 40 parts of $CaCO_3$ and 3 parts of nanoclay presented the maximum piezoelectric coefficient, d_{33} of 7.4 pC/N. For stretched nanocomposites, the volume resistivity and dielectric properties of hybrid nanocomposite containing 40 parts of $CaCO_3$ and 3 parts of nanoclay decreased gradually with R presumably due to its porous structure, as observed in SEM. However, stretched hybrid nanocomposites consistently exhibited enhanced piezoelectricity where the highest d_{33} value of 30.6 pC/N at R of 5 was obtained, which is attributed to the almost 100% β phase content and dipolar orientation induced by stretching and subsequent poling.

5.2 Introduction

PVDF has been the subject of significant research interest in the last few decades due to its excellent ferroelectric and piezoelectric properties leading its way to numerous applications as energy harvesting devices, flexible detectors, sensors and actuators of modern information and electronic industries [6, 13, 43, 126]. Based on its chain conformation, PVDF exhibits five different phases (α, β, γ, δ, ε) where only α, β and γ are the most commonly encountered. While the non-polar α phase is the most stable crystalline phase, β phase is the polar one with highest dipolar density and exhibits strong piezoelectric properties. γ phase as well is a polar phase with relatively lower dipole density and consequently, with lower piezoelectric performance [42]. As of now, a large number of studies have been conducted on the transformation of non-polar α to polar β phase using different techniques such as mechanical stretching, fillers addition, etc. [43, 127]. For example, Gomes, et al. [58] showed that stretching performed at different draw ratios and

temperatures enhances the β phase content and increases the piezoelectric coefficient, d_{33}, of PVDF.

Lately, the incorporation of fillers, especially ceramic nanofillers, has been proven to be an efficient way to improve the ferroelectric properties of PVDF because of their inherently high dielectric and piezoelectric properties [5, 6]. Among them, barium titanate, $BaTiO_3$, and lead containing perovskites, particularly PZT (lead zirconium titanate), have been most widely studied [5-7], although it is desirable to replace them due to their environmental and health concern. Therefore, other nanofillers, such as carbon nanotubes [47], nanoclays [8-13], gold [115], silver [63] are also being used in PVDF because of their additional benefit of being effective even at very small content.

Until recently, it has been reported by several researchers that organically modified nanoclays not only enhances the polar β-PVDF content and improves the piezoelectric properties of PVDF [10, 11, 13, 14], but also improves its dielectric and thermomechanical properties [13]. For instance, Patro, et al. [11] showed that organic surfactant modified montmorillonite clay could almost completely transform the α phase to β-PVDF at very low content. They attributed this enhancement to the mobility of silicate layers and fibre like structure of β phase. Similar result was reported by Priya and Jog [8], Priya and Jog [10] where they showed that a small amount of modified clay could introduce significant percentage of β phase and improve the storage modulus. Zhang, et al. [14] reported a maximum d_{33} value of 5.8 pC/N for poled PVDF/Mt nanocomposite. However, the complete conversion of α to β phase or hindering the unwanted conversion of α phase to less electroactive γ phase [12] of PVDF/silicate nanocomposite remain as major challenges yet to be explored.

The crystalline phases and their content in PVDF are strongly dependent on the processing technique, temperature, pressure and other parameters [42, 47]. The most commonly used technique reported in the literature to prepare PVDF nanocomposite films is first, dissolving the polymer and the filler in a suitable solvent and then preparing the film from this solution by solvent casting [5, 6, 47], spin coating [128], compression molding [5], and electrospinning [129] under various conditions. Since these techniques lack in potential for large scale production and often ends with porous structures [13], commercially viable mass production methods, such as melt blending along with calendaring, demands extended studies.

In this work, a new material approach of hybrid filler (micro-$CaCO_3$ + nanoclay) doped PVDF nanocomposite has been demonstrated with improved piezoelectric properties manufactured by melt-extrusion and then stretched to different draw ratios, R. Effectiveness of hybrid fillers (micro-$CaCO_3$ + nanoclay) in introducing higher amount of polar β phase in PVDF was demonstrated in the recent work [130] and the effect of stretching to further increase the β-PVDF content was also explained. Therefore, piezoelectric coefficient along with mechanical, thermomechanical, electrical and dielectric properties of hybrid nanocomposites (both stretched and unstretched) are characterized in this study by taking into account the roles of fillers to correlate the amount of polar β phase and crystalline characteristics obtained from the previous study [130]. The properties of hybrid nanocomposites were compared and analyzed with respect to the corresponding properties of two phase nanocomposites (PVDF/nanoclay and PVDF/$CaCO_3$) as well as pristine PVDF.

5.3 Experimental

5.3.1 Materials

PVDF (Kynar 720) was supplied by Arkema, USA. Nanomer I44P ((dimethyl hydrogenated tallow quaternary ammonium ion exchanged montmorillonite); density 1.4 g/cm^3) was purchased from Nanomer Inc. The micro-filler calcium carbonate ($CaCO_3$) (particle size: 3-13 μm, density: 2.7 g/cm^3) was supplied by Univar, Surrey, BC, Canada and was used without further purification.

5.3.2 Film Preparation

The films of pristine PVDF and its micro and nanocomposites were prepared using a tightly intermeshing co-rotating twin-screw extruder (for mixing) and a calendar (for forming the films). The composition of the developed PVDF/$CaCO_3$/clay (x-y-z) nanocomposite samples is presented in Table 5.1, where x, y and z correspond to the parts of PVDF, $CaCO_3$ and nanoclay, respectively. In the compounding process, first, weighted amounts of PVDF and fillers were compounded in the extruder to prepare small pellets and then the pellets were passed through the extruder again pulled by the calendar to prepare the film with a thickness in the range of 80-100 μm. All the films were prepared using a constant screw rotation speed of 100 rpm with the temperature of compounding zone being 195°C. Details of the extrusion/calendaring process is described in ref. [130].

Table 5.1: Details of the sample composition used in this study.

Elements	Content of $CaCO_3$	Content of nanoclay	Sample ID
PVDF	0	0	100-0-0
PVDF/clay	0	3	100-0-3
PVDF/$CaCO_3$	40	0	100-40-0
PVDF/$CaCO_3$/clay	30	3	100-30-3
PVDF/$CaCO_3$/clay	35	3	100-35-3
PVDF/$CaCO_3$/clay	40	3	100-40-3

5.3.3 Uniaxial Stretching

All the samples were stretched uniaxially using an Instron (ElectroPlus^{TM} E3000) equipped with an environmental (heating) chamber. The temperature of the chamber was set to 90 °C and the stretching speed was fixed to 2.5 mm/min. Only the stretching ratio, R (final length/initial length) was varied from 4 to 5 (4, 4.5 and 5) represented as R4, R4.5 and R5 respectively, in the following sections. R0 denotes the unstretched sample.

5.3.4 Characterization Techniques

Tensile characterization was performed on dog bone shape samples at a cross head speed of 5 mm/min using an Instron (ElectroPlus^{TM} E3000) equipped with a 500 N load cell. The tests were performed in the extrusion direction only. Dynamic mechanical analysis (DMA) was carried out in the tension mode on both melt-extruded and uniaxially-stretched samples by using a Q2980 DMA (TA Instruments, Newcastle, DE) at a frequency of 1 Hz in the temperature range of -90 °C to 130 °C at a ramp of 5 °C/min. The amplitude was set to 30 μm. Scanning electron microscope (SEM) images were obtained from field emission scanning electron microscope (JEOL JSM-7600TFE) at 15 kV. Dielectric measurements were performed on both melt-extruded and uniaxially-stretched films using a high precision impedance analyzer (Agilent 4294A) in the frequency range of 100 Hz to 1 MHz. DC volume resistivity (ρ_v) of both melt-extruded and uniaxially-stretched samples has been measured using an electrometer (6517B, Keithley instrument) equipped with a Keithley 8009 resistivity test fixture. The measurements were performed at 40 V and the electrification time was 300 seconds. The samples were corona poled at a constant electric field of 90 V/μm at room

temperature for 10 min. In order to choose an optimum polarization field and polarization time, a number of poling experiments were performed at an electric field from 40 V/μm to 100 V/μm on the neat PVDF (since pure PVDF has the lowest dielectric constant) until breakdown happened at 100 V/μm, assuming that full polarization takes place before 100 V/μm. For the sake of conformity in experimental parameters and comparison of different samples, 90 V/μm was chosen as the polarization field although it is not confirmed that the polarization field is strong enough for complete polarization of all samples. A quasi-static setup was used to measure the piezoelectric d_{33} coefficient by applying a direct piezoelectric effect where a force, F = 0.98 N, was applied on the sample by placing a mass , m= 100 g or by removing it [80]. The d_{33} coefficient was then calculated as ; d_{33}= Q/F where Q denotes the accumulated charge on the electrodes due to the applied force. Due to the ease of removal than applying the force on the sample, a static force of 0.98 N was applied initially on the sample for a longer time and after 10 s of load removal, the accumulated charge was read from the electrometer. For each sample, the procedure was repeated 3 times and the average value of Q was taken for d_{33} calculation.

5.4 Results and Discussion

5.4.1 Tensile Properties

Tensile characterization was performed on melt extruded neat PVDF and its nanocomposites in order to investigate their mechanical performance. The stress-strain curves of the extruded samples are presented in Figure 5.1 and the relevant experimental data is shown in Table 5.2. The tensile strength remained unaltered upon the addition of 3 parts of nanoclay (100-0-3), however, it decreased significantly (by around 47%) with the addition of 40 parts of $CaCO_3$ and by around 36% for hybrid nanocomposites (PVDF + $CaCO_3$ + nanoclay) regardless of $CaCO_3$ concentration. Therefore, hybrid filler ($CaCO_3$ + nanoclay) exhibited a negative effect on the tensile strength of PVDF, which could be attributed to the weaker affinity between the untreated $CaCO_3$ and PVDF due to the low surface energy of PVDF [126].

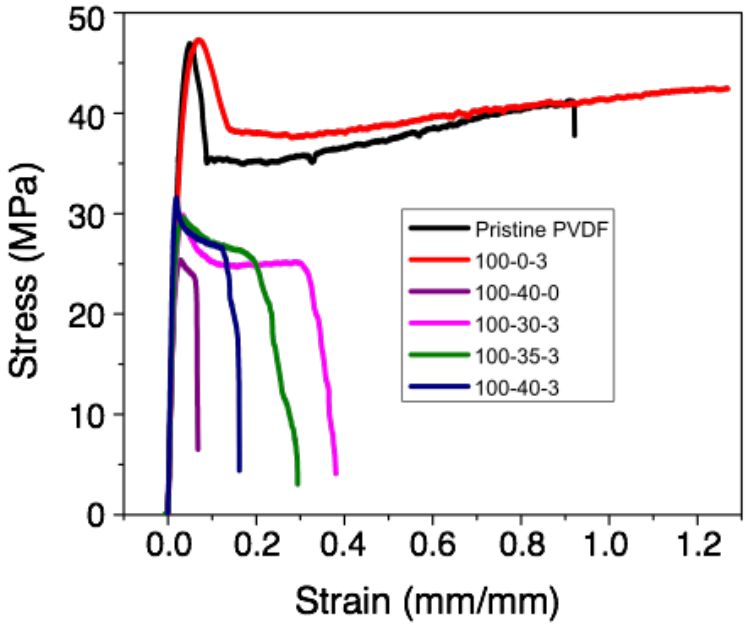

Figure 5.1: Tensile stress-strain curves of neat PVDF and its nanocomposites in the extrusion direction.

Table 5.2: Tensile properties of extruded neat PVDF and its composites.

Sample	**Tensile strength (MPa)**	**Young's modulus (GPa)**	**Elongation at break (%)**
100-0-0	46.9	1.71	92.1
100-0-3	47.3	1.56	No break
100-40-0	25.4	1.63	6.8
100-30-3	29.9	1.60	39.0
100-35-3	29.7	1.64	29.4
100-40-3	31.6	1.56	18.3

Also, Young's modulus of PVDF nanocomposites reduced slightly compared to neat PVDF. This made the PVDF nanocomposite more flexible and easy to deform under load, which is favorable for the improvement in piezoelectric properties [129].

The elongation at break (%) largely increased by the addition of 3 parts of nanoclay into PVDF. No sign of sample tearing was observed for 100-0-3 nanocomposite within the range of available instrument whereas all other samples failed at some point. This significant enhancement could be attributed to the plasticizing effect of nanoclay [13]. For hybrid nanocomposites, the elongation at break decreased gradually with increasing $CaCO_3$ content, which was expected since higher $CaCO_3$ content could hinder the plasticizing effect of nanoclay in the PVDF matrix.

5.4.2 Dynamic Mechanical Analysis (DMA)

In order to characterize material stiffness as a function of temperature, DMA was performed on neat PVDF and its hybrid nanocomposites (PVDF + $CaCO_3$ + nanoclay). Figure 5.2(a) describes the storage modulus (E') as a function of temperature at a constant frequency of 1 Hz for all samples in unstretched condition. The characterization was performed in extrusion direction. The storage modulus of PVDF was greatly affected by the addition of $CaCO_3$ and nanoclay fillers while both of them individually induced clear improvement. Interestingly, a synergistic improvement in the storage modulus was observed for hybrid fillers ($CaCO_3$ + nanoclay) incorporated PVDF nanocomposites and increased gradually with increasing $CaCO_3$ fraction. This increase in storage modulus due to hybrid filler inclusion can be attributed to their effectiveness in transferring the interface stress and limiting the segmental motion of polymer chains [131].

The effect of draw ratio, R, on the storage modulus of 100-0-3 and 100-40-3 nanocomposites is shown in Figure 5.2 (b and c). Stretching seemed to affect 100-0-3 and 100-40-3 samples inversely. While the storage modulus increased remarkably for stretched 100-0-3 nanocomposites at various draw ratios, it decreased noticeably for 100-40-3 film (Figure 5.2c). Compared to unstretched samples, stretched ones had more molecular orientation in both crystalline and amorphous regions due to stretching [132], which contributed to the enhanced storage modulus of 100-0-3 (containing nanoclay only). However, for 100-40-3 nanocomposite, containing both $CaCO_3$ and nanoclay, molecular orientation was also present in the stretched sample compared to the unstretched, a higher percentage of voids were present, as observed in SEM images in Figure 5.3. These voids were due to the interfacial delamination between the $CaCO_3$ solid filler and the PVDF matrix, leading to a significant decrease in the storage modulus.

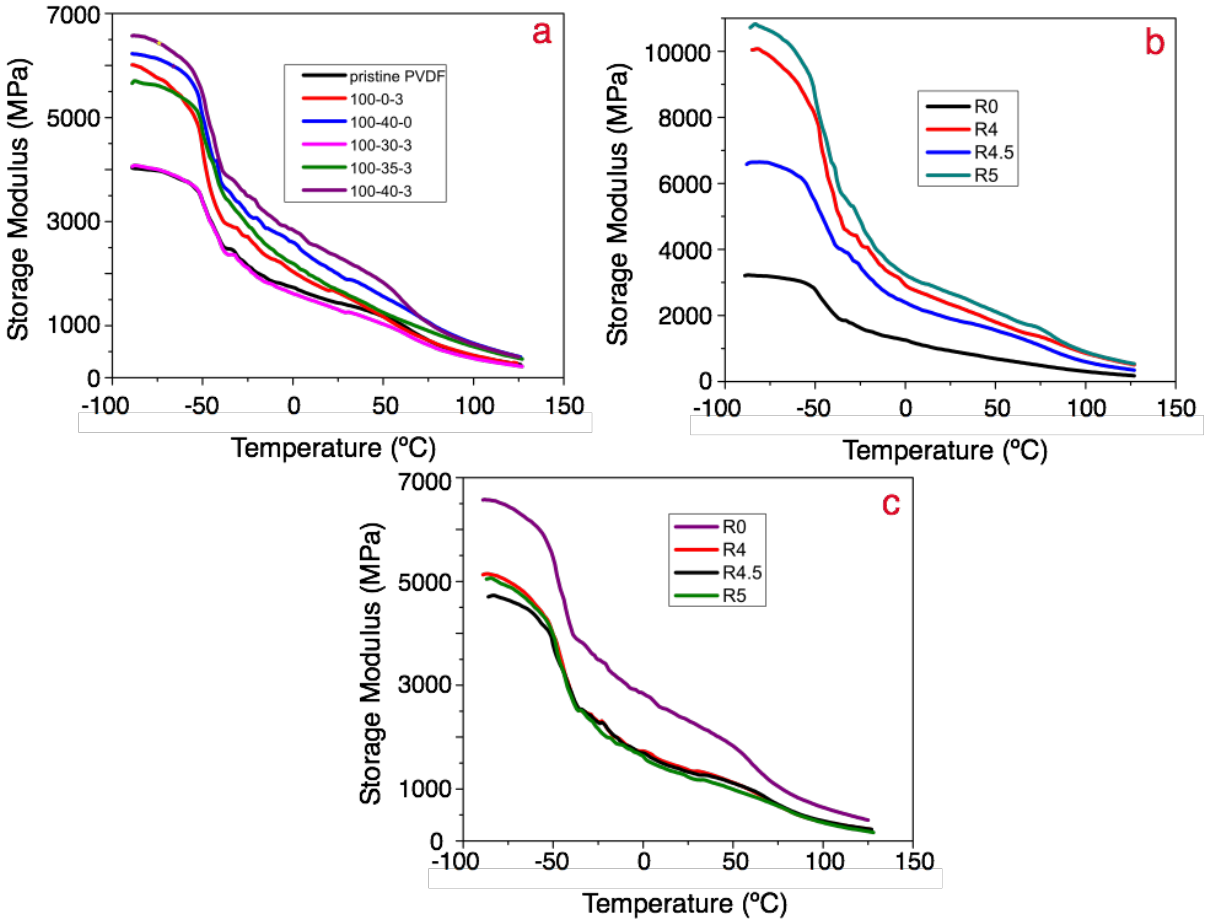

Figure 5.2: Temperature dependence of tensile storage modulus of (a) unstretched extruded samples, and (b, c) 100-0-3 and 100-40-3 samples, respectively stretched at various draw ratios, R.

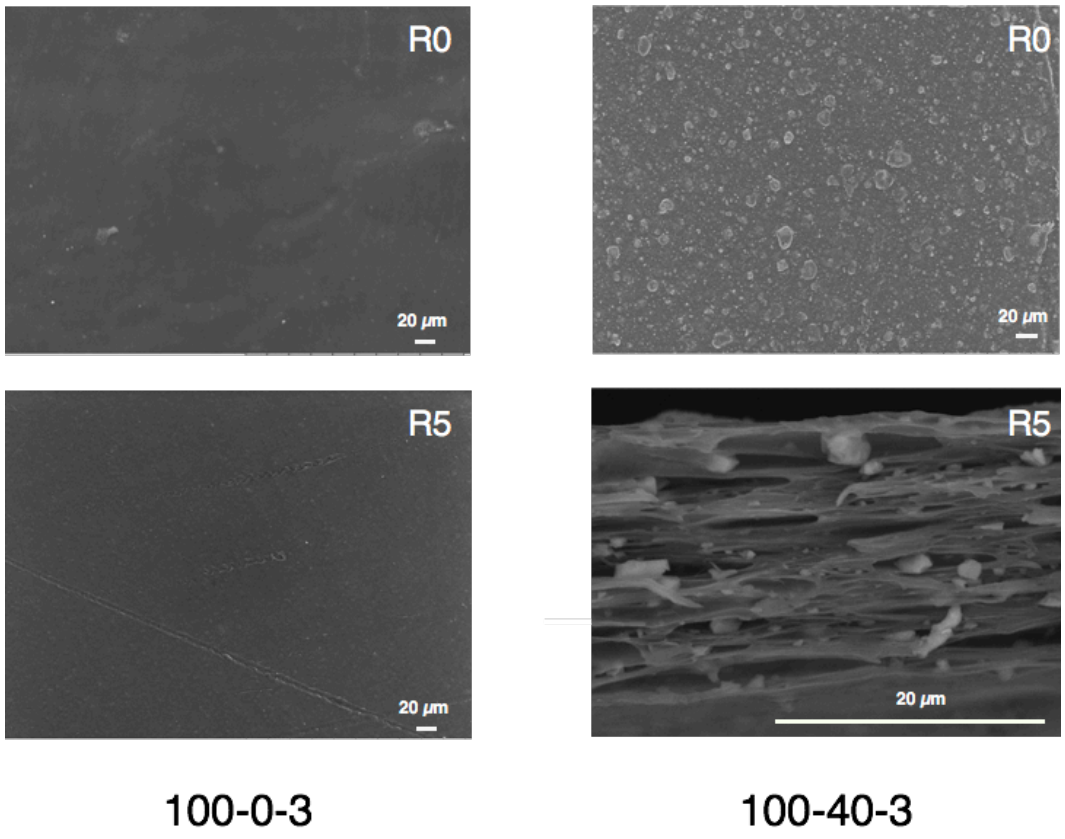

Figure 5.3: SEM images of (left) 100-0-3 nanocomposite and (right) 100-40-3 composite.

5.4.3 Dielectric Properties

The frequency dependent dielectric constant (ε_r) at room temperature of neat PVDF and its nanocomposites in the frequency range of 100 Hz to 1 MHz is shown in Figure 5.4(a). In the whole frequency range, all PVDF micro and nanocomposites exhibited higher ε_r than pristine PVDF. For example, 100-40-0 showed an ε_r of 11.3 compared to 7.9 for pristine PVDF at 1 kHz. While both nanoclay and $CaCO_3$ fillers independently enhanced the dielectric constant of PVDF to some extent, synergistic increment was observed in the case of the hybrid filler (nanoclay + $CaCO_3$). With increasing fraction of $CaCO_3$ in the hybrid nanocomposite, the dielectric constant increased gradually. The highest dielectric constant of 14.8 at 1 kHz was achieved for 100-40-3 hybrid nanocomposite film, which is two times larger than that obtained for neat PVDF and 47% higher than that of the PVDF/clay nanocomposite (100-0-3).

In the case of PVDF nanocomposites, the PVDF matrix is the dominant phase which determines the dielectric characteristics. The dielectric constant of PVDF is ruled by the number of orientable dipoles present in the matrix and their ability to orient under the applied electric field [6, 133]. At lower frequencies, the free dipoles in the PVDF chains can orient themselves, which results in higher dielectric constant. However, as the field frequency increases, the larger dipolar groups cannot orient themselves at the same pace with the frequency of the alternating field. Therefore, the contributions of these dipolar groups to the dielectric constant keep diminishing, which ultimately results in a gradual decrease of PVDF dielectric constant with increasing field frequency [6, 133].

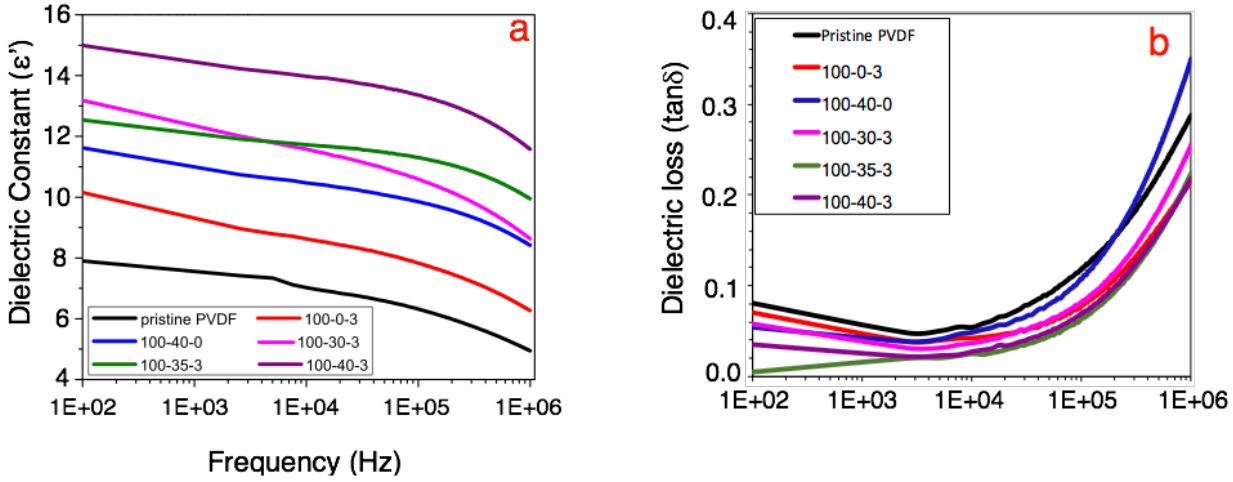

Figure 5.4: Dielectric constant (ε') (a) and dielectric loss (tanδ) (b) of unstretched pristine PVDF and its composites.

Lately, it has been believed that the dielectric constant of a nanocomposite material is not only dependent on the dipolar orientation but also on the degree of polarization including, electronic, ionic, interfacial and orientation polarization. All these polarizations are believed to have a positive effect on the dielectric properties at low frequency level. Also, the dielectric properties of nanocomposites depend on the physical properties of polymer matrix as well as the filler, filler size and concentration, nanocomposite preparation method and the interfacial interaction between the polymer and filler. It has already been established that PVDF has a very high dipole moment due to the presence of electronegative fluorine atoms in its molecular structure. In response to an alternating electric field, PVDF is also susceptible to interfacial polarization

(known as Maxwell Wagner Sillars (MWS) polarization) commonly observed at the interface of α and β phases and/or at the filler-PVDF interface [134, 135]. Due to the difference in the ε_r of the inorganic fillers and PVDF, a large amount of charge carriers (in this case electrons) accumulated at the interface. Since the polar group on the modified nanoclay surface and the amorphous-crystalline interface could act as charge scatterers effectively trapping the charges, the overall mobility of charges reduced and eventually resulted in decreased electrical conductivity and enhanced ε_r [134, 136]. As reported by Roy, et al. [137], the advantage of adding micro-fillers is that they do not conform to the polymer chain length and enhance the occurrence of MWS type interfacial polarization arising from the difference of dielectric constant between the polymer and filler. Therefore, the enhanced ε_r of hybrid nanocomposites (100-30-3, 100-35-3 and 100-40-3) can also be attributed to this phenomenon.

Table 5.3: Percentage of β phase, crystallinity and crystallite size of pristine PVDF and its nanocomposites obtained in the previous study [130]. Data are presented for both stretched and unstretched composites.

Draw ratio	**R0**				**R4**		**R4.5**		**R5**	
Sample	**F(β)**	**χ_C (%)**	**L_α (nm)**	**L_β (nm)**	**F(β)**	**χ_C (%)**	**F(β)**	**χ_C (%)**	**F(β)**	**χ_C (%)**
Neat PVDF	0	42.5	31.7	0	59±1.5	52	55±2	52	62±2	68
100-0-3	50±1	43	23.2	16.1	70±2	49	72±1.5	50	70±2	53
100-40-0	58±1	42	21.8	15.2	63±1	44	66±1.8	48	76±1	51
100-30-3	58±2	56	19.0	15.3	67±1.5	--	73±0.5	--	73±1	--
100-35-3	80±3	53	11.5	6.2	100	--	100	--	93±2	--
100-40-3	80±2	39	10.1	4.1	100	49	100	50	100	55

Also, as shown in Table 5.3, the crystallite size decreased with increasing $CaCO_3$ fraction in the hybrid nanocomposite since the inorganic filler particles acted as nucleation sites [130]. Under an alternating field, it was easier for the smaller crystallites to be switched or aligned, which resulted in improved ε_r [138]. Moreover, the dielectric permittivity of PVDF and its nanocomposite was strongly affected by the amount of β phase or dipoles it contains [139]. Since samples

containing the hybrid filler (i.e., 100-40-3 and 100-35-3) had the highest amount of β phase (Table 5.3), they exhibited the higher ε_r.

The fillers, especially the hybrid $CaCO_3$-nanoclay fillers in PVDF, not only increased the dielectric constant of the nanocomposite but also suppressed the dielectric loss (tanδ) of the system (Figure 5.4(b)). Generally, the addition of an inorganic filler in the PVDF matrix increases the tanδ value of the nanocomposite since the filler could act as a source of charge carrier in the matrix [6, 7, 47]. Hence, the lower tanδ values for nanocomposites obtained in this study can be attributed to the occurrence of limited electrical charge movement through PVDF chains and smaller interfaces due to smaller crystallites [133]. Similar result of enhanced ε_r and decreased tanδ was reported by Singha et al. [133] for epoxy/ZnO nanocomposites.

The frequency dependence of the dielectric constant (ε_r) and dielectric loss (tanδ) of 100-0-3 and 100-40-3 nanocomposites stretched at various draw ratios (R) is presented in Figure 5.5(a-d). While the drawing process yielded enhanced ε_r in 100-0-3 nanocomposite, it reduced the ε_r of the stretched hybrid nanocomposite (100-40-3).

In the case of 100-0-3 nanocomposite, enhanced ε_r due to stretching can be attributed to the enhanced dipole density, improved crystallinity, increased β phase content and chain alignment (data shown in Table 5.3). According to Tang, et al. [127], stretching not only transforms the crystal structure from α to β in PVDF but also modifies the interface between the crystalline and amorphous phases by molecular orientation and this conversion from normal crystalline phase to electroactive phase eventually enhances the ferroelectric properties as well as the dielectric response and suppresses the loss tanδ. On the other hand, in the case of hybrid nanocomposite (100-40-3), although the crystallinity and F(β) increased with R, the probability of electric conduction due to the presence of higher percentage of voids (Figure 5.3) could explain the decrease of ε_r and the simultaneous increase of tanδ. Similar effect of voids on decreasing ε_r of PZT-P(VDF-CTFE) nanocomposite was reported by Choi et al. [7].

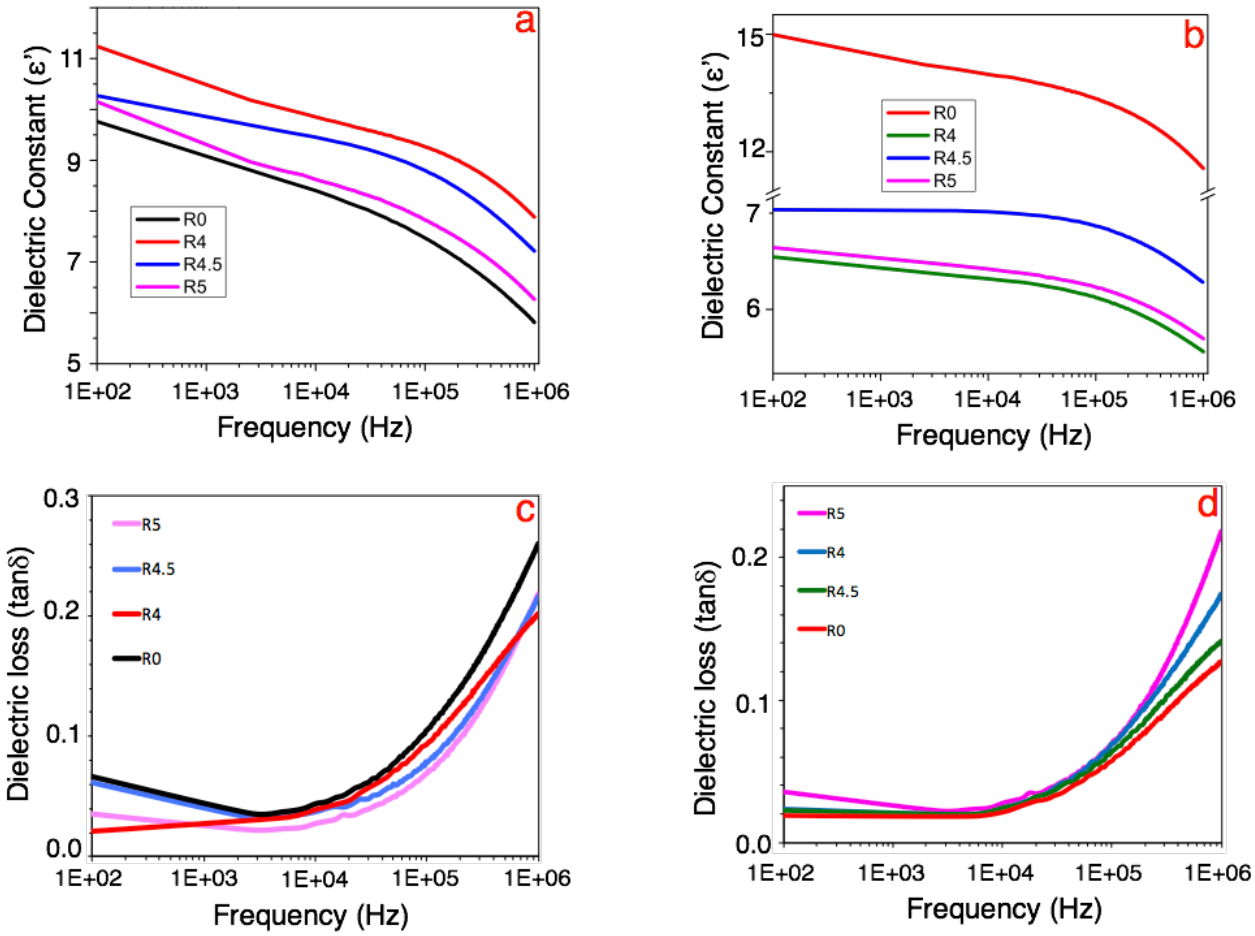

Figure 5.5: Dielectric constant (ε') (a, b) and dielectric loss (tanδ) (c,d) of 100-0-3 and 100-40-3 composites, respectively stretched at different draw ratios.

5.4.4 DC Volume Resistivity

The DC volume resistivity (ρ_v) of PVDF and its micro and nanocomposites were measured to investigate and compare the effect of the hybrid filler (nanoclay + $CaCO_3$) loading on the electrical properties of PVDF. The variations of ρ_v with respect to filler concentration in PVDF nanocomposites are shown in Figure 5.6(a) and relevant data has been listed in Table 5.4. For the same processing conditions, the addition of fillers increased ρ_v of PVDF composites. For example, the volume resistivity of neat PVDF increased from 46E+12 to 172E+12 ohm-cm when only 3 parts of nanoclay were added. More interestingly, almost seven times enhancement in ρ_v was

observed for hybrid filler induced PVDF nanocomposite (100-30-3) but displayed a downtrend with increasing $CaCO_3$ loading beyond 30 part (100-35-3 and 100-40-3).

It is known that the dc volume resistivity of filled nanocomposites is greatly influenced by the formation of interfacial layers around the nanofillers, as explained by Tsagaropoulos and Eisenberg [140] in dual nanolayer theory. According to this theory, two nanolayers form around the nanofiller. The closest one is considered to be tightly-bonded to the nanofillers where the polymer chains are immobile and the second polymer layer, slightly thicker than the first layer, is lightly bound to the fillers where the polymer chains or other additives are relatively mobile. Under an applied electric field, free charge carriers are generated from electrodes, fillers and impurities present in the loosely bonded polymer in the extended layer [9]. Therefore, this extended layer acts as a convenient medium to carry charges in the bulk of the nanocomposites towards the electrode with opposite polarity and controls the conductance in the insulating polymer matrix.

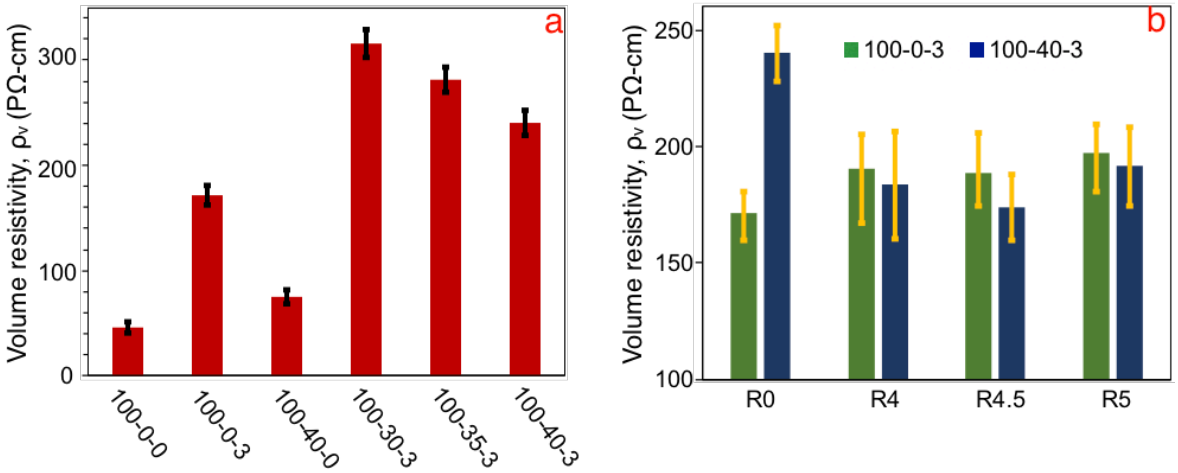

Figure 5.6: Volume resistivity of (a) unstretched extruded neat PVDF and its composites, and (b) stretched 100-0-3 and 100-40-3 composites.

Since the surface functionalization of nanoclay created strong bonds with PVDF chains, and restricted their mobility , or in other words, created a deeper trap to localize the free charges [141], an increased ρ_v was observed for 100-0-3 composite. On the other hand, the relatively lower increase in ρ_v of 100-40-0 micro-composite was attributed to the untreated surface of the micro $CaCO_3$ particles, which lacked in charge trapping capability.

The large resistivity increase for hybrid nanocomposites (100-30-3) could be attributed to the inert/resistive nature of the micro $CaCO_3$ particles. The electron conduction was hindered not only by the strong bonding between modified clay and PVDF chains but also by the presence of $CaCO_3$ filler in the loosely bound polymer layer acting as a barrier to the conduction path and increasing the distance between the nanoclay platelets. Therefore, the resistivity increased almost seven times.

Further addition of $CaCO_3$ lowered the ρ_v of the hybrid 100-35-3 and 100-40-3 nanocomposites, which can be explained by the solid nature of $CaCO_3$ micro-particles, as mentioned in ref. [142]. Increasing the micro $CaCO_3$ filler content in the nanocomposite was expected to increase the distance between the clay platelets and weaken the chance of creating the conduction path. However, this filler existed as solid micro-particles in the PVDF matrix during the melt mixing for the preparation of the nanocomposite, therefore, the nanoclay only dispersed and bonded with the PVDF matrix. Hence, with increasing $CaCO_3$ concentration, a fraction of the PVDF was used in creating an interface with the $CaCO_3$, thus, the amount of PVDF available for nanoclay to bond decreased gradually. Because of the balance between these two factors, only a slight decrease in resistivity was observed for 100-35-3 and 100-40-3 nanocomposites. Liao, et al. [143] showed that, for LDPE/Mt nanocomposites, ρ_v decreased with increasing Mt concentration. They attributed this phenomenon to the reduced charge mobility due to the large interfacial area between the Mt fillers and LDPE matrix.

The above results can also be explained by the crystallinity of the nanocomposites already measured in the previous work [130]. According to Yang, et al. [144], the conduction of electrons took place mostly through the PVDF amorphous phase rather than the crystalline phase. The crystallinity measured by DSC for 100-0-0, 100-0-3 and 100-40-0 nanocomposites was approximately similar and close to 43% (Table 5.3). Their corresponding resistivity measured was also similar (Table 5.4), not to mention crystallinity is one of the many parameters affecting the conductance of semi-crystalline polymers. The crystallinity for 100-30-3 nanocomposite was the highest and so was the volume resistivity. Results for 100-35-3 and 100-40-3 nanocomposites showed that with increasing $CaCO_3$ filler content, both crystallinity and ρ_v decrease, which again proved their mutual dependence [136].

Table 5.4: Piezoelectric coefficient d_{33} and dc volume resistivity ρ_v of both stretched and unstretched pristine PVDF and its composites.

Draw ratio	**R0**		**R4**		**R4.5**		**R5**	
Sample	**ρ_v (PΩ-cm)**	**d_{33} (pC/N)**	**ρ_v (PΩ-cm)**	**d_{33} (pC/N)**	**ρ_v (PΩ-cm)**	**d_{33} (pC/N)**	**ρ_v (PΩ-cm)**	**d_{33} (pC/N)**
Neat PVDF	46.2±5	0		6.2±0.4		6.4±0.4		7.6±0.2
100-0-3	171.7±9	2.3±0.3	190.3±15	12.8±0.5	188.6±17	11.9±0.7	197.4±12	12.3±0.7
100-40-0	74.9±7	0	--	4.5±0.2	--	4.9±0.2	--	8.5±0.4
100-30-3	316.1±13	3.6±0.5	--	20.6±0.7	--	19±1.1	--	25.2±0.8
100-35-3	281.5±12	7.2±1.0	--	26.2±1.3	--	26.1±3.2	--	29.1±3.0
100-40-3	240.3±12	7.4±0.9	183.5±23	22.3±2.5	174.0±14	24.8±2.8	191.6±17	30.6±3.3

The effect of drawing (i.e. draw ratio, R) on the ρ_v of 100-40-3 and 100-0-3 nanocomposites has been shown in Figure 5.6. While the ρ_v of 100-0-3 increased with increasing the draw ratio, R, it decreased gradually for hybrid 100-40-3 nanocomposite where stretching not only increased the distance between the clay particles, but also generated micron-size voids inside the sample (SEM images in Figure 5.3) due to PVDF/$CaCO_3$ interfacial delamination. These voids led to increased dc electrical conduction leading to a decreased volume resistivity of the stretched hybrid nanocomposites [47].

5.4.5 Piezoelectric Properties

The piezoelectric coefficient, d_{33} for poled PVDF and its micro and nanocomposites are shown in Figure 5.7a and data listed in Table 5.4. While pristine PVDF and 100-40-0 nanocomposite did not exhibit any piezoelectricity, 100-0-3 and all other hybrid nanocomposites showed a slight piezoelectric behavior. A maximum d_{33} value of 7.4 pC/N was obtained for the 100-40-3 nanocomposite film.

The polar β-phase crystallinity of the extruded PVDF-based nanocomposites played a crucial role in obtaining a piezoelectric behavior after poling at appropriate conditions. It was quite reasonable to expect higher piezoelectricity for samples with higher amount of β phase. However, the orientation of β-PVDF dipoles had a much pronounced effect on d_{33} than the amount of β phase inside the PVDF-based nanocomposite [47, 145]. Additionally, according to Mohammadi et al. [145], although mechanical stretching could preferably orient the crystallites, it was not capable of orienting the molecular dipoles, and for that reason the piezoelectricity measured directly after the uniaxial/biaxial stretching was quite low. This indicates the necessity of electrical poling even after mechanical stretching. Poling in appropriate conditions resulted in enhanced dipole orientation and, hence, increased piezoelectricity was observed in the previously stretched samples due to the additional polarization induced by poling. Therefore, although the β-PVDF content in the unstretched neat PVDF and its nanocomposites was more than 50% (even 80% in case of 100-35-3 and 100-40-3 hybrid nanocomposite samples), piezoelectricity is still low due to the random orientation of β-PVDF dipoles in unstretched samples. Since the electric field for poling had been applied on the direction perpendicular to the film surface (along the thickness direction), the dipoles in the crystallites intended to rotate towards the direction of the electric field. The randomly oriented dipoles in the unstretched samples were less susceptible to this preferable rotation, which narrows down the crystallite distribution [47]. In the case of filled nanocomposites, not only the orientation of the β-dipoles could affect the piezoelectricity, but also the filler-polymer and/or crystalline-amorphous interface could also largely contribute. As mentioned in the previous section, smaller crystallites in the case of PVDF hybrid nanocomposites could facilitate the interface charge storage conceding an increased efficiency of dipolar polarization and hence, better piezoelectric response. Not only that, according to Baur, et al. [146], the presence of fillers (in this case both nanoclay and $CaCO_3$) in the PVDF matrix might enhance the local electric field and increase domain mobility of generally localized stress points, therefore, contribute improving polarization to some extent.

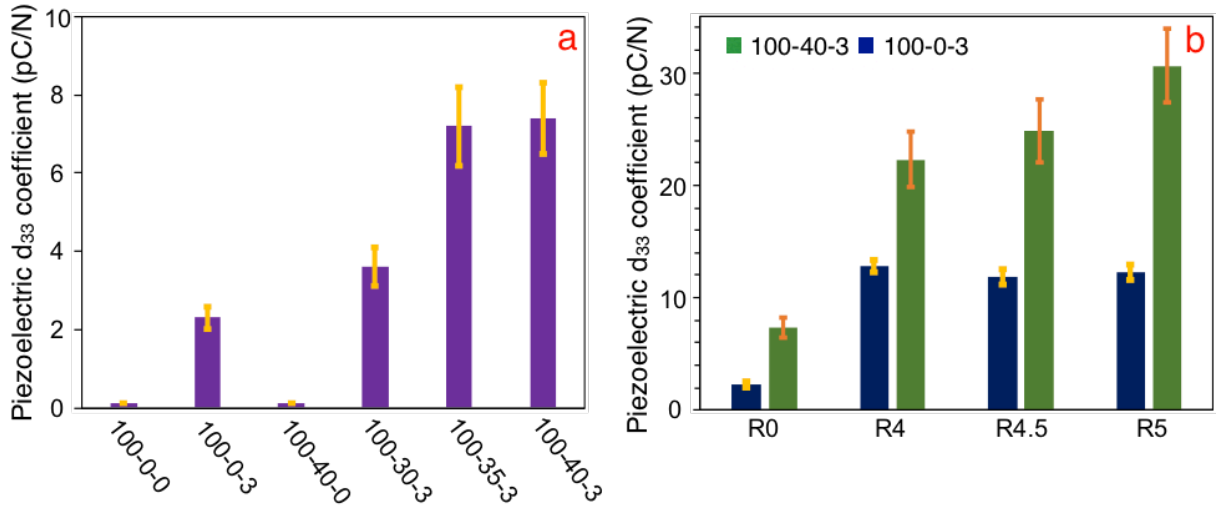

Figure 5.7: d_{33} values of (a) unstretched nanocomposites including neat PVDF and (b) stretched 100-0-3 and 100-40-3 composites.

In the case of stretched samples (Figure 5.7b), stretching not only induced almost 100% of the β-PVDF phase (especially in the case of hybrid nanocomposites), but also oriented the crystallites in the drawing direction. Therefore, under the given electric field during poling perpendicular to the surface of the stretched film, the preliminarily oriented crystallites continued to be more oriented in the poling direction and this orientation was stronger than in the unstretched samples, leading to enhanced d_{33} coefficient. In addition, since the stretching of hybrid PVDF-based nanocomposites resulted in higher percentage and larger size voids, the electric field applied to orient the dipoles could also be strong enough to breakdown the gas in the voids (such as creating electrets) to some extent and create more dipoles, which might also contribute to the improved piezoelectricity.

5.5 Conclusion

The effect of micro-$CaCO_3$ and uniaxial stretching on the mechanical, dielectric, electrical and piezoelectric properties of PVDF/clay based hybrid nanocomposites prepared through melt-blending extrusion was investigated. Due to the enhanced β phase crystallinity, reduced crystallite size and oriented structure, hybrid nanocomposites yielded the highest piezoelectric response (7.4 pC/N for 100-40-3) among the extruded composites. The best d_{33} value (30.6 pC/N) was obtained when they were stretched to a draw ratio of 5 presumably due to the increased crystallinity along

with the occurrence of almost 100% β-PVDF and dipole orientation in the latter case. Similarly, the hybrid nanocomposite exhibited the most enhanced dielectric properties compared to other samples. Stretching surely has a positive effect in enhancing the ferroelectric properties of nanocomposite samples. While the dielectric properties enhanced for 100-0-3 after stretching at various draw ratio, it reduced significantly for 100-40-3 probably due to the presence of higher percentage of voids which presumably caused electrical conduction under the applied field. However, the piezoelectric coefficient d_{33} of stretched samples improved significantly for all cases, especially for the oriented hybrid composites. It is expected that this study will be a guideline for developing commercially viable, low cost piezoelectric materials.

5.6 Acknowledgement

The authors acknowledge the technical support from Mr. Richard Silverwood and Ms. Claire Cerclé and the financial support from FRQNT (Fond de Recherche du Quebec en Nature et Technologie) and NSERC (Natural Sciences and Engineering Research Council of Canada).

CHAPTER 6 ARTICLE 3: EFFECT OF THE INFLATION STRATEGY ON THE PIEZOELECTRIC RESPONSE OF CELLULAR PVDF FERROELECTRET

Nusrat Jahan[1,2], Frej Mighri,[1,3], Denis Rodrigue[1,3], Abdellah Ajji[1,2*]

[1]CREPEC, Research center for high performance polymer and composite systems

[2]Department of Chemical Engineering, Polytechnique Montréal,
C.P. 6079, Montreal, QC, H3C 3A7, Canada

[3]Department of Chemical Engineering
Université Laval, Quebec, QC, G1V 0A6, Canada

Submitted in : Smart Materials and Structures

6.1 Abstract

Cellular poly(vinylidene fluoride) (PVDF)-Montmorillonite (Mt-clay)-calcium carbonate ($CaCO_3$) based piezoelectret films were produced using uniaxial stretching and various gas diffusion expansion (GDE) treatments followed by corona charging. The cross-section micrographs revealed that a cellular structure was developed at the interface between the solid $CaCO_3$ particles and the polymer matrix. Sample characterization showed that the piezoelectric coefficient (d_{33}) was a function of the external gas pressure and treatment temperature, as well as the way they were applied. The results also showed that the maximum d_{33} was obtained when the inflation pressure was increased stepwise from 3 MPa to 5 MPa at a constant treatment temperature of 130 °C for a certain period of time. Finally, the overall electromechanical performance of the cellular PVDF piezoelectrets is discussed in terms of the GDE procedure and the developed microstructures.

6.2 Introduction

Piezoelectrets are polarized cellular polymers exhibiting a piezoelectric response. They are comprised of macroscopic dipoles which are space charge electrets of opposite charges on the internal surface of the voids along the applied field direction. Cellular polypropylene (PP) is one of the most widely investigated piezoelectret since it exhibits piezoelectric coefficient (d_{33}) about one order of magnitude higher compared to commercial or laboratory-synthesized piezoelectric materials [16, 19, 76], as well as intrinsic piezoelectric PVDF and its copolymers [46, 95, 130]. However, one drawback of PP piezoelectrets is their poor thermal stability limiting their working temperature below 60 °C [80, 85-87]. Therefore, developing thermally stable piezoelectrets has drawn a significant attention in recent years [147, 148].

Among the thermally stable piezoelectrets, perfluoropolymers, such as polytetrafluoroethylene (PTFE) and fluoroethylenepropylene (FEP) ferroelecterts, are known to have superior charge stability at both polarities [28]. However, these materials are expensive, difficult to process into desired shapes and to form via conventional melt processing techniques because of their high processing temperature, degradation tendency during manufacturing (with the possibility of releasing hydrofluoric acid, HF), and poor stretching properties. Hence, further studies are required to optimize the processing conditions of these fluoropolymers. However,

PVDF presents some obvious advantages over the other fluoropolymers such as ease of processability, relatively lower manufacturing temperature and less degradation [149].

In general, a cellular structure can be produced by stretching a polymer-filler compounded film [23, 150] or by using a supercritical gas as a physical foaming agent in a foaming process, [25, 72] which is then followed by adjusting the voids geometry under high ambient gas pressure. Typically, film thickness (or density) following gas inflation, film cellular structure (the number and the shape of the resulting voids) and the nature of the gas inside the voids influence the charging process, and thus the resulting piezoelectric response. Since the number of voids and their associated dipole concentration become fixed after film preparation, the voids shape and therefore the dipoles sizes are the only parameters to be modified. This modification can be done using suitable inflation treatment at an elevated pressure. Various inflation techniques have been suggested to improve the piezoelectric response of cellular PP, FEP, PTFE, PETP, and cyclo-olefins [18, 19, 70, 76, 78, 81, 151]. However, any comprehensive study in this regard is yet to be reported.

Generally, solid filler particles in a polymer matrix act as mechanical stress concentrators during stretching and can create voids around themselves. To facilitate the process, typical fillers of poor compatibility with the polymer matrix are chosen. In this study, PVDF is chosen as the host polymer because of its stable chemical structure, ease of processing, excellent charge retaining capacity and superior thermal stability [152, 153]. The filler is a hybrid mixture of micro-$CaCO_3$ and Mt-clay which are readily available and cost-effective. The prism/rhombohedral shape of $CaCO_3$ generates enough stress-concentration to create lens-shaped cavities, while the layered montmorillonite (Mt-clay) improves the β phase content of PVDF and increases the composite system stretchability. In previous studies [95, 130], the mechanical and ferroelectric properties of PVDF/hybrid filler (micro-$CaCO_3$ + nanoclay (Mt-clay)) was reported with respect to filler concentration and drawing parameters. The aim of the current study is to investigate the piezoelectric properties of various cellular PVDF ferroelectrets prepared from the same PVDF/hybrid filler composite with respect to various inflation procedures. Inflation conditions, such as pressure, temperature, and time are the key parameters in the study and are applied either in a single or in multiple steps.

The transport coefficient of a gas depends on various parameters associated with the specific polymer-gas system. Typically this includes the polymer crystallinity, the polarity of both polymer and gas, the polymer thermal history, the gas molecular properties, and the gas diffusion expansion (GDE) conditions such as the pressure, temperature and treatment time. With an optimized control of these parameters, one can prepare stable piezoelectrets with low density and reduced elastic modulus. In this study, the PVDF foam samples and inflation gas were kept constant for all the inflation techniques, while only the GDE parameters were changed.

The inflation procedures were evaluated on the basis of sample thickness changes due to gas diffusion and changes in void geometry (void height) which were then correlated with the piezoelectric coefficient. To the best of our knowledge, there is no similar report in the literature on cellular PVDF and this study will shed some light on their inflation as well as their piezoelectric properties.

6.3 Experimental procedure

6.3.1 Materials

PVDF (Kynar 720) ($M_w = 2.65\times10^5$ g mol^{-1}, T_m = 165 to 172 °C, density = 1.78 g/cm^3, PDI = 2.3, MFR = 5-29 g/10 min at 450 °C under 3.8 kg load) is an extrusion grade polymer from Arkema (USA). Nanomer I44P (dimethyl hydrogenated tallow quaternary ammonium ion exchanged montmorillonite ; density 1.4 g/cm^3) was purchased from Nanomer Inc. and used as a filler to prepare the PVDF composites. The $CaCO_3$ micro-filler (particle size: 3-13 μm, density: 2.7 g/cm^3) was supplied by Univar (Canada). It is an industrial grade filler and was used without further purification. Nitrogen (N_2) (purity ~ 99.99%, supplied by Air Liquide, Canada) was chosen as the inflation gas because it is inexpensive, readily available and “relatively-neutral” with respect to PVDF [77].

6.3.2 Film Preparation

Neat PVDF, $CaCO_3$ and nanoclay were vacuum dried overnight at 70 °C before compounding. The polymer (PVDF) was fed to the extruder main hopper using a volumetric feeder and the fillers ($CaCO_3$ and nanoclay) were introduced using a high precision powder feeder. The materials were fed at a constant rate to maintain the specific composition. PVDF films with 40

parts (~ 30 wt.%) of $CaCO_3$ and 3 parts (~ 2.7 wt.%) of nanoclay were prepared using a tightly intermeshing co-rotating twin-screw extruder equipped with a typical compounding screw including two kneading blocks zones and fitted with a strand die and a pelletizer. The pellets were then re-extruded with the same extruder equipped with a slit die (20 cm × 1.8 mm) and a calendaring three-roll system for film forming. The extrudates were pulled by the calendar to prepare films with a 80-100 μm thickness range. Since the extrudate velocity at the die exit was constant, the draw ratio or the film thickness was controlled by the pulling speed of the calendar's rolls. Besides natural air cooling, a controllable air knife was installed at the die exit to supply sufficient air to the film surface. A constant extruder speed of 100 rpm with a constant temperature profile (195 °C) was used in each case.

6.3.3 Uniaxial Stretching

The PVDF/$CaCO_3$/montmorillonite composite films were uniaxially stretched in the direction perpendicular to the extrusion direction using an Instron machine (ElectroPulse^{TM} E3000) equipped with an environmental (heating) chamber using a pneumatic grip of 1 kN. The samples were cut into a rectangular shape (width of 4.5 cm and length of 1 cm = gauge length). The temperature of the environmental chamber was set to 90 °C, the stretching speed was fixed at 2.5 mm/min, and the stretching ratio (final length/initial length) was set to 5. To maintain the thermal equilibrium between the samples surface and interior, an equilibrium time of 8 min was applied before stretching. Finally, the stretched samples were cooled down to room temperature in natural air. The final film thickness ranged between 35 and 42 μm.

6.3.4 Gas Diffusion Expansion

To obtain a lens-like cellular structure to make the film more compressible and thus highly piezoelectric [17, 25, 72, 78], several inflation treatments were performed combining the GDE parameters (pressure, temperature and time). The pressure treatment was performed in a closed vessel pressurized with pure N_2. The temperature treatment was carried out either in series or in parallel with the pressure treatment using an oil bath attached to the closed pressure vessel heating jacket. To achieve better N_2 penetration (combining both permeation and diffusion) into the films, the pressure was varied from 3 MPa to 5 MPa and the temperature was chosen from room

temperature to 140 °C, which are above the critical pressure and temperature of nitrogen (P_c = 3.4 MPa and T_c = 126.4 K) [154]. Since the PVDF melting temperature (T_m) is around 163 °C and its glass transition temperature (T_g) is around -35 °C, the selected temperature was high enough to ensure chain mobility and consequently to facilitate N_2 intrusion.

In the first set of experiments (GDE-I and GDE-II), pressure and temperature treatments were performed in series (Figure 6.1(I, II)). The samples were inflated at a constant pressure of 5 MPa and room temperature for 3 h followed by a temperature treatment at 115 °C for 2 h or 4 h keeping the pressure constant.

In the second set of experiments (GDE-III), the samples were treated at constant pressure (5 MPa) while the temperature was increased from 50 to 115 °C in four steps with a 2 h residence time for each step, except for the last one which lasted 4 h (Figure 6.1(III)).

In the third set of experiments (GDE-IV, GDE-V, GDE-VI), the inflation pressure was increased stepwise, starting from 3 MPa up to 5 MPa with a dwelling time of 2 h for the first two pressure levels and 4 h for the last one at 5 MPa. Each GDE experiment was performed at a constant temperature of 115 °C (GDE-IV), 130 °C (GDE-V) and 140 °C (Figure 6.1(IV, V, VI)).

In the fourth set of experiments (GDE-VII, GDE-VIII), the treatment time and pressure were set to 24 h and 5 MPa, respectively. Only the inflation temperature was different: one at room temperature (GDE-VII) and the other at 50 °C (GDE-VIII), as shown in Figure 6.1(VII, VIII).

At the end of each GDE procedure, the imposed pressure was rapidly reduced to atmospheric and the samples were cooled down to room temperature. In general, the pressure treatment was aimed at saturating the voids with gas at higher pressure, while the temperature treatment was intended to increase the gas transport inside the voids by softening the polymer matrix as well as to stabilize the newly formed cellular structure.

A thickness tester (ProGage, Thwing-Albert Instrument Co., USA) was used to measure any change in sample thickness after each GDE procedure.

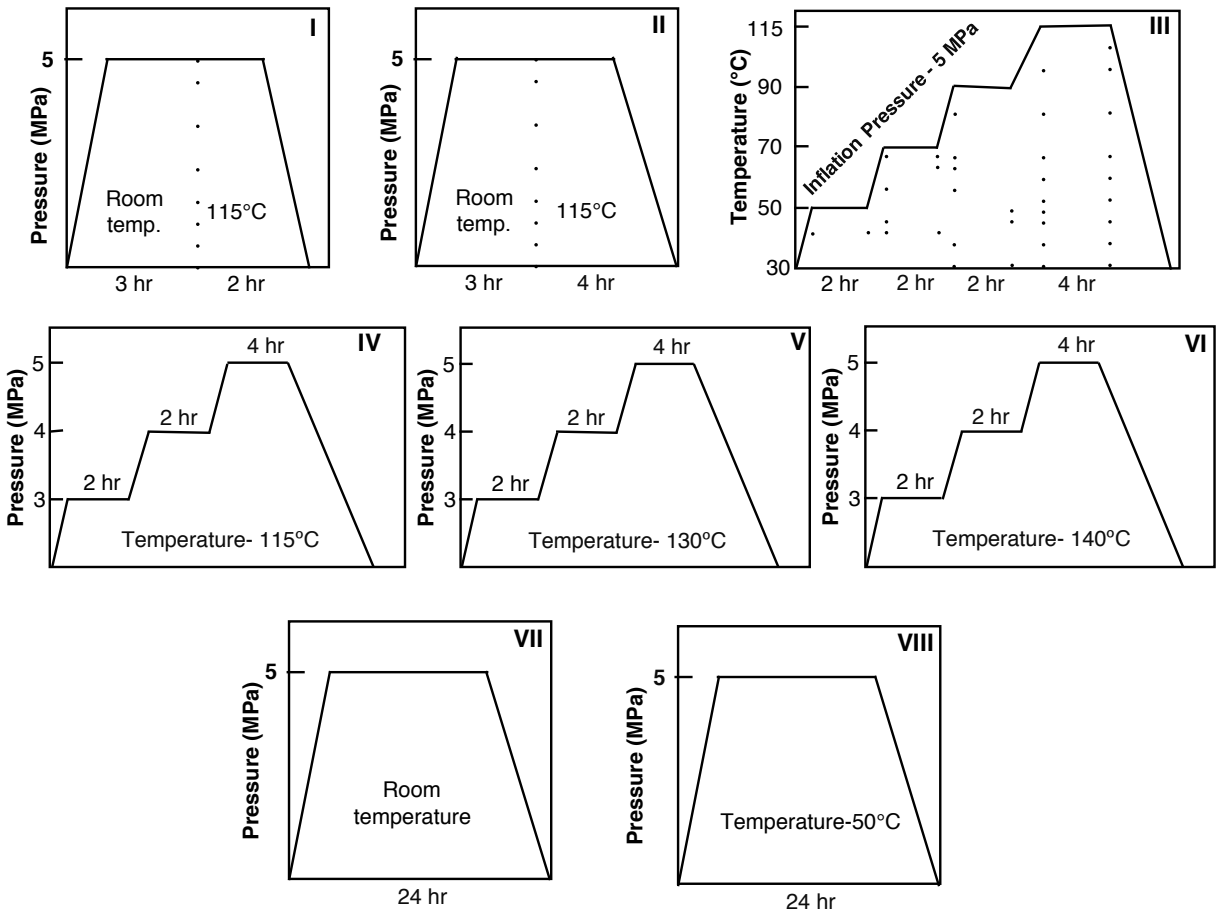

Figure 6.1: Schematic diagrams of the different inflation procedures for the gas diffusion expansion (GDE).

6.3.5 Scanning Electron Microscopy

The morphology of the films cross-section before and after the GDE treatments was studied using a table-top scanning electron microscope (TM3030 plus, Toshiba) without any metallic coating. The samples were prepared by cryogenic fracture in liquid nitrogen to have a neat fracture surface and the fracture was done in the stretching direction. For a complete study of the cellular structure, including the void shape, height, size, etc., a software package "ImageJ" was used to analyze the SEM images. Void boundaries were detected automatically by fitting an ellipse to obtain the required data, as shown in Figure 6.2 (a,b).

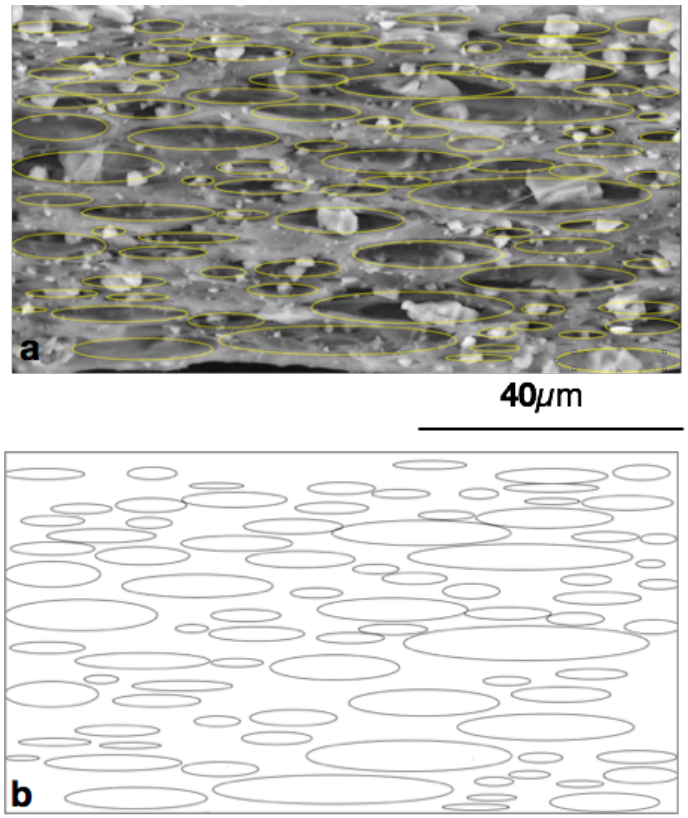

Figure 6.2: Ellipses fitting of the voids using the software ImageJ.

6.3.6 Corona Discharge

Building-up of oriented dipoles is required for a material to be piezoelectric; i.e. to form ferroelectrets. In order to create these oriented macro-dipoles inside the voids, the inflated films were electrically charged during 10 min in a tip-to-plane corona setup with a needle voltage of +27 kV. Charging was performed at room temperature in a closed chamber filled with N_2 at 200 kPa. The high voltage needle tip was set 4 cm above the sample surface. Finally, the samples were metallized with a conductive silver (Sigma-Aldrich, Canada) coating on both surfaces for electromechanical measurement.

6.3.7 Quasi-static Piezoelectric Coefficient (d_{33})

A quasi-static setup was used to measure the piezoelectric coefficient: a force F was applied on the sample by placing a mass m and by removing it after few seconds [80]. The d_{33} value was then calculated as :

$$d_{33} = Q / F \quad (6\text{-}1)$$

where Q denotes the accumulated charge on the electrodes due to the applied force (F=m g). A parallel capacitor of 100 nF was connected to the grounded sample in parallel. Compared to the parallel capacitor, the capacitance of the sample is very small so that the accumulated charges on the sample electrode are entirely transferred to the parallel capacitor [148]. A static force of 500 g was initially applied on the sample for 8-10 min and after 10 s of load removal, the accumulated charge was measured using a NI-9239 data acquisition system attached to a USB carrier NI-9162 (National Instruments, USA) connected to the capacitor in parallel and recorded using a LabVIEW interface. For each sample, the procedure was repeated 3-5 times and the average value is reported.

6.4 Results and Discussion

To investigate the effect of GDE parameters on void geometry and on the final piezoelectric response of cellular PVDF samples, multiple inflation experiments were performed as shown in Figure 6.1. These tests indicate that a pressure higher than 3 MPa is required to initiate the inflation of the stretched PVDF film. This pressure limit can be coupled with temperatures higher than 100 °C to obtain the desired inflation level.

Following the inflation treatment, the samples were stored and their thickness was recorded over the next two days at random intervals. For each GDE procedures of Figure 6.1, the respective increase in sample thickness (from the original value) due to the rise in void height over the two days' period is shown in Figure 6.3. The final cross-sectional micrographs for each cellular PVDF sample are shown in Figure 6.4 (also see Figure S6-1 in supporting information for larger area view of the micrographs), which shows the formation of lens-shaped voids inside the films, achieved by means of the stretching-inflation process. These developments in void-morphology via the GDE treatments can be compared with the untreated sample microstructure shown in Figure 6.4x. The voids are closed and inhomogeneous in all samples, including both treated and untreated, with different size and height distributions. The minor axes of the fitted ellipses (as shown in Figure 6.2) are taken as the void heights and their respective distributions are shown in Figure 6.5. These figures suggest that most of the voids have a height below 3.5 μm while voids with smaller heights (< 2 μm) dominate the samples morphology. The voids aspect ratio (AR = cell length divided by cell height) is calculated (form the ImageJ data) and the corresponding values are in the range of 4

to 9. However, no specific correlation was found between the average AR associated with their inflation techniques and their corresponding film piezoelectric response. Finally, Figure 6.6 presents the measured piezoelectric d_{33} coefficients for cellular PVDF piezoelectrets as a function of the various inflation treatments.

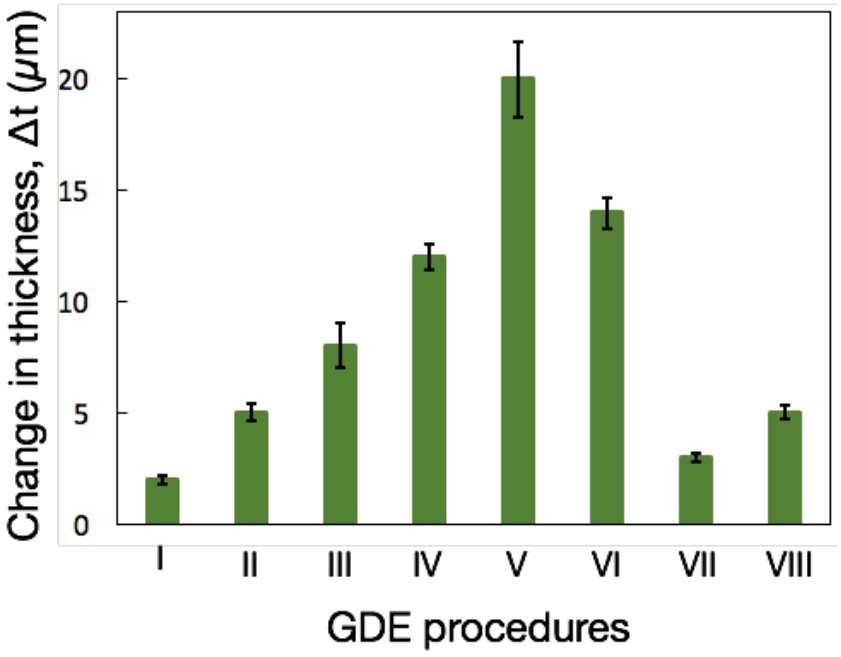

Figure 6.3: The change in sample thickness (Δt) of cellular PVDF electrets due to inflation using various GDE procedures. Each measurement is the average of at least 3 measurement points on the samples.

In GDE-I and GDE-II (Figure 6.1), the inflation chamber was pressurized externally under 5 MPa for 3 h at room temperature to induce gas-saturation of the voids through a pressure difference. Following the saturation, GDE-I and GDE-II samples were annealed at 115 °C for 2 and 4 h respectively, to soften the films for further gas intrusion as well as to stabilize the inflated structure. However, both treatments led to negligible changes in the respective sample thicknesses, as shown in Figure 6.3. This observation is contrary to previous studies on PP and cyclo-olefin polymers (COP) [17, 18, 79, 81, 155], where two to three-fold increase in sample thickness has been reported for similar inflation treatments. This can be attributed to the better penetration of

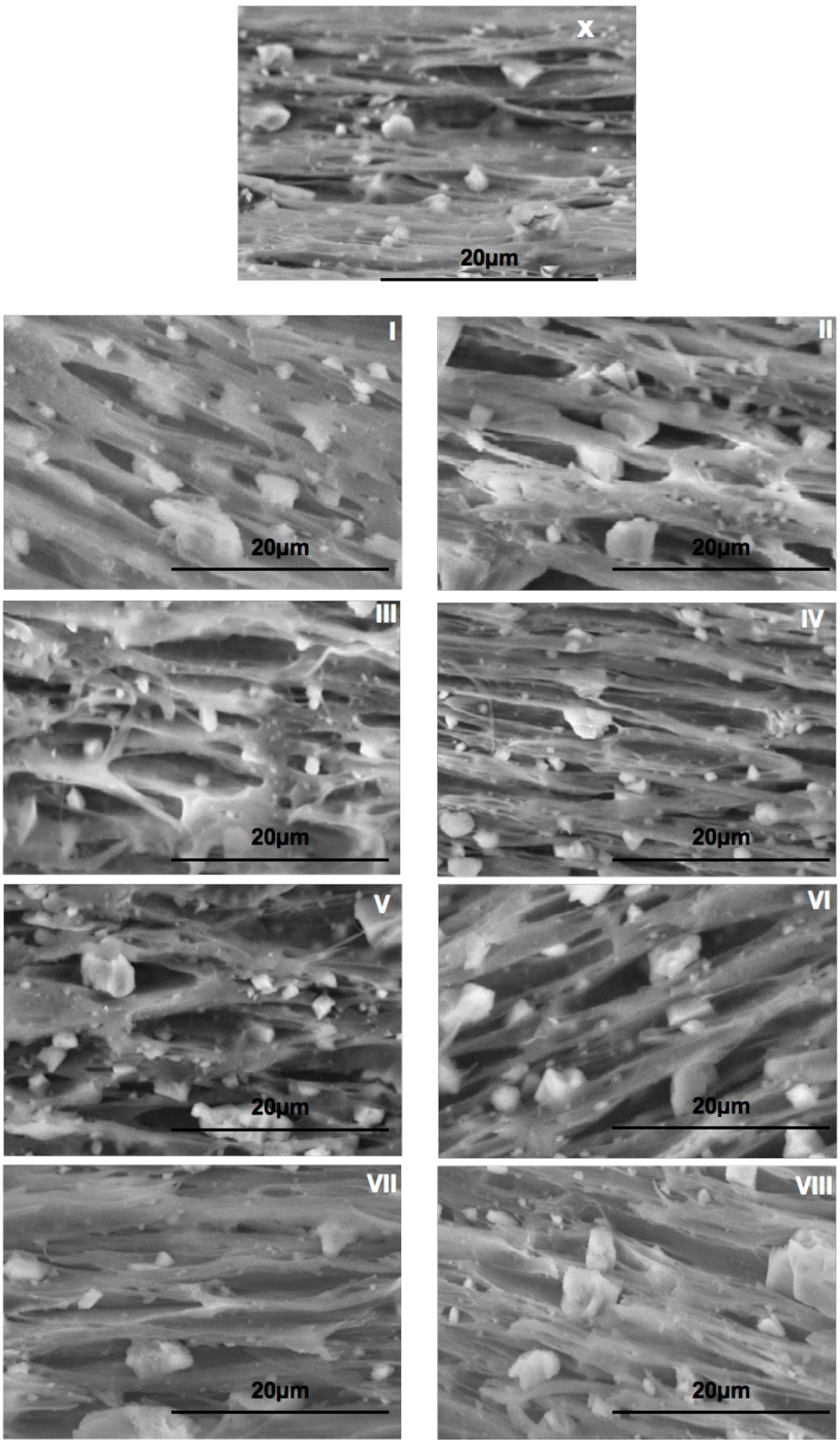
X
20µm
I
20µm
II
20µm
III
20µm
IV
20µm
V
20µm
VI
20µm
VII
20µm
VIII
20µm

Figure 6.4: Scanning electron micrographs of the cross-section of cellular PVDF samples inflated at various GDE procedures. ‘x’ represents the cross-section of sample without inflation treatments after stretching. The other micrographs represents the samples treatd with various inflation procedures. See supporting information for larger area micrographs.

conventional inflation gases, such as N_2, in polypropylene than in polar polymers like PVDF, even at room temperature [77]. Due to the stable PVDF chemical structure, slow segmental motion of the main polymer chain, and the presence of polar fluorine groups, PVDF films are less permeable to gases than non-polar PP or COP [156]. Moreover, the macromolecular chain orientation in PVDF developed during film extrusion and mechanical stretching could also contribute to the lack of correlation with the gas transport characteristics [77, 157].

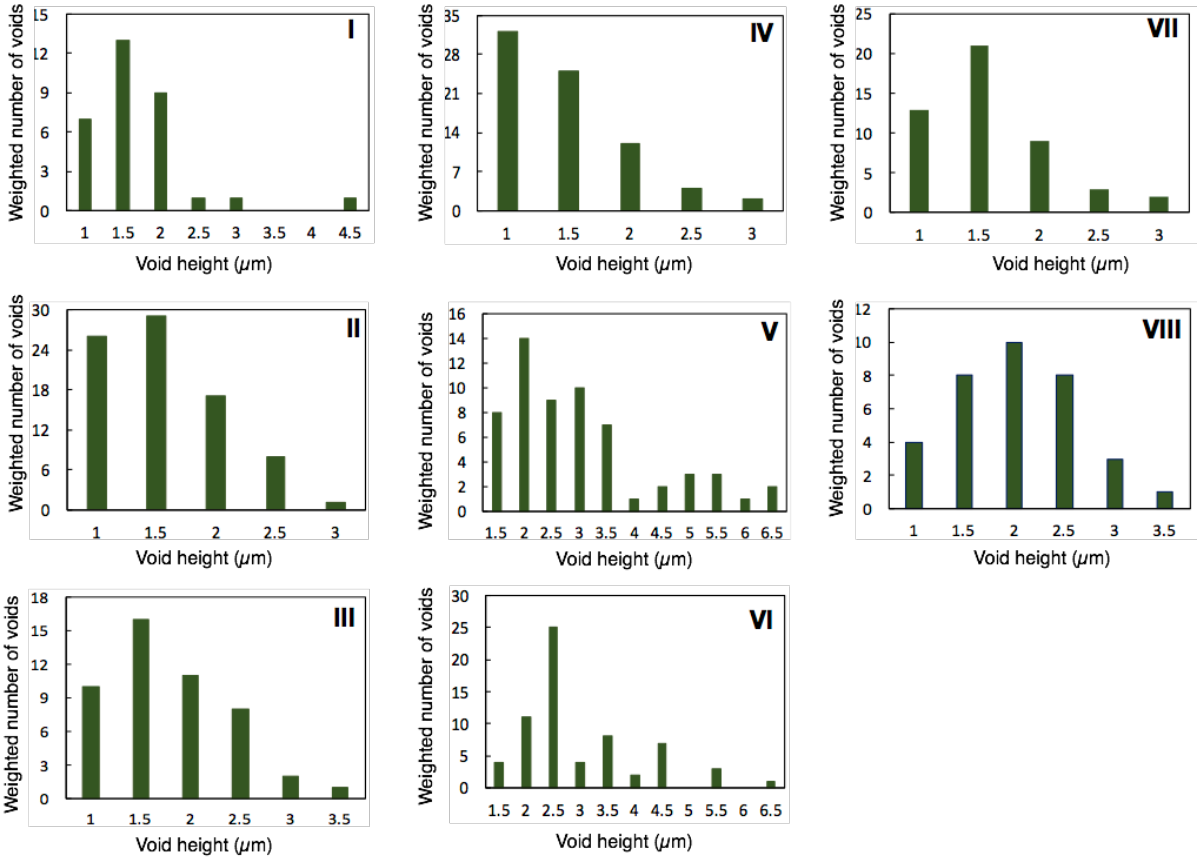

Figure 6.5: Void height distribution for samples treated by various inflation techniques obtained by analyzing their respective SEM images.

Despite the trivial change in sample thickness (Δt) after the inflation treatments, the number of voids increases in both GDE-I and GDE-II samples compared to that in the untreated sample. This increase is more pronounced for GDE-II, as shown in the SEM micrographs (Figure 6.4 (I, II)). This is likely because the inflation gas (in terms of pressure and temperature) was consumed to inflate the existing but very thin voids as shown in Figure 6.4x. Void height distribution in Figure 6.5 reveals that both the number of voids and the average void height are larger for GDE-II samples than those for GDE-I samples. The optimum void number and height required to maximize the piezoelectric response upon suitable electrical charging depend on multiple parameters associated with the processing technique. However, with high compressibility, lens-shaped voids forming high dipoles concentration during charging show the highest piezoelectricity and the lowest stiffness. In comparison, flat and circular voids show the lowest compressibility and the maximum stiffness leading to poor piezoelectric response [26]. Figure 6.4 (I and II) suggest that the voids in both GDE-I and GDE-II treated samples assume flat shapes, which eventually lead to a marginal d_{33} coefficient improvement as shown in Figure 6.6. Here, the two sample categories have a respective increase of 4 and 10 pC/N in their coefficients over the original d_{33} value of 41 pC/N for untreated samples.

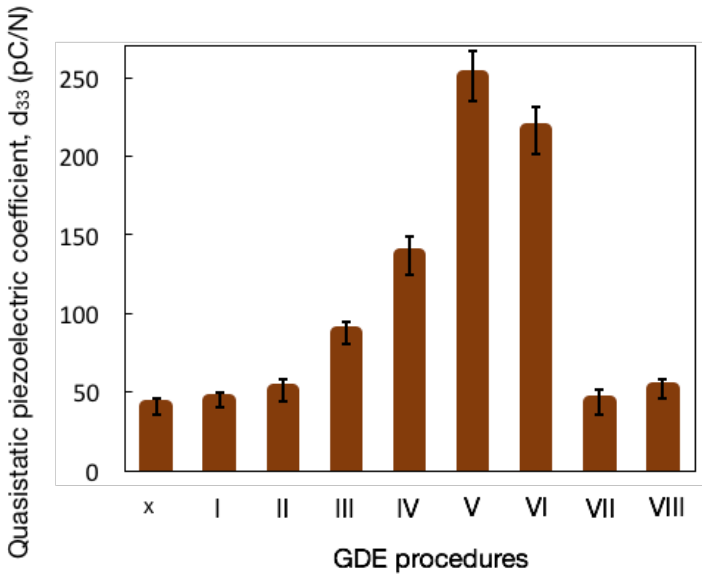

Figure 6.6: Piezoelectric d_{33} coefficients of the cellular PVDF electrets obtained after various inflation treatments followed by corona charging.

Since the results in these two inflation procedures (GDE-I and GDE-II) did not yield significant improvement, a multistep incremental scheme in temperature from 30 °C to 115 °C was implemented in GDE-III (Figure 1(III)) along with a constant inflation pressure of 5 MPa was applied. This allowed a gradual PVDF structure softening to facilitate gas penetration into the voids. As shown in the SEM micrograph in Figure 6.4 (III) the cellular structure is clearly visible in this case unlike for pristine samples (Figure 6.4x). There is also a higher sample thickness increase up to around 8 μm over the initial untreated thickness, as shown in Figure 6.3. However, the number of voids is lower than that in GDE-II film indicating inadequate gas transport into the sample. This implies that the limited permeation coefficient of the relatively-neutral N_2 gas in the polar polymer cannot complete the inflation. The reason for this limited inflation level could be explained by the study of Flaconnèche et al. [77]. The authors showed that at 10 MPa, the N_2 permeation coefficient in a 2 mm thick PVDF film can increase from 0.18×10-7 to 0.78×10-7 cm^3(STP)/cm.s.MPa with a temperature increase from 69 to 102 °C. These values show the weak tendency of N_2-intrusion compared to polar gases like CO_2 having a permeation coefficient of 4.85×10^{-7} cm^3(STP)/cm.s.MPa for the same PVDF film even at 70 °C under similar conditions. Moreover, Corona-charging predominantly creates the dipoles in voids with higher thickness leading to larger dipoles [16]. Therefore, because of the generation of larger number of relatively thicker voids in GDE-III treated samples (Figure 6.5), the resulting d_{33} coefficient is higher (88 pC/N in Figure 6.6) compared to the previous procedures.

In GDE-IV, GDE-V and GDE-VI (Figure 6.1(IV, V, VI)), the temperatures were constant at 115, 130 and 140 °C, respectively. The pressure was however increased in three steps from 3 to 4, then to 5 MPa in all three treatments. The idea is to soften the polymer from the very beginning to induce higher gas transport into the cavities. This stepwise pressure increase creates a progressive path for gas intrusion, even into smaller voids, and prevents any potential collapse [76]. The higher applied temperatures here were motivated by the limited cellular structure and piezoelectric coefficients improvements through the earlier inflation treatments (GDE I, II and III) at 115 °C. As shown in Figure 6.3, the thickness of all three samples significantly increased compared to that of the previous cases. A maximum of 20 μm increase in sample thickness is observed for GDE-V sample. Here, 130 °C seems to be the optimum temperature as higher temperature (140 °C in GDE-VI) is close to the PVDF melting point (162-163 °C) [130]. This in

turn may cause partial collapse/softening of the voids leading to the lower thickness for the GDE-VI sample. The SEM images in Figure 6.4 (IV, V, VI) present the cross-section morphology of the samples treated by the three respective procedures. A well-developed cellular structure is observed for the GDE-V samples, associated with thickness improvement (Figure 6.3). The void height distributions in Figure 6.5 (IV, V, VI) also support this observation. Although GDE-IV samples have a large voids number, the majority of their heights remain below 2 μm (Figure 6.5(IV)). Only a negligible fraction can achieve a thickness greater than 3 μm. The largest voids number appear following the GDE-V treatment, which generates a good fraction with a height distribution between 3.5 to 6.5 μm (Figure 6.5(V)). The rest (below 3.5 μm) have an average height of 2.5 μm. Finally, the average void height produced by the GDE-VI treatment remained between 2.5 and 3.0 μm with a moderate fraction between 3.5 and 6.5 μm (Figure 6.5(VI)). The relatively large void-fractions found above 3 μm in GDE-V and VI treated samples can be attributed to the increase in permeability of N_2 gas in PVDF with increasing temperature (0.78×10^{-7} cm^3(STP)/cm.s.MPa at 102 °C to 2.8×10^{-7} cm^3(STP)/cm.s.MPa at 129 °C, keeping other variables unaltered [77]). This results in improved piezoelectric d_{33} coefficients with values of 137, 251 and 217 pC/N for GDE-IV, V and VI treated samples, respectively.

In the final two sets of experiments (GDE-VII and GDE-VIII in Figure 6.1), the effect of extended inflation period on the piezoelectric response of cellular PVDF films using the simplest approach of direct application of pressure and temperature was studied. Therefore, the inflation pressure and time were constant at 5 MPa and 24 h respectively, in both GDE-VII and VIII samples, while only the temperature was changed; the former being held at 25 °C and the latter at 50 °C. In both cases, the sample thickness decreased from an initial high value measured immediately after the end of the GDE procedures to values close to their original thickness after the two-day period (Figure 6.3). The observed increase thickness is 3 and 5 μm, respectively. This implies that higher treatment temperature with a multistep pressure scheme (which is not present in these two categories) can stabilize the cellular structure by altering the crystallinity degree and via defects relocation [87, 97]. For instance, the crystallinity degree of untreated, GDE-V and GDE-VIII treated samples is 54.2, 62.4 and 54.7 % respectively, which supports the above statement. Although the voids number is larger in GDE-VII than in GDE-VIII, these samples are thicker than GDE-VIII samples where the majority of voids remained below 3 μm (Figure 6.5 (VII, VIII)). This

can be attributed to the relatively higher treatment temperature in GDE-VIII samples. The corresponding piezoelectric coefficients are also shown in Figure 6.6 (44 and 52 pC/N, respectively) which are limited improvement over the untreated specimen (41 pC/N).

6.5 Conclusion

In summary, the effect of various inflation techniques on the piezoelectric properties of cellular PVDF electrets were investigated. The inflation techniques with stepwise-pressure application were more efficient than the direct pressure application. Micrographs and d_{33} results on samples with direct pressure application revealed that the sample inflations are far from being adequate to produce significantly enhanced piezoelectric response. On the other hand, stepwise pressure application opens up the voids, increases the sample thickness and leads to higher piezoelectric response. For example, the piezoelectric d_{33} coefficient for stepwise pressure application ranges from 137 to 251 pC/N depending on the treatment temperature, while it is only 45-52 pC/N for direct pressure treatments. Also, higher treatment temperature (> 115 °C) applied at the beginning of the treatment yields larger amount of voids with higher thickness by increasing the gas transport and thus creates larger dipoles during corona charging. For instance, stepwise pressure application at a constant temperature of 130 °C produced the maximum piezoelectric coefficient of 251 pC/N, while the one inflated at 115 °C gave 137 pC/N. This gas inflated, electromechanically active voided PVDF film is believed to be suitable for sensor and actuator applications, as well as for acoustical transducers.

6.6 Acknowledgement

The authors acknowledge the technical support from Mr. Richard Silverwood (Polytechnique, Montreal) and Mrs. Claire Cerclé (Polytechnique, Montreal) and the financial support from FRQNT (Fond de Recherche du Québec en Nature et Technologie) and NSERC (Natural Sciences and Engineering Research Council of Canada).

6.7 Supporting information

Effect of the inflation strategy on the piezoelectric response of cellular PVDF ferroelectret

Nusrat Jahan[1,2], Frej Mighri,[1,3], Denis Rodrigue[1,3], Abdellah Ajji[1,2*]

[1]CREPEC, Research center for high performance polymer and composite systems

[2]Department of Chemical Engineering, Polytechnique Montréal,
C.P. 6079, Montreal, QC, H3C 3A7, Canada

[3]Department of Chemical Engineering
Université Laval, Quebec, QC, G1V 0A6, Canada

6.7.1 Supporting information content

1. Supporting Figure

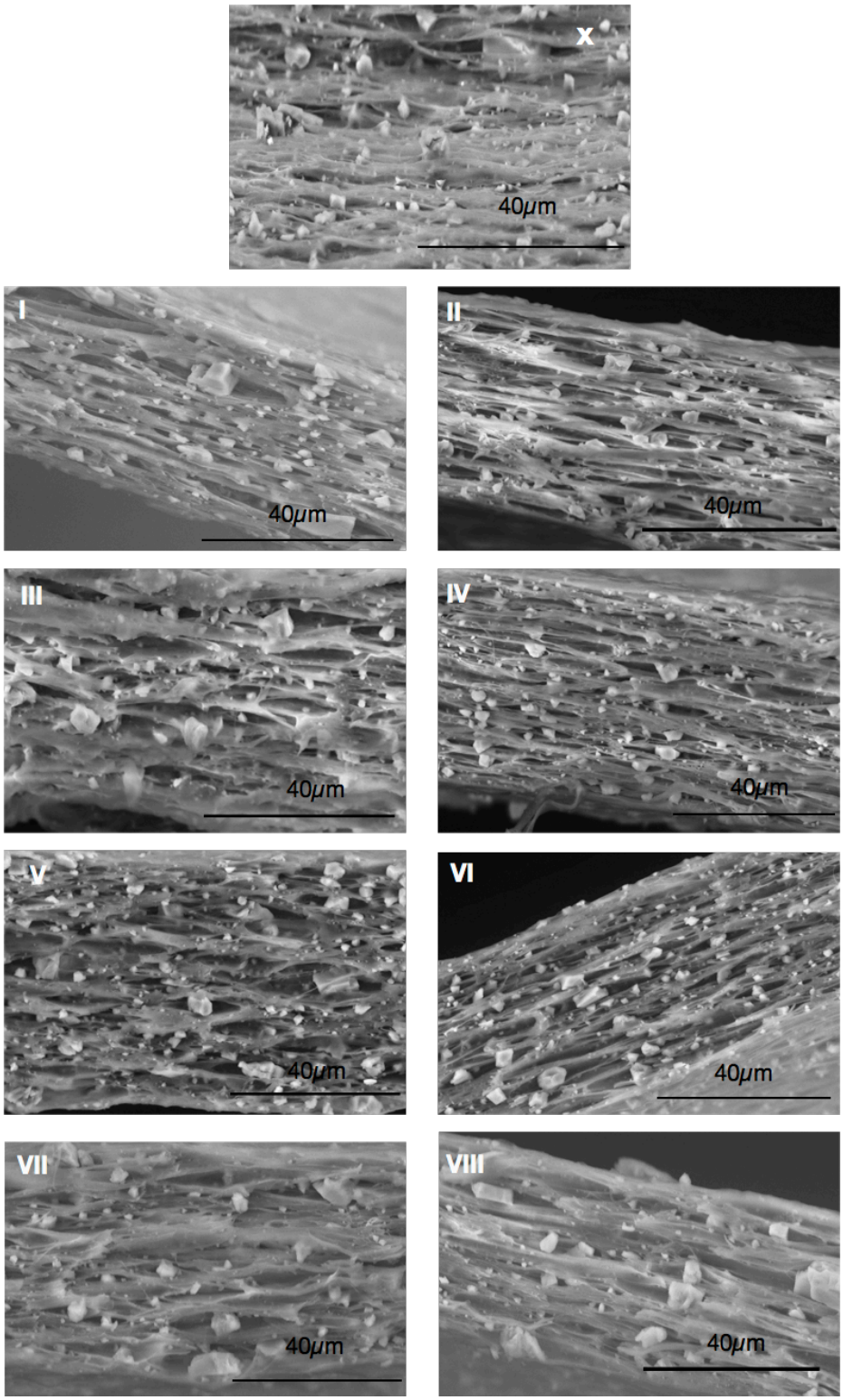

Figure S6-1: Enlarge area micrographs of Figure 6.4 in the original manuscript.

CHAPTER 7 ARTICLE 4: THERMALLY STABLE CELLULAR PVDF FERROELECTRETS: OPTIMIZATION OF CO_2 DRIVEN INFLATION PROCESS

Nusrat Jahan[1,2], Frej Mighri,[1,3], Denis Rodrigue[1,3], Abdellah Ajji[1,2*]

[1]CREPEC, Research center for high performance polymer and composite systems

[2]Department of Chemical Engineering, Polytechnique Montréal,
C.P. 6079, Montreal, QC, H3C 3A7, Canada

[3]Department of Chemical Engineering
Université Laval, Quebec, QC, G1V 0A6, Canada

Submitted in: Smart materials and structures

7.1 Abstract

Electrically charged cellular ferroelectrets can show excellent thermally stable piezoelectric activity and are therefore progressively used in electrochemical transducers. In this paper, we report on the influence of various gas diffusion expansion (GDE) or inflation procedures on the piezoelectric d_{33} coefficient and thermal stability of cellular poly(vinylidene) (PVDF) ferroelectrets. Given that an optimized cellular structure is a key for improving charge density and the associated piezoelectric properties in this material, we investigated the required CO_2 inflation treatment using various inflation procedures to enhance the internal voids expansion and compare with the results obtained by N_2 inflation as reported in our previous study [158]. The maximum d_{33} coefficient for CO_2-inflated samples is found to be around 30% higher than that of N_2-inflated samples (327 pC/N compared to 251 pC/N). The key parameters addressed in the inflation procedures are the changes in sample thickness, morphology and the void-height distribution in both treatments. The ferroelectrets show excellent thermal stability for up to four days at 90, 110 and 120 °C, which is suitable for high temperature applications.

7.2 Introduction

Ferroelectrets, also known as electrically charged polymer foams, have been the subject of significant research in recent years. Because of their excellent piezoelectric response d_{33} (several hundred pC/N), their light weight and mechanical flexibility, they are used in a wide range of microelectronic applications [18, 23, 89, 150]. To prepare a cellular polymer film, a mixture of polymer and filler is extruded and stretched using suitable conditions. The piezoelectricity of ferroelectrets arises from macroscopic dipoles generated by opposite charges deposited on the opposite inner walls of lens-shaped voids. The charge-deposition is achieved by applying an electric field in the direction perpendicular to the film surface. The resulting piezoelectricity is proportional to the degree of polarization achieved in the voids. In cellular ferroelectrets however, the possibility to modify the amount of voids and in turn the number of dipoles is very limited beyond the film preparation step. At this stage, the voids height remains the only parameter; thus the size of the resulting dipoles can only be modified by choosing suitable inflation parameters [18]. This treatment requires a high external pressure applied for a certain period of time (with/out any specific temperature) allowing gas diffusion into the voids. The process is applied until the internal void pressure equals the external pressure at the source, and finishes with a sudden release

of the applied pressure. Although the correlation between the charging process and the resulting piezoelectric response in such systems has been improved in recent years [16, 147, 150, 159], the relationships between void geometry and electromechanical properties are yet to be completely understood.

One of the key steps in the inflation procedure is gas transport through cellular films, which in semi-crystalline polymers is a complex phenomenon, especially under high temperatures and pressures [77, 78, 154]. The transport coefficients, including gas permeation, diffusion and solubility are function of several parameters associated with the polymer and the gas properties. Typically, this dependence may arise from the degree of polymer crystallinity, polarity of both polymer and gas, polymer thermal history, gas molecular size [160], as well as the inflation parameters such as pressure, temperature and treatment time. While non-polar ferroelectrets, such as polypropylene (PP) [78, 150, 161], poly(ethylene terephthalate) (PET) [26, 27], fluoroethylene propylene (FEP) [28], and polyethylene naphthalate (PEN) [162], exhibited satisfactory inflation behavior either with N_2 or CO_2, the inflation behavior of polar polymer foams, such as polyvinylidene fluoride (PVDF) or polylactic acid (PLA) [96], is still not clear and requires a fundamental understanding of the interaction between the polymer matrix and the inflation gas.

Cellular PP ferroelectrets are widely used materials in microelectronics because of their easy and cost-effective processing compared to other non-polar piezoelectrets [18, 98, 150]. However, poor thermal stability of PP electrets above 60 °C has limited their industrial implementation [92]. Several other ferroelectrets (polymer foams) have been investigated in the last few years including perfluoropolymers such as polytetrafluoroethylene (PTFE) and FEP. The excellent charge storage ability of PTFE and FEP up to 120 °C made them excellent choices for various electromechanical applications [97, 148]. However, they are cost-intensive and difficult to process through conventional polymer processing methods because of their very high melt viscosity and tendency to degrade releasing hydrofluoric acid [30] during manufacturing.

In this context, we have recently reported the piezoelectric response of cellular PVDF ferroelectrets with various inflation techniques using N_2 as the inflation gas [158]. Although a new ferroelectret material was produced, the reported N_2 gas inflation treatment had limitations. Because of its relatively neutral nature, N_2 permeation is limited by the PVDF polar groups (C-F bonds). This introduces a lack of understanding of void inflation inside such polar polymers. To

overcome these limitations, we investigated CO_2 as the inflation gas which is polar in nature with respect to PVDF. The inflation performances between CO_2 and N_2 have been compared using various inflation procedures. Finally, the study reports on the thermal stability of the cellular PVDF ferroelectrets produced.

7.3 Experimental Procedure

7.3.1 Materials

PVDF (Kynar 720) ($M_w = 2.65\times10^5$ g mol^{-1}, T_m = 165-172 °C, density = 1.78 g cm^{-3}, PDI = 2.3, MFR = 5-29 g/10 min at 450 °C under 3.8 kg) is an extrusion grade polymer supplied by Arkema (USA). Nanomer I44P (dimethyl hydrogenated tallow quaternary ammonium ion exchanged montmorillonite, density 1.4 g cm^{-3}) was purchased from Nanomer Inc. (USA) and used as a filler to prepare the PVDF nanocomposites. The micro-filler, calcium carbonate ($CaCO_3$) (particle size: 3-13 μm, density: 2.7 g cm^{-3}), was supplied by Univar (Canada). It is an industrial grade filler used without further purification. Both gases, nitrogen N_2 (purity ~ 99.99%) and carbon dioxide CO_2 (purity ~ 99.9%), supplied by Air Liquide (Canada), were used as the inflation gases. The critical pressure and temperature are respectively 7.38 MPa and 304.13 K for CO_2, and 3.40 MPa and 126.19 K for N_2. These two gases were chosen based on their different properties as N_2 is less polar than CO_2 and therefore acts as a more 'neutral' gas in terms of interactions with PVDF [154].

7.3.2 Sample Preparation

The samples used in this study are cellular PVDF films prepared by unidirectional stretching of PVDF/hybrid filler ($CaCO_3$+ nanoclay) extruded films. More details on the extrusion process and uniaxial stretching can be found in our previous work [158], as well as in the supporting information.

The stretched PVDF films were then inflated with CO_2 in a closed pressurized vessel equipped with a heating jacket to perform the temperature treatments. In our previous study [158], eight N_2 inflation schemes (I-VIII) were divided into 4 sets. In this work, four of them (schemes II, III, V and VIII) were chosen based on the best results obtained, one from each set of experiments. Figure 1 presents these inflation procedures, but more details can be found in the

supporting information [158]. The charging was performed in a tip-to-plane corona setup filled with N_2 at 200 kPa for 10 min using a needle voltage of +27 kV. Finally, the samples were metallized on both surfaces using conductive silver paste and the piezoelectric measurements were performed. Details of the d_{33} measurement and scanning electron microscopy (SEM) is reported in the supporting information and also in ref. [158].

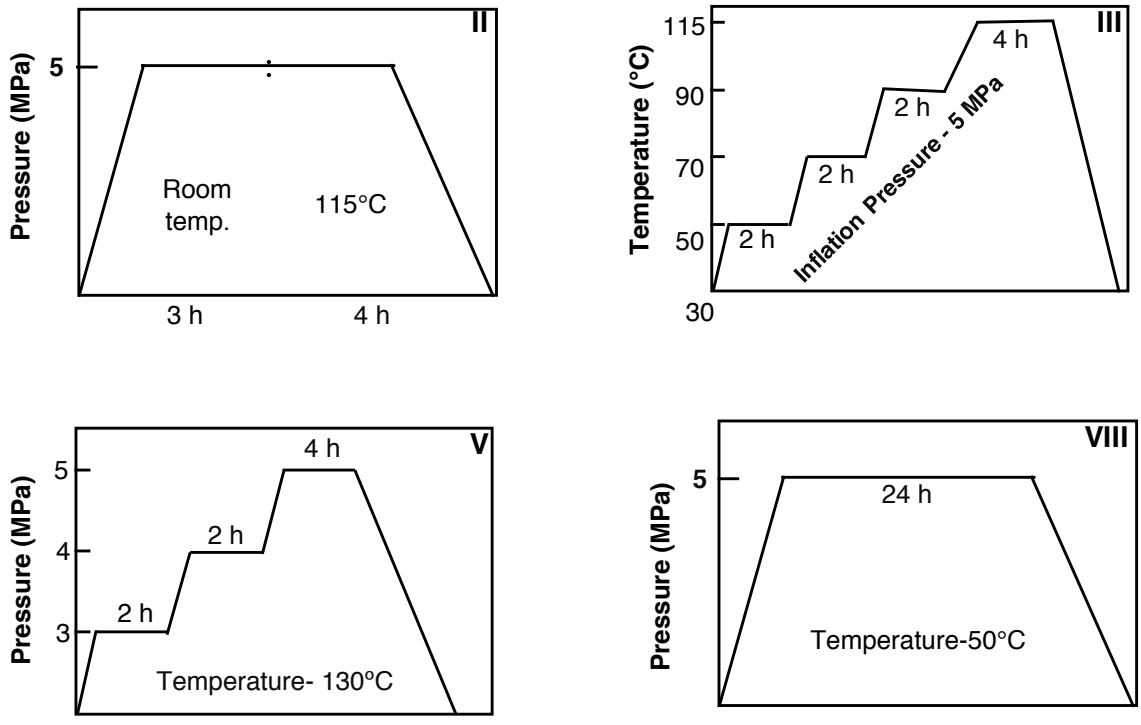

Figure 7.1: Schematic representation of the inflation procedures, reprinted from [158].

The heat flow curve obtained from differential scanning calorimetry (DSC Q1000, TA Instruments, USA) was used to estimate the crystallinity level of samples inflated with both gases. The samples were heated to 220 °C at 15 °C/min in a N_2 atmosphere. The degree of crystallinity (χ_c) was determined as [47]:

$$\chi_c = \frac{\Delta H_m \times 100}{\Delta H(1-w)} \text{----------(7-1)}$$

where ΔH_m is the melting enthalpy of the sample (J/g), ΔH is melting enthalpy for 100% crystalline PVDF (103.4 J/g) [47], and w is the filler weight fraction (0.327).

7.4 Results and Discussion

7.4.1 Morphological Analysis

A morphological analysis was done first to determine the effects of both inflation gases (N_2 and CO_2) on the cellular structure of the uniaxially stretched PVDF hybrid composite samples. The results are presented in Figure 7.2 and Figure 7.3, as well as Figure S7-1 and S7-2 in the supporting information. The inflation treatments were carried out in four different schemes (Figure 7.1). Figure 7.2 andFigure 7.3 reveal the formation of closed voids at the polymer/filler interface (in this case PVDF/$CaCO_3$). The inhomogeneous voids distribution (in terms of both size and height) can be attributed to the wide $CaCO_3$ particle size distribution (3-13 μm). Moreover, homogeneous voids distribution across the sample implies a uniform fillers distribution in the PVDF matrix during film preparation.

The electromechanical properties of electrically charged cellular polymer foams are known to depend on the cellular morphology in terms of cell size, shape and distribution [163]. The evolution of cell-morphology occurs in two steps. Firstly, by stretching the polymer film filled with solid particles and then by inflating the stretched film with gases at high pressure. The latter has a more pronounced effect on the morphology evolution. Due to the different behavior of both polar CO_2 and neutral N_2 inflation gases [154], the resulting cellular morphology features such as the number of voids, voids geometry and the porosity level are also different in both cases based on their interaction with the host polymer (PVDF) system (Figure 7.2 and Figure 7.3). To explain in details the inflated samples cellular structure, the histograms of voids height, taken as the minor axis of the fitted ellipses, are presented in Figure 7.4 andFigure 7.5. The increase in sample thickness (Δt) following each inflation treatment is shown in Figure 7.6. The voids height plays a critical role both in charge separation during electrical charging and on the film stiffness during d_{33} measurement [78]. Since the inflation treatment does not change the amount of polymer in the cellular structure, the resulting sample thickness increase for each treatment arises from the gas pressure created inside the voids and the PVDF swelling because of gas absorption is assumed negligible.

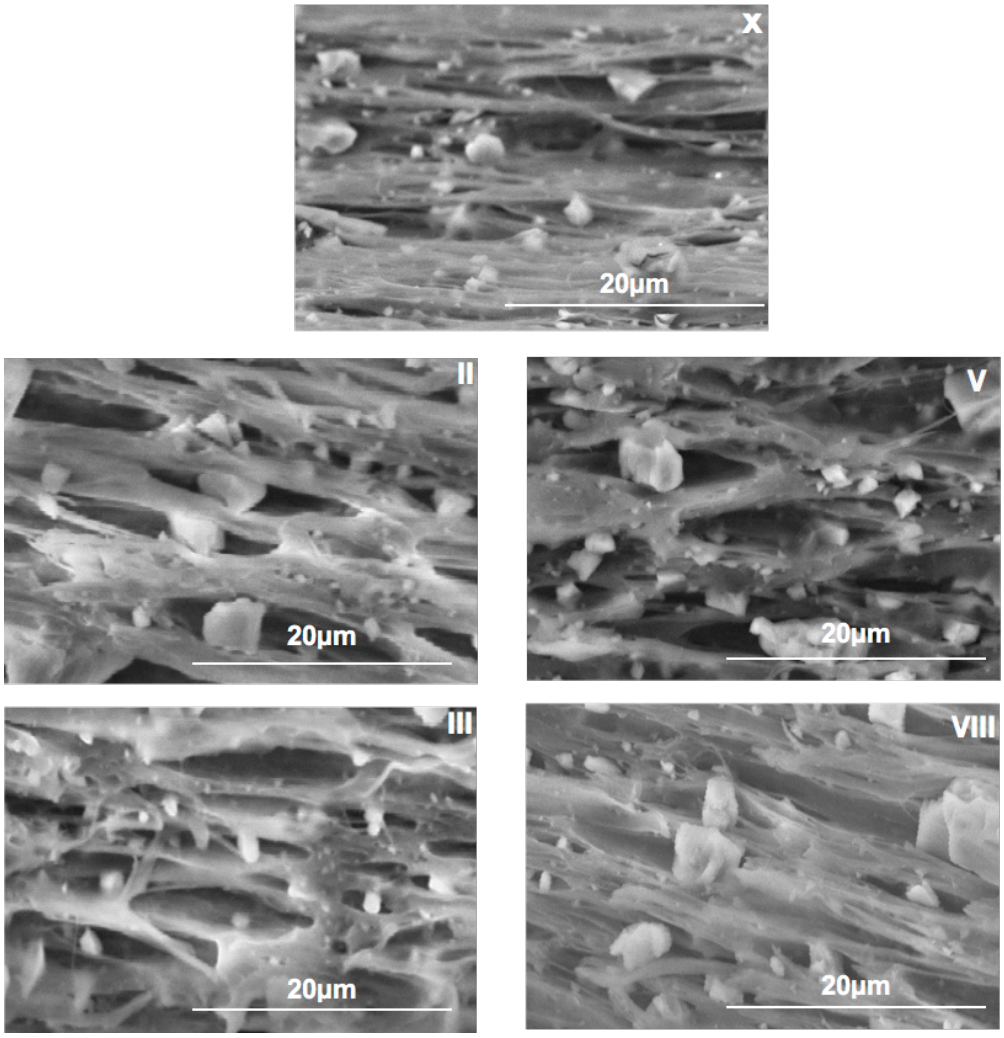

Figure 7.2: Scanning electron micrographs of the cross-section of the N_2-inflated samples, reprinted from [158]. The roman numbers on the top right corner represents the inflation procedures explained in Figure 7.1. 'X' represents the sample without any inflation treatment.

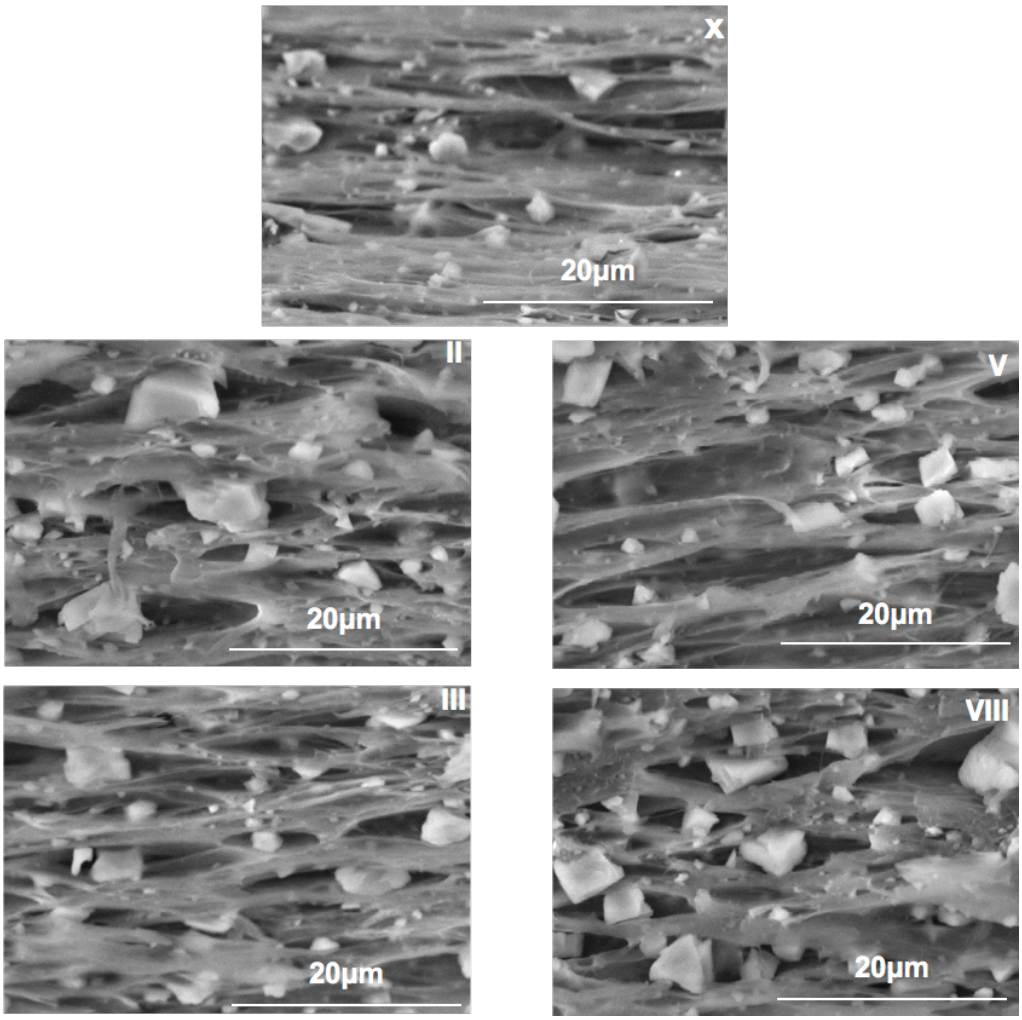

Figure 7.3: Scanning electron micrographs of the cross-section of the CO_2-inflated samples. The roman numbers on the top right corner represents the inflation procedures of Figure 7.1 and 'X' represents the sample without any inflation treatment.

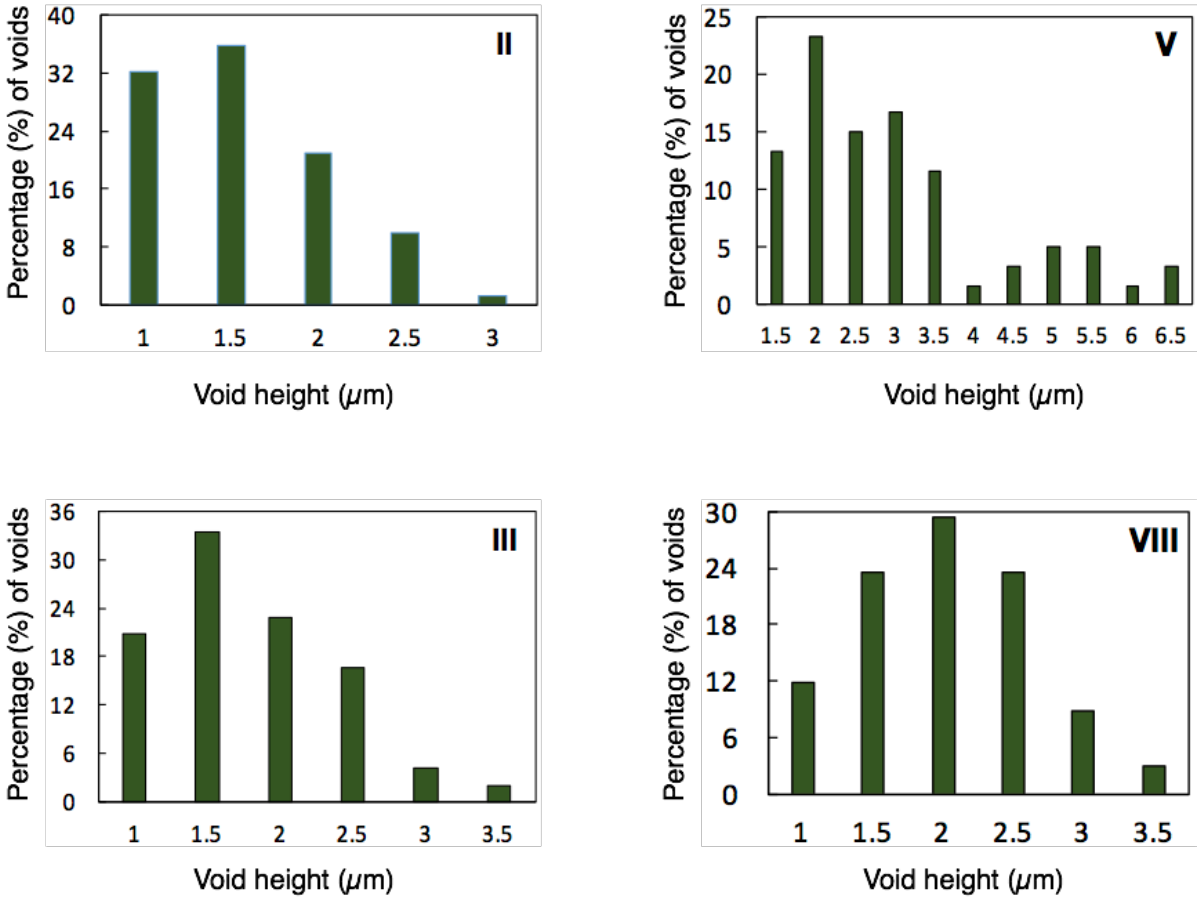

Figure 7.4: Histograms of void height distribution of N_2-inflated samples, taken from ref [158]. The roman numbers (II, III, V and VIII) on the top right corner represents the inflation procedures described in Figure 7.1.

As shown in Figure 7.6, Δt is always higher for CO_2-inflated samples compared to N_2-inflated ones. This suggests that CO_2 penetration into the PVDF voids is more important than that of N_2 under the same temperature, pressure and time length. For CO_2 treatment, the maximum Δt obtained was 24 μm (65% increase over the initial thickness) with the GDE-V scheme, while this value was 20 μm (54% increase compared to the initial thickness) for N_2 inflation with the same GDE procedure. Along with the effect of pressure difference and temperature treatments, this difference can also be attributed to stronger CO_2 interaction with PVDF compared to N_2. The highly electronegative C-F bonds in PVDF tend to interact more strongly with the polar CO_2 molecules than with N_2. In addition, the interaction between CO_2 and C-F bonds are stronger than that between the polymer chain segments [77, 154]. The interaction of polar PVDF with the quadruple moment

of CO_2 via the electronegative oxygen makes the CO_2 penetration in PVDF film easier [164, 165]. No such interaction is reported for N_2 because of its inertness even if they have similar molecular diameter (315 pm for N_2 and 334 pm for CO_2) [160]. Therefore, N_2 inflation is mainly attributed to the pressure difference between the outer and inner voids surface depending on the applied temperature [78, 158]. Moreover, Shen et al. [166] reported strong chemical stability of inorganic-mineral-filler in permeating gases inside PVDF. Also, it is assumed that both CO_2 and N_2 do not cause any significant degradation or adsorption of the fillers used.

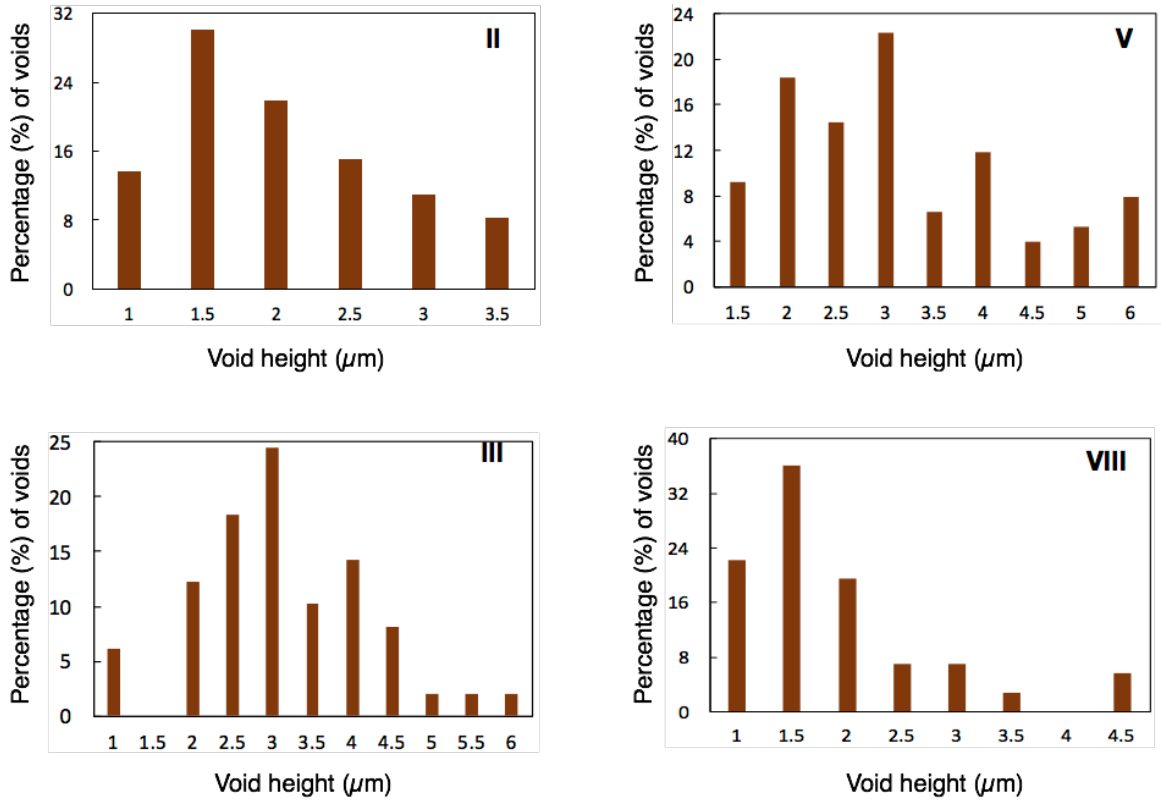

Figure 7.5: Histograms of void height distribution of CO_2-inflated samples. The roman numbers (II, III, V and VIII) on the top right corner represents the inflation procedures described in Figure 7.1.

In a previous work, Flaconnèche et al. [77] suggest that temperature has a more prominent effect on the transport coefficient of CO_2 than for N_2 in PVDF. As shown in Figure 7.4 and Figure 7.5 for GDE-V treated samples, CO_2 inflation at 130 °C and a stepwise applied pressure of up to 5 MPa leads to a higher voids number than N_2. Furthermore, the number of voids having a thickness

above 4 μm in CO_2 treated samples is almost twice than for N_2-inflated samples, which is likely due to the higher permeation of CO_2 than N_2. It was shown that at 130 °C and 5 MPa, CO_2 has about 9 times higher permeability and 9 times higher solubility than N_2 despite their similar diffusion coefficients [77]. This effect is also consistent at relatively lower temperatures. In particular, the GDE-III treatment (temperature applied in a stepwise manner form 30 °C to 115 °C at a constant pressure of 5 MPa) results in Δt value twice as high for CO_2-inflated samples than for N_2-inflated ones. This is shown via the histograms in Figure 7.4 and Figure 7.5, which confirm that the number of thicker voids is much higher for CO_2-inflation than for N_2-inflation treatments.

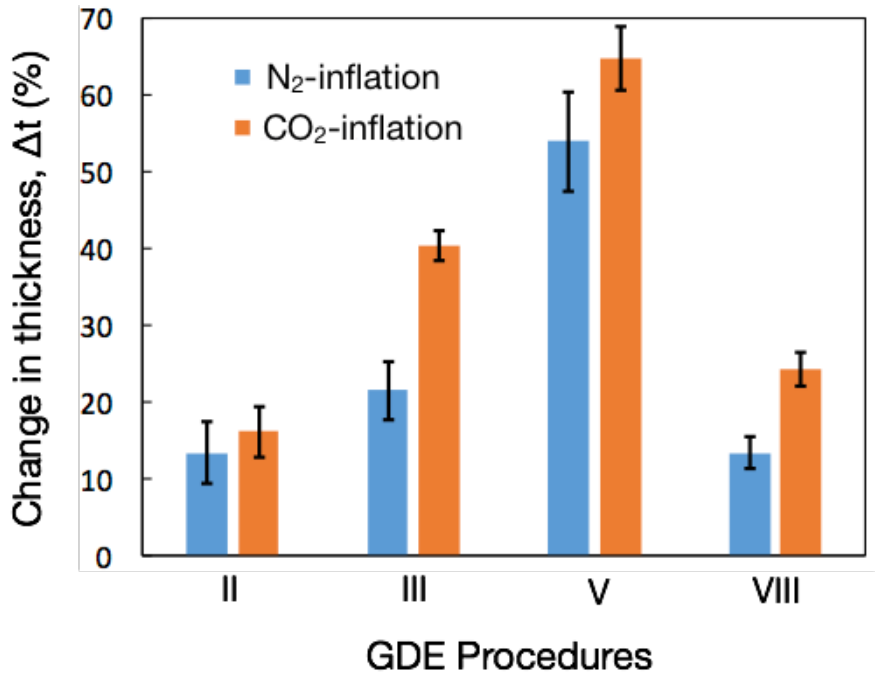

Figure 7.6: Change in sample thickness (Δt) of both N_2 and CO_2-inflated samples. The thickness value for N_2 inflation is taken and recalculated in percentage (%) from ref. [158].

A similar effect was observed for the GDE-VIII scheme where a constant 50 °C combined with 5 MPa drove the inflation for 24 h. This could again be attributed to better CO_2 permeation than N_2 even at this lower temperature as reported in ref. [77] since the CO_2 permeability and solubility coefficient are 10-12 times higher than that of N_2 (at 70 °C). This is consistent with the observed thickness increase of CO_2 inflated films (Figure 7.6) in this study, where the amount of

thicker voids is higher (Figure 7.4 and Figure 7.5). However, Δt is still low in both gases (5 μm in N_2 and 9 μm in CO_2 for GDE-VIII). This is probably because inflation at high pressure and low temperature only increases the elastic nature of the film expansion and thus impedes the permanent expansion of the film thickness [78]. A similar argument also applies to the slightly higher Δt value (Figure 7.6) and the larger number of expanded voids (Figure 7.4 and Figure 7.5) in CO_2-inflated samples for GDE-II.

7.4.2 Piezoelectric d_{33} Coefficient

During corona charging, the ambient gas and the voids inside the film play an important role in electrical breakdown, as well as in their piezoelectric response. Figure 7.7 shows the quasi-static piezoelectric d_{33} coefficient for both N_2 and CO_2-inflated samples corona charging in N_2 atmosphere. An ambient gas with larger dielectric breakdown strength allows a larger potential difference across the film surfaces during charging, resulting in higher charge density and hence stronger piezoelectric d_{33} coefficient. Because of that, N_2 having a breakdown voltage of 1.15 V (uniform DC field at 1 atm [16]) was used as the ambient gas in our studies in preference to CO_2, which has a lower breakdown voltage of 0.95 V under identical conditions.

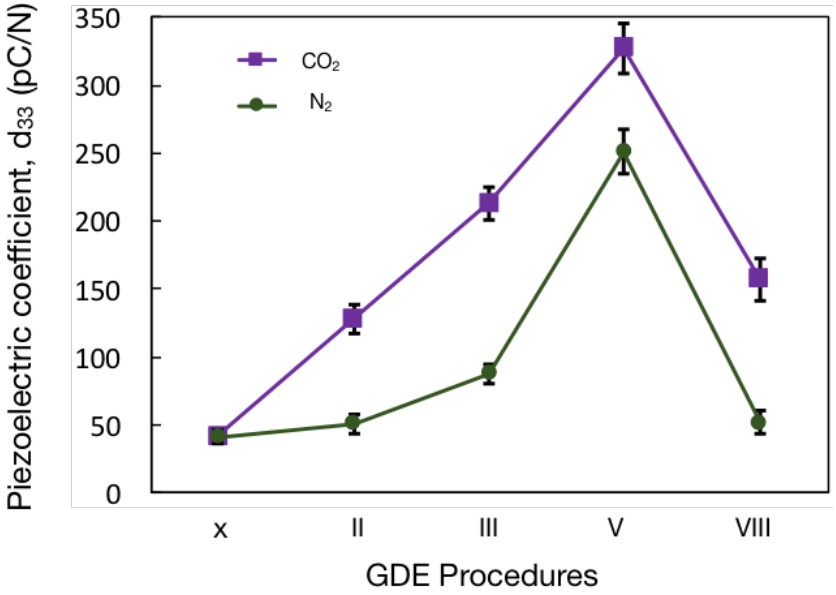

Figure 7.7: Quasi-static piezoelectric d_{33} coefficients of both N_2 and CO_2-inflated samples. 'X' represents the uninflated sample and the GDE procedures are described in Figure 7.1. The lines are a guide for the eyes. The d_{33} value for N_2 inflation is taken from ref. [158] for comparison.

The d_{33} coefficient in CO_2-inflated samples varies between 128 and 327 pC/N, while the N_2-inflated samples yield d_{33} values in the range of 51-251 pC/N following the corona charging process (Figure 7.7). The optimum d_{33} value of 327 pC/N was obtained for CO_2-inflated sample via GDE-V. This 25-50% piezoelectric response improvement for CO_2-inflated samples can be attributed to better charge separation across the thicker voids, lower stiffness of the same voids (assumed from their larger Δt as shown in Figure 7.6), as well as the larger dipoles size (void height distribution in Figure 7.5). Because of the inhomogeneous cellular structure, the potential difference across the sample surface was not uniform resulting in piezoelectric coefficient varying by 18% for different samples of the same batch.

7.4.3 Thermal Stability of the Ferroelectret

The key to improve charge stability is the very low electrical conductivity of the polymer matrix (10^{-16} /Ω.m or less) [97, 99]. The PVDF composite used in this study exhibits very high volume resistivity (2×10^{16} Ω.m [95]), making this system a promising candidate for thermally stable electret material. Moreover, unidirectional stretching of the PVDF composite film at a suitably higher temperature was reported to improve the crystallinity level [130], which is attributed to the reorganization of macromolecular chains during stretching. The improved crystallinity not only enhanced charge stability, but also provided thermal stability in the mechanical properties [97].

Cellular PVDF films (‘stretched-inflated-charged’) were heat-treated in an oven for 5 h at 90 °C to investigate the short-term thermal stability of the generated piezoelectric coefficient. Both N_2 and CO_2–inflated samples were included in the heat treatment for comparison. Following the heat treatment, the samples were cooled down to room temperature before measuring the d_{33} coefficient again. The recorded d_{33} coefficient before and after this heat-treatment are presented in Figure 7.8. It can be seen that the decays in the piezoelectric responses are only limited to a maximum of 16 and 10% of the original values (before heat treatment) for N_2 and CO_2-inflated samples, respectively. The CO_2-inflated samples show a better charge stability than N_2-inflated samples due to enhanced crystallinity and larger cell number. The pores along with crystalline/amorphous interfaces and polymer/filler interfaces act as a source of high energy regions in the samples. These features can produce a high concentration of structural defects, broken chains, double bonds and free radicals in the CO_2 samples (compared to N_2 treated

samples), resulting in a high concentration of trapped charges [97, 101]. At elevated temperatures, the charges (electrons) stored at these interfaces break away because of higher mobility via thermal energy, which can cause a decay in the ferroelectrets piezoelectric characteristics as shown in Figure 7.9 (discussed below in more details).

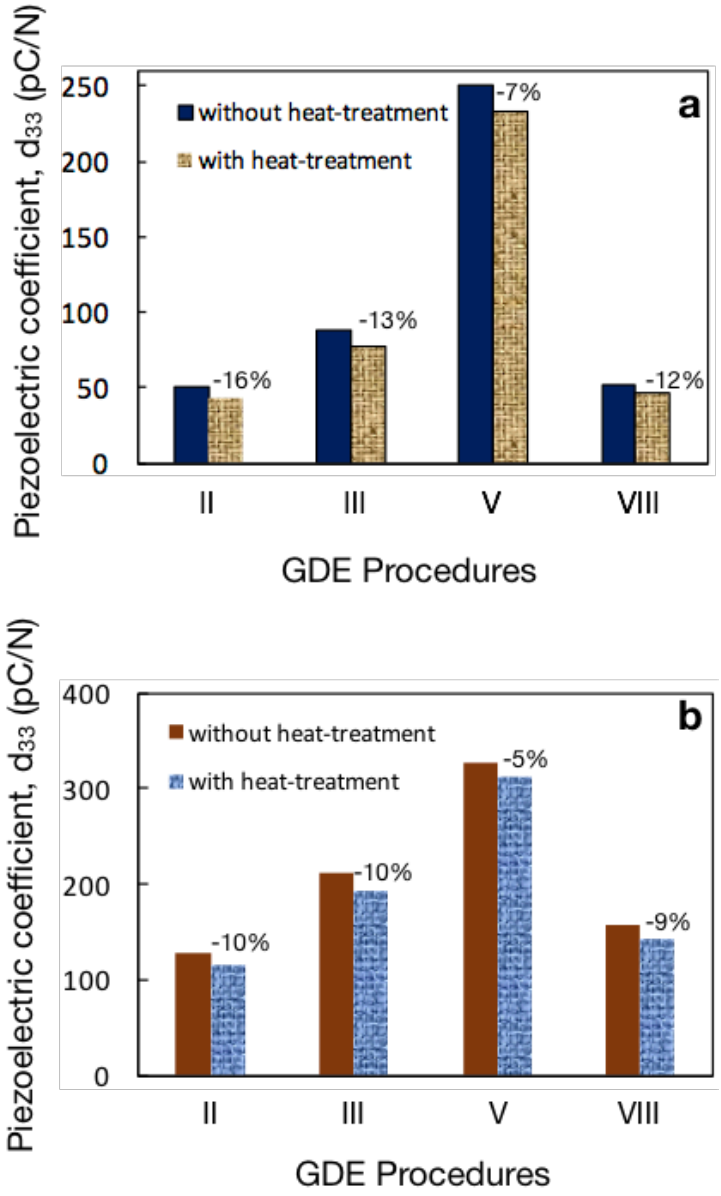

Figure 7.8: Quasi-static piezoelectric d_{33} coefficients of both (a) N_2 and (b) CO_2-inflated samples heat treated for 5 h at 90 °C. For comparison, the d_{33} coefficients before heat treatment are also shown. The percentage (%) value represents the decay of d_{33} coefficients due to the heat treatment

compared to the samples without heat treatment. The d_{33} value of 'without heat treatment' in Figure (a) is taken from ref. [158] for comparison.

The crystallinity of the inflated samples in both N_2 and CO_2 with the defined procedures was calculated using Equation (7-1) and the values are listed in Table 7.1. The data confirms the increased crystallinity via inflation for all the samples. The crystallinity of CO_2 and N_2-inflated samples are very close, but CO_2 treated samples are slightly higher. This has a direct effect on the respective piezoelectric responses as discussed above (Figure 7.8) with improved thermal stability. Therefore, the effect of cell structure and crystallinity degree are combined to produce excellent stability in the d_{33} values.

Table 7.1: Crystallinity data for both N_2 and CO_2-inflated samples. 'X' represents the sample without inflation and the GDE procedures described in Figure 7.1.

	N_2- inflation		CO_2-inflation	
	ΔH_m	χ_c	ΔH_m	χ_c
X	37.6	54.2	37.6	54.2
II	37.4	54.0	38.1	55.0
III	38.1	55.0	42.3	61.0
V	43.2	62.4	47.0	67.8
VIII	37.9	54.7	39.8	57.4

The stable range of working temperature for PVDF electrets prepared using the GDE-V scheme with both gases was investigated by recording the decay of the piezoelectric d_{33} coefficient. The films were heat-treated at 90, 110 and 120 °C for different time periods up to 96 h. The results of Figure 7.9 and Table 7.2 show an initial fast decay in d_{33} values followed by a stabilization over the 96 h period. For all heat-treatment temperatures, the values stabilize after 24 h and remain constant thereafter. Only the 120 °C treated samples show a slight variation in the d_{33} decay profile within 5-15 h of treatment, beyond which the values stabilize. These trends confirm the improved charge stability in PVDF electrets over the GDE untreated samples, which is due to the increased amount of internal voids, crystallinity and structural defects. Although the electrical conductivity of the intrinsic porous PVDF is very low, mobilization of the detrapped charges toward the interfaces and in the PVDF bulk lead to the observed charge decay. As pointed above, this loss of

stored charge at the interfaces is more likely to occur at elevated temperatures [97], in agreement with the data of Figure 7.9 and Table 7.2.

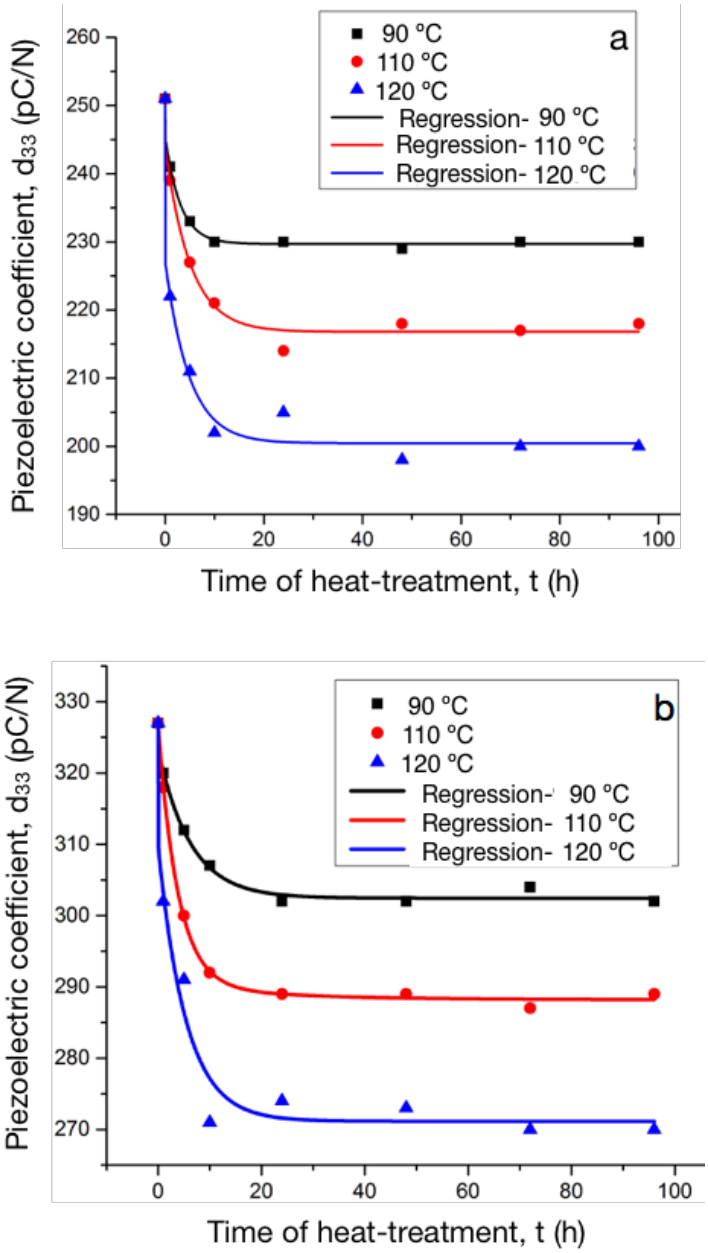

Figure 7.9: Quasi-static piezoelectric d_{33} coefficients as a function of heat treatment time (h) of both (a) N_2 and (b) CO_2-inflated GDE-V samples at various temperature. The solid lines represent fitting to Equation (7-2) with the parameters of Table 7.3.

Moreover, it has been reported that fillers addition results in enhanced polymer composites electret properties and charge stability [92, 96, 98]. For example, the stability of PVDF electret can be strongly influenced by $CaCO_3$ and nanoclay addition. This improvement can be attributed to several factors. Firstly, it introduces trap-centers at the interface boundary with the PVDF matrix [93, 94]. Secondly, the fillers can induce the Maxwell-Wagner-Sillar polarization at the PVDF boundary via conductivity difference through various phases [95]. Thirdly, the physical adsorption of PVDF on the solid filler surface decreases chain mobility resulting in a more stable electromechanical response via lower relaxation rates [96]. Finally, the voids generated in each case by the fillers (Figure 7.4 and Figure 7.5) hinder the drift/depolarization process by increasing the path-length for the carriers across the film [92, 97-99].

Table 7.2: d_{33} values measured after heat treatment at various temperature for different time periods.

Heat treatment Time (h)	d_{33} coefficient (pC/N)					
	N_2			CO_2		
	90 °C	**110 °C**	**120 °C**	**90 °C**	**110 °C**	**120 °C**
0	251	251	251	327	327	327
1	241	239	222	320	318	302
5	233	227	211	312	300	291
10	230	221	202	307	292	271
24	230	214	205	302	289	274
48	229	218	198	302	289	273
72	230	217	200	304	287	270

The experimentally data (Figure 7.9) were fitted to an exponential decay model as:

$$y(t) = y_0 + A_1 \exp\left(-\frac{t}{t_1}\right) + A_2 \exp\left(-\frac{t}{t_2}\right) \qquad (7\text{-}2)$$

where y_0 is the offset value, while A_1 and A_2 are the amplitude and t_1 and t_2 are time constants. The second part of the equation represents the initial decay, while the third part gives the level of residual charge. The fitting parameters are listed in the Table 7.3.

Table 7.3: Fitting parameters for Equation (7-2).

Fitting parameters	N_2			CO_2		
	90 °C	**110 °C**	**120 °C**	**90 °C**	**110 °C**	**120 °C**
A_1	15.7	27.26	23.9	3.67	36.4	17.45
t_1 (h)	3.11	5.07	0.006	0.2	3.79	0.06
A_2	5.6	6.94	16.69	20.87	2.22	38.64
t_2 (h)	0.018	0.013	4.89	7.29	0.33	6.38
Decay rate, k_1 ($1/t_1$) (1/h)	0.32	0.20	180.83	6.00	0.26	17.07
Decay rate, k_2 ($1/t_2$) (1/h)	56.52	78.62	0.20	0.14	2.98	0.16
Determination coefficient, R^2	0.995	0.975	0.970	0.986	0.996	0.943

As expected, the d_{33} values decreased faster with increasing heat treatment temperature. As seen from Table 7.3, no correlation between the decay rate (k_1) and the temperature was found. However, k_1 is always higher at 120 °C: 0.970 and 0.943 for N_2 and CO_2, respectively.

The exponential decay for both N_2 and CO_2 inflated samples was used to generate an Arrhenius equation as:

$$k = k_1 + k_2 = A\, exp(-\frac{E_a}{k_b T}) \qquad (7\text{-}3)$$

where A represents the probability of a decay interaction taking place with respect to temperature (T) and activation energy (E_a), while k_b is the Boltzmann constant. Thus, a system with higher activation energy has a lower tendency of charge decay. The activation energy also provides insights of the charge trapping inside the system. Therefore, using the data from Table 7.3, the E_a of N_2-inflated samples is 0.43 eV, while a value of 0.52 eV for CO_2-inflated ones indicating the better stability of the latter.

7.5 Conclusion

This study reports different inflation treatments performed on PVDF in both CO_2 and N_2 gases, where CO_2 treated samples yield ~30% higher piezoelectric d_{33} coefficient than the N_2 treated samples. Owing to better interaction of polar CO_2 with PVDF, especially at elevated temperatures, the number of thicker voids is larger in CO_2-inflated samples regardless of the inflation technique. Nevertheless, the d_{33} coefficient was maximized by GDE-V (in both gas treatments) where the elevated temperature from the onset of the experiment facilitated the gas permeation. Hence, a

maximum of 65% increase in sample thickness over the initial thickness and a corresponding maximum in d_{33} coefficient (327 pC/N) was obtained in CO_2-inflated cellular PVDF electret with GDE-V. Moreover, excellent short-term (up to 96 h) thermal stability was obtained in both cases, especially for CO_2-inflated samples. This was attributed to higher crystallinity degree and the presence of a larger amount of porosities. The interfaces obtained between small crystals, at the filler-polymer interface and also at the void-polymer in the samples act as charge trapping centers, which along with the space-charge in electrets improved charge stability. The results were fitted to an exponential decay function to extract temperature dependency for each showing that the CO_2 value is higher than for N_2 (0.52 vs 0.43 eV) confirmation of the better thermal stability for CO_2-inflated samples.

7.6 Acknowledgement

The authors acknowledge the technical support from Mr. Richard Silverwood (Polytechnique, Montreal) and Mrs. Claire Cerclé (Polytechnique, Montreal), as well as the financial support from FRQNT (Fond de Recherche du Québec en Nature et Technologie) and NSERC (Natural Sciences and Engineering Research Council of Canada).

7.7 Supporting information

Thermally Stable Cellular PVDF Ferroelectrets: Optimization of CO_2 Driven Inflation Process

Nusrat Jahan[1,2], Frej Mighri,[1,3], Denis Rodrigue[1,3], Abdellah Ajji[1,2]*

[1]CREPEC, Research center for high performance polymer and composite systems

[2]Department of Chemical Engineering, Polytechnique Montréal,
C.P. 6079, Montreal, QC, H3C 3A7, Canada

[3]Department of Chemical Engineering
Université Laval, Quebec, QC, G1V 0A6, Canada

7.7.1 Supporting information content

1. Supporting Figures
2. Film preparation and charaterization techniques

7.7.1.1 Film preparation

Pure PVDF, $CaCO_3$ and nanoclay were vacuum dried overnight at 70 °C before compounding. The polymer (PVDF) was fed from the main hopper using a volumetric feeder and the fillers ($CaCO_3$ and nanoclay) were introduced in the extruder using a high precision powder feeder. The materials were fed at a constant rate to maintain the specific composition. PVDF films with 40 parts (~ 30 wt.%) of $CaCO_3$ and 3 parts (~ 2.7 wt.%) of nanoclay were prepared using a tightly intermeshing co-rotating twin-screw extruder (for mixing), equipped with a typical compounding screw provided with two kneading block zones, fitted with a small pellets die and pelletizer. The pellets were then extruded again with the extruder end equipped with a slit die (20 cm × 1.8 mm) and a calendar (film forming). The extrudate was pulled by the calendar to prepare the film with a thickness in the range of 80-100 μm. Since the extrudate velocity at the die exit was constant, the draw ratio (the film thickness) was controlled by the pulling speed of the calendar rolls. Besides natural air cooling, a controllable air knife was installed at the die exit to supply sufficient air to the film surface. The film was prepared using a constant extruder speed of 100 rpm with a constant temperature profile in the compounding zone (195 °C).

7.7.1.2 Uniaxial stretching

The PVDF/$CaCO_3$/montmorillonite composite films were uniaxially stretched in the direction perpendicular to the extrusion direction using an Instron (ElectroPlus ™ E3000) instrument equipped with an environmental (heating) chamber and pneumatic grips of 1 kN. The samples were cut in rectangular shape (width of 4.5 cm and length of 1 cm = gage length). The temperature of the chamber was set to 90 °C, the stretching speed was fixed to 2.5 mm/min, and the stretching ratio (final length/initial length) was set to 5. To maintain the thermal equilibrium between the surface and inside the samples, an equilibration time of 8 min was applied before stretching. Finally, the stretched samples were cooled to room temperature in natural air. The thickness of stretched film ranges from 35-40 μm.

7.7.1.3 Gas diffusion expansion (GDE)

To obtain a lens-like cellular structure that make the film more compressible, and thus highly piezoelectric [17, 25, 72, 78], several inflation treatments were performed by combining the GDE (gas diffusion expansion) parameters (pressure, temperature and time). The pressure

treatment was performed in a closed vessel pressurized with pure nitrogen (CO_2) gas. The temperature treatment was carried out either in series or in parallel with the pressure treatment using an oil bath attached to the closed pressure vessel heating jacket. To achieve better N_2 transportation (combining both permeation and diffusion) into the films, the pressure was selected from 3 MPa up to 5 MPa and the temperature from room temperature to 140 °C which are well above the critical pressure and temperature of nitrogen (P_c = 3.4 MPa and T_c = 126.4 K) [154]. Since the melting temperature (T_m) of used PVDF is around 163°C and its glass transition temperature (T_g) is around -35°C, the selected temperature was high enough to ensure the chain mobility of PVDF to facilitate N_2 intrusion.

In GDE-II, pressure and temperature treatments were performed in series (Figure 1(II)). The samples were inflated at a constant pressure of 5 MPa and room temperature for 3 h followed by a temperature treatment at 115 °C for 2 h or 4 h keeping the pressure constant.

In GDE-III, the samples were treated at constant pressure (5 MPa) while the temperature was increased from 50 to 115 °C in four steps with a 2 h residence time for each step, except for the last one which lasted 4 h (Figure 1(III)).

In GDE-V, the inflation pressure was increased stepwise, starting from 3 MPa up to 5 MPa with a dwelling time of 2 h for the first two pressure levels and 4 h for the last one at 5 MPa. The whole experiment was performed at constant temperatures of 115, 130 or 140 °C, respectively (Figure 1(V)).

In GDE-VIII, the treatment time and pressure were set to 24 h and 5 MPa, respectively, only the inflation temperature was different; one at room temperature (GDE-VII) and the other at 50 °C (GDE-VIII) as shown in (Figure 1(VIII)).

At the end of each GDE procedure, the pressure was rapidly decreased to ambient and the samples were cooled down to room temperature. In general, the pressure treatment was aimed at saturating the voids with gas at higher pressure and the temperature treatment was intended to increase the gas transportation inside the voids by softening the polymer matrix as well as to stabilize the newly formed cellular structure.

A thickness tester (ProGage, Thwing-Albert Instrument Co., USA) was used to measure the change in sample thickness after each GDE procedures.

7.7.1.4 Scanning Electron Microscopy

The morphology of the cross-section of the films before and after GDE treatments was studied using a table top scanning electron microscope (TM3030 plus, Toshiba) without any metallic coating. The samples were prepared by cryogenic fracture in liquid nitrogen to have a neat fracture surface and the fracture was done in the stretching direction. For a complete study of the cellular structure including the void shape, height, size etc. by analyzing the obtained SEM images, a software package "ImageJ" was used.

7.7.1.5 Quasi-static piezoelectric coefficient (d_{33})

A quasi-static setup was used to measure the piezoelectric coefficient by applying a direct piezoelectric effect: a force was applied on the sample by placing a mass (m = 500 g) and by removing it [80]. The d_{33} value was then calculated as; $d_{33} = Q / F$, where Q denotes the accumulated charge on the electrodes due to the applied force. A parallel capacitor of 100 nF was connected to the grounded sample in parallel. Compared to the parallel capacitor, the capacitance of the sample is very small so that the accumulated charges on the sample electrode are entirely transferred to the parallel capacitor [167]. A static force of 500 g was initially applied on the sample for 8-10 minutes and after 10 s of load removal, the accumulated charge was measured using a NI-9239 data acquisition system attached to a USB carrier NI-9162 (National Instruments) connected to the capacitor in parallel and recorded using a LabVIEW interface. For each sample, the procedure was repeated 3-5 times and the average value is reported.

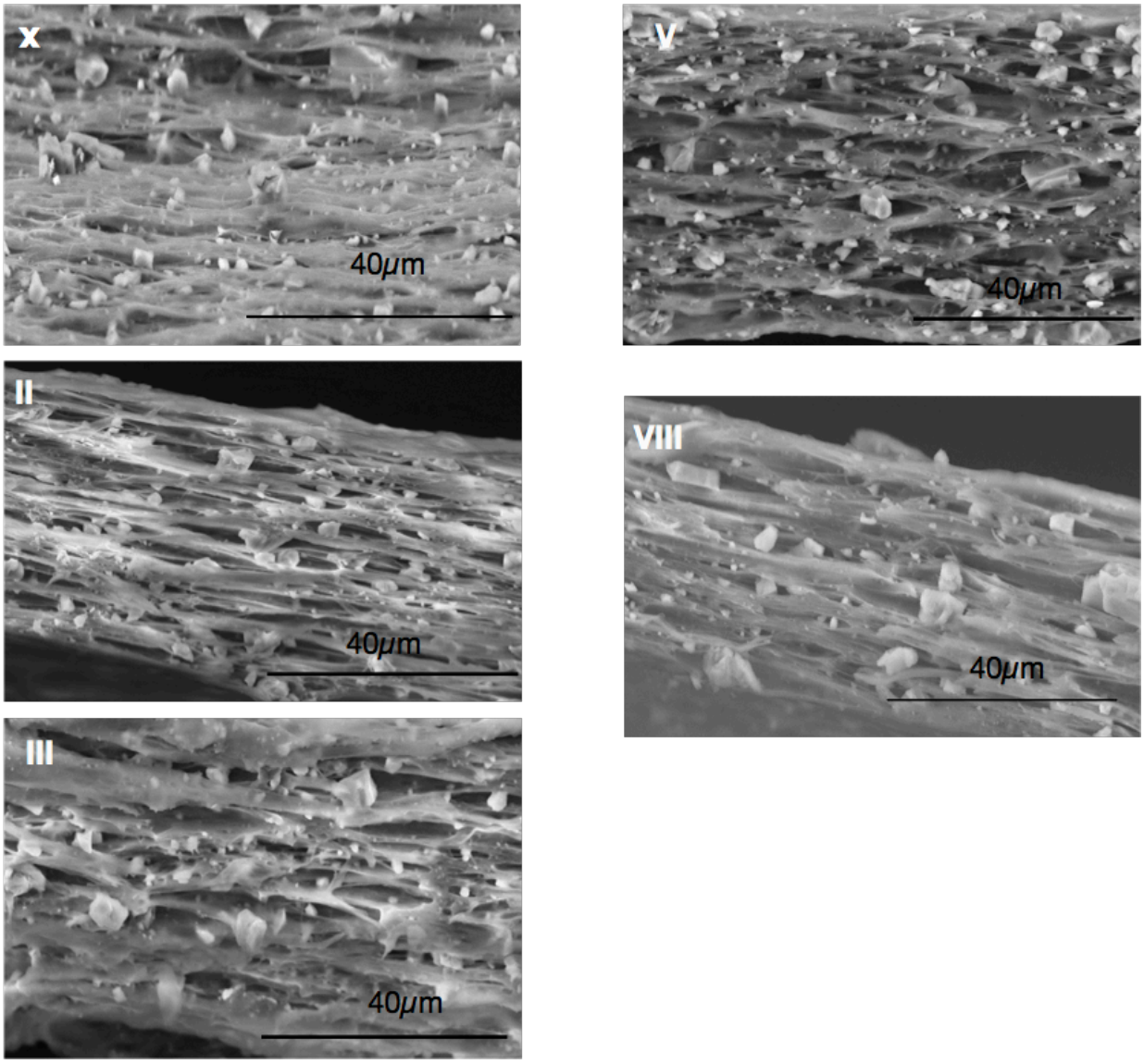

Figure S7-1: Large area view of the samples shown in Figure 7.2 in original manuscript.

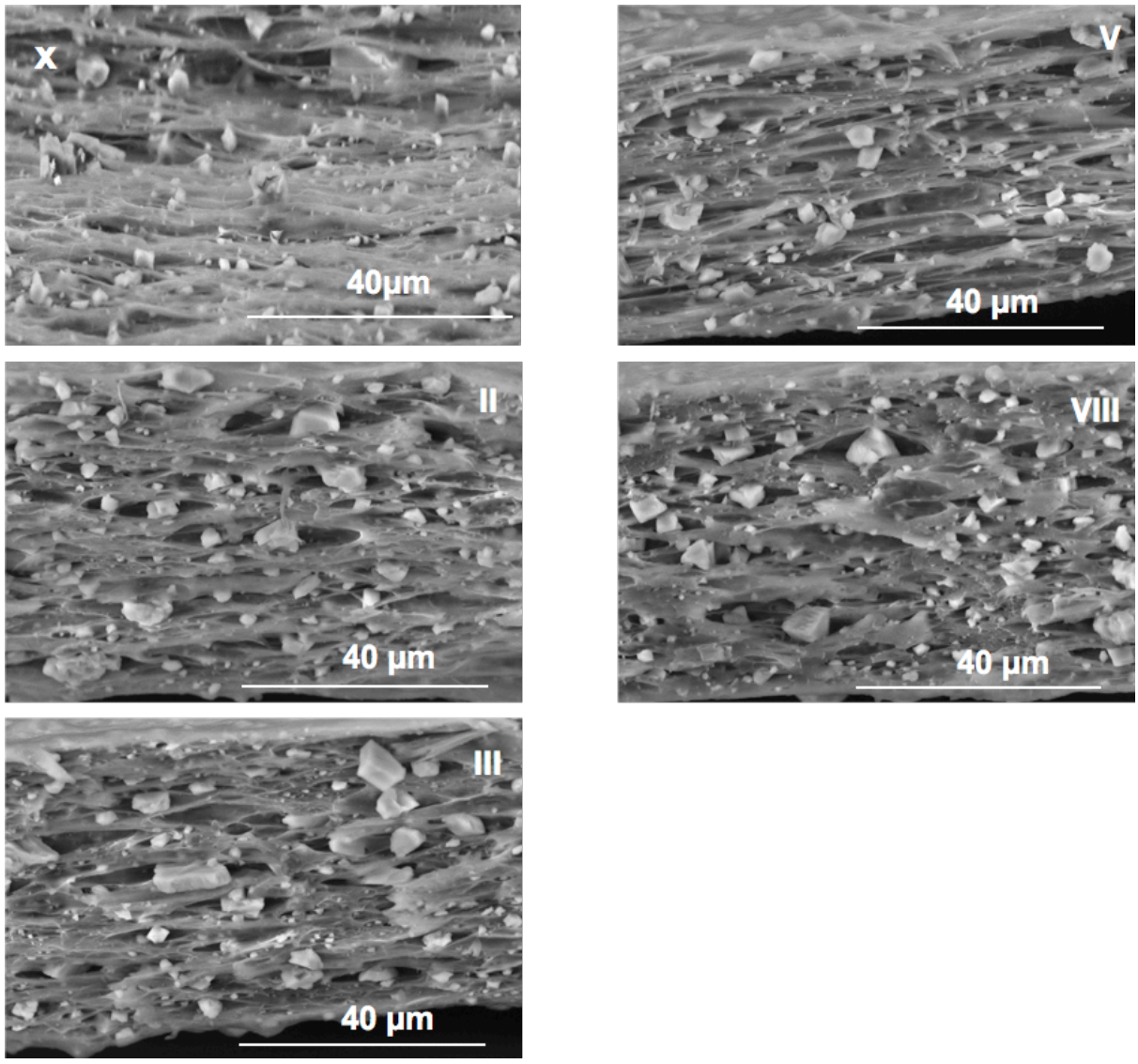

Figure S7-2: Large area micrograph of Figure 7.3 in the original manuscript.

CHAPTER 8 GENERAL DISCUSSION

In order to prepare commercial PVDF based piezoelectric materials, the materials have to be cost-effective, the manufacturing process has to be industrially feasible and the obtained piezoelectric response has to be strong and stable enough to be applied in various applications. To obtain a maximum piezoelectric response from PVDF, one must prepare the precursor film with the maximum amount of polar β phase, or in other words, the film must have the maximum amount of polarizable dipoles able of reorienting under an applied electric field (electrical poling/corona charging). It has already been confirmed by researchers that larger amount of β-PVDF can enhance the possibility of increased piezoelectric activity for PVDF based materials. However, the maximum attainable piezoelectric d_{33} coefficient for a system also depends on the degree of alignment of the randomly oriented dipoles (or dipole moment) under an applied electric field as well. It has been reported in the literature that rolling or stretching of PVDF films prior to electrical poling could facilitate dipole alignment. This is because the mechanical force induces preferential alignment of the polymer chain and thus the dipole moments in the oriented crystallites are most likely to be distributed in the direction perpendicular to the stretching direction. Furthermore, stretching can change the chain conformation from α to β-PVDF. Thus, the ideal piezoelectric PVDF polymer system would have larger amount of β phase oriented in the applied field direction (i.e. the sample thickness).

Several fillers such as $BaTiO_3$, PZT, CNT, gold and silver have been extensively reported in the literature to improve the β phase content of PVDF. However, these fillers are usually costly and, in some cases, hazardous. Moreover, the most common method of filler addition in the PVDF matrix is solvent/solution casting which sometimes results in structurally fragile films and is not industrially possible. Additionally, aligning the dipoles in solvent cast films is difficult leading to low d_{33} coefficient (20-34 pC/N), which is also in the range of d_{33} values obtained in other lab scale film preparation. Therefore, a lot of work has been done on cost-effective fillers such as organoclay reinforced PVDF films prepared by large scale melt mixing techniques. However, besides the difficulty of nanoclay dispersion in the PVDF matrix, the tendency to induce less piezoelectric γ phase and to form an inadequate amount of β-PVDF are few drawbacks of nanoclay doped PVDF systems.

Therefore, in the first phase of the study, various amounts of hybrid fillers (combination of micron size $CaCO_3$ and nanoclay) were added to PVDF via melt extrusion to prepare around 100 μm thick films. Both $CaCO_3$ and nanoclay are cost-effective fillers, easily available and several studies already exist in the literature reporting on their physical, chemical and manufacturing properties. The results obtained in this study showed that hybrid filler incorporation improves the amount of polar β-PVDF compared to pristine PVDF, PVDF/clay or PVDF/$CaCO_3$ films confirmed by FTIR and XRD. Moreover, with increasing $CaCO_3$ concentration in the hybrid filler, the amount of β-PVDF increased gradually. The crystallite size also decreased with increasing amount of $CaCO_3$ indicating a more uniform nucleation process influenced by $CaCO_3$. Additionally, stretching of the hybrid composite resulted in almost 100% β-PVDF regardless of the draw ratio, which is not the case for single filler systems. Based on these results, it was established that the polar groups on the montmorillonite clay surface play an important role in reorienting the polymer chains into the β-phase and the effect is stronger in the presence of micron size unmodified $CaCO_3$. Therefore, a synergistic effect was found for the hybrid filler system in enhanced β-PVDF content and the effect is more pronounced for stretched samples. Therefore, to observe the effect of the hybrid filler, mechanical stretching, crystallite size, as well as the amount of β-PVDF on the PVDF mechanical, electrical and piezoelectric properties have been investigated in this part of the study. The results showed that the tensile properties (tensile strength and elongation at break) decreased for PVDF hybrid composites due to the weak interaction between PVDF and unmodified $CaCO_3$. However, the Young's modulus remained almost constant irrespective of the filler concentration. It is worth mentioning that the elastic modulus has an inverse relationship with the piezoelectric d_{33} coefficient. The dielectric permittivity (ε_r) of the hybrid composites increased progressively with increasing filler content. The filler/polymer and amorphous-crystalline interfaces could act as charge trapping centers for the system and thus increasing the amount of filler can hinder the charge mobility and enhance the permittivity. Additionally, the micro filler ($CaCO_3$) does not conform to the PVDF chain length and enhances the chance of interfacial polarization. The smaller crystallites resulting from the addition of hybrid filler in PVDF again contributed in increasing ε_r since smaller crystallites are easier to switch or align under an applied electric field. Interestingly, the dielectric loss (tanδ) was also suppressed with increasing filler content, which is contrary to the main findings in the literature. Lower tanδ

is associated to the limited charge movement through the PVDF chain due to the presence of $CaCO_3$ and smaller interfaces from the smaller crystallites. Subsequent stretching of the hybrid PVDF composite films gradually decreased the ε_r value and increased tanδ with increasing draw ratio (R). Stretching creates voids in the sample and these voids can contribute in increasing the leakage current. The volume resistivity of the hybrid composites was sevenfold higher than the pristine PVDF system which indicated its better charge retention capability. Since voids in the PVDF films can raise their electrical conduction, stretched hybrid films showed slight but gradual decrease in volume resistivity. Finally, the piezoelectric d_{33} coefficient of hybrid composites increased with increasing amount of $CaCO_3$ compared to pristine PVDF or single filler system. However, the value is still quite low around 7 pC/N (maximum). Subsequent stretching significantly improved the d_{33} value of the hybrid composite to 30 pC/N. Besides the amount of β phase, the dipoles alignment play a major role in enhancing the d_{33} value. Since the dipoles are randomly oriented in extrusion cast PVDF films and the $CaCO_3$ filler can hinder their reorientation under an applied field, the d_{33} value is quite small. On the other hand, mechanical stretching of the extruded hybrid film mainly orients the crystallites and makes them easier to reorient in the next step of poling.

Ferroelectrets are a relatively new class of piezoelectric materials exhibiting excellent piezoelectric response and improved charge stability. The difference between ferroelectrics and ferroelectrets lies in their piezoelectric origin. While the piezoelectricity in ferroelectrets originates from the deformation of charged voids or in other words, from the change in dipole moment, ion displacement in the lattice is the reason for piezoelectricity in ferroelectric materials. Among the investigated polymers, fluoropolymers such as FEP and PTFE based ferroelectrets are good choices because of their strong piezoelectric coefficient and excellent charge retention ability arising from their chemical structure containing fluorine atoms. However, their cost and processing using conventional manufacturing techniques (i.e. melt extrusion) is a challenge because of their very high melt viscosity and elevated processing temperature. Therefore, PVDF was chosen as the base material containing the alternating $-CF_2$ group to prepare ferroelectrets with excellent chemical, mechanical and electrical properties. Preparing a ferroelectret consists of three main steps: (a) creating a cellular structure in the polymer film by physical foaming or by stretching a film having fillers already in the polymer, (b) controlling the voids geometry by high pressure gas inflation and heat treatment to optimize its compressibility, and (c) electrically charging the film to create dipoles

in the voids followed by metallization on both sides. Optimization of these steps is important because the final piezoelectric d_{33} coefficient depends on their combined effect.

Inflation is one of the most important steps to optimize the cellular structure and to maximize the film compressibility by controlling the void geometry. It is especially important for uniaxially stretched films because the degree of stretching is limited in uniaxial stretching compared to a biaxial stretching setup. Among the inflation parameters, pressure, temperature and time are the system variables mainly affecting the inflation level. The influence of the type of gas (neutral or polar), the interaction of the permeating gas with the polymer chain and the way to apply the pressure and temperature are especially complex for polar polymers like PVDF. While the inflation process involves the penetration of high pressure gas into the voids inside the film, to understand this process, interaction of the gas with the polymer is crucial to optimize the inflation process. In this part of the study, the piezoelectric response of cellular PVDF ferroelectrets was investigated by optimizing the inflation procedure using two different inflation gases and various inflation procedures. Each inflation procedure varied in the way the pressure and/or temperature treatment was performed. For instance, pressure was applied either directly or in step-wise manner with either parallel or subsequent heat treatment for a different time period. The heat treatment is particularly important to stabilize the inflated cellular structure. It was also found that the heat treatment during high pressure inflation also helps in gas penetration and thus improves the inflation level. Since PVDF is a polar polymer, two different types of gas were chosen for inflation: one neutral (N_2) and the other polar (CO_2). The inflation performance was evaluated from their thickness change and morphology evolution. The result also showed that because of its polar nature, CO_2 has a stronger interaction with PVDF than N_2 and thus a higher permeation in the cellular film regardless of the inflation strategy. Therefore, the overall d_{33} coefficient is higher for CO_2–inflated samples in every inflation strategy studied. Moreover, when the pressure is applied in a stepwise manner at a temperature close to the PVDF melting point, gas penetration was easier and increased the inflation level for both gases. On the other hand, direct application of pressure comes with the possibility of void collapsing leading to very low inflation levels. The ultimate piezoelectric d_{33} coefficient was higher for CO_2 inflated samples for all the inflation strategies studied as compared to the N_2-inflated films. Also, the ferroelectrets showed very strong thermal stability up to 120 °C for both gases. The degree of crystallinity of CO_2 inflated samples are higher than in N_2 inflated samples. The interfaces offered by crystalline-amorphous, air-polymer and

filler-polymer act as charge trapping centers. Besides the inherent charge retention ability of PVDF arising from its chain conformation, the interfaces contribute in increasing the charge stability by trapping these charges. The more the interfaces and the deeper the trapping, the better is the charge stability in the system.

CHAPTER 9 CONCLUSION AND RECOMMENDATIONS

9.1 Conclusions

This dissertation investigated the piezoelectric properties of hybrid filler (combination of micro-$CaCO_3$ and montmorillonite clay) reinforced poly(vinylidene fluoride) (PVDF) films prepared through cast extrusion. To this end, two types of piezoelectric PVDF films were prepared: solid ferroelectric films where the piezoelectricity originates from the molecular dipoles (β-PVDF) and cellular films with internal dipoles into the voids (ferroelectret).

In the first phase of the study, we examined the effect of filler content and subsequent mechanical stretching (drawing ratio, R) on the polar β crystalline phase formation in PVDF hybrid composites prepared through cast film extrusion. The amount of $CaCO_3$ particles was varied in the range of 30-40 parts with 3 parts of clay and R was selected from 4-5. Stretching of composite films at 90°C to a draw ratio of 4 to 5 was shown to be an effective way to maximize the β phase in hybrid films. The result showed that the amount of β phase gradually increased in both un-stretched and stretched samples with increasing $CaCO_3$ content and R value. For instance, a maximum of 80% and almost 100% β phase was observed in unstretched (as extruded) and stretched samples having 40 parts of $CaCO_3$ respectively. Moreover, the degree of crystallinity decreased with increasing $CaCO_3$ concentration due to the increasing nucleation events, whereas it increased gradually with increasing draw ratio (R) for the same samples. Therefore, the crystallinity and amount of β phase have an inverse relationship in un-stretched samples while having a relatively direct relationship in stretched samples with respect to the $CaCO_3$ content.

After obtaining almost 100% β phase, the mechanical, dielectric, electrical and piezoelectric properties of these PVDF based hybrid nanocomposites were investigated in this next step of the study. Due to the enhanced β phase crystallinity, reduced crystallite size and oriented structure, hybrid nanocomposites yielded the highest piezoelectric response (7.4 pC/N for 100-40-3) among the extruded and unstretched composites. The best d_{33} value (30.6 pC/N) was obtained when the samples were stretched to a draw ratio of 5. This could be attributed to the increased crystallinity along with the occurrence of almost 100% β-PVDF and dipole orientation. Since mechanical stretching to an optimum condition before corona charging could reorient the dipole to some extent, a larger d_{33} value for stretched sample is expected. Similarly, the hybrid

nanocomposites exhibited the most enhanced dielectric properties compared to other samples and mechanical stretching seemingly has a positive effect in enhancing the electrical properties of hybrid samples. As expected, the dielectric constant increased gradually with increasing filler content while the loss tangent decreased. Even though the dielectric properties increased for PVDF/clay film after stretching at various draw ratio, they were significantly mower for the hybrid composite (100-40-3) probably due to the presence of higher void content, which presumably caused electrical conduction under the applied field.

Ferroelectrets are able of exhibiting excellent piezoelectric response and strong thermal charge stability depending on the base polymer. Highly compressible films exhibit enhanced piezoelectricity and their compressibility is controlled by the size, shape and amount of voids. Therefore, adjusting the cellular structure of polymer films by high pressure gas inflation is one of the crucial steps in ferroelectret preparation. In this phase of the study, the effect of various inflation techniques on the piezoelectric properties of cellular PVDF ferroelectrets were investigated. The pressure was applied either directly or on a step-wise manner, either in parallel or subsequently with a temperature treatment. The result showed that the inflation treatment with stepwise-pressure application in an isothermal condition were more efficient than the direct pressure application in terms of increasing the void thickness and leading to higher d_{33}. For example, the piezoelectric d_{33} coefficient for a stepwise pressure application ranged from 137 to 251 pC/N depending on the treatment temperature, while it was only 45-52 pC/N for direct pressure treatments in N_2 gas. Also, higher treatment temperature (> 115 °C) applied at the beginning of the treatment yielded larger amount of voids with higher thickness by increasing the gas transport and thus created larger dipoles during corona charging. For instance, stepwise pressure application at a constant temperature of 130 °C produced the maximum d_{33} coefficient of 251 pC/N, while the one inflated at 115 °C gave 137 pC/N. While it is customary to study the effect of pressure, temperature and time on the inflation level, the type of inflation gases has far more influence on the ultimate properties of cellular films. In this section of the study, the effect of both CO_2 and N_2 gases on the inflation level of cellular PVDF films has been compared. The results showed that the inflation treatments performed in CO_2 yielded up to 30% higher piezoelectric d_{33} coefficient than N_2 treated samples. Owing to better interaction of polar CO_2 with PVDF, especially at elevated temperatures, the number of thicker voids was larger in CO_2-inflated samples regardless of the inflation technique. Hence, a maximum increase in d_{33} coefficient to 327 pC/N was obtained in CO_2-inflated

cellular PVDF electrets compared to the 251 pC/N in corresponding N_2 treated samples. Moreover, excellent short term (up to 96 h) thermal stability was obtained in both cases especially for CO_2-inflated samples, which is attributed to their higher degree of crystallinity and the presence of larger amount of porosity. The interfaces obtained between fine crystals, at filler-polymer and also at air-polymer interfaces in the samples act as charge trapping centers, which along with the inherent charge retention capability of PVDF enhances charge stability. It is expected that this study will be a guideline for developing commercially viable and low cost piezoelectric materials.

9.2 Original Contribution

The key novelty of this study lies in using a cost-effective hybrid filler in improving the piezoelectric response of ferroelectric β-PVDF and developing a new ferroelectret from the same filler/polymer system with enhanced properties.

In view of the obtained experimental results, it was found that besides improving the piezoelectric response of PVDF, hybrid filler enhanced the dielectric properties and the volume resistivity of PVDF films as well. Moreover, subsequent mechanical stretching further improved the piezoelectric properties.

A new ferroelectret based on PVDF hybrid composite was developed and characterized with strong piezoelectric response and excellent thermal stability. Most importantly, the combination of these properties was obtained in a system prepared via the most commonly studied stretching-inflation-charging method.

Little attention has been paid in the literature to the optimization of the inflation level to prepare cellular polymer films. In particular, the nature of the inflation gas, the interaction of the gas with the polymer, and various inflation strategies are few of the inflation parameters that have hardly been investigated in the literature. In this part of the study, these inflation parameters have been investigated to prepare the cellular structure of PVDF and finally their effect was observed on the piezoelectric d_{33} coefficient of PVDF ferroelectret and on its thermal stability.

Taking all these aspects into consideration, the investigated piezoelectric PVDF films will be a choice of material for advanced piezoelectric applications.

9.3 Recommendation

The following topics could be studied for future work:

- The working mechanism of hybrid filler in enhancing the properties of ferroelectric PVDF needs to be investigated.
- Further research is necessary to improve and optimize the cellular structure of the ferroelectrets. Under the studied experimental conditions, the average void height remains in between 2-3 μm, which could be increased and optimized by changing the inflation parameters. Various combinations of inflation parameters could be used to obtain an optimized cellular structure. Moreover, by using fillers with more uniform size range, the cellular structure could be more uniform and therefore making the system possible for industrial production in mass volume.
- Further characterizations can be performed such as measuring surface potential, degree of porosity, thermally stimulated discharge (TSD) to choose the working temperature and polarization characteristics, as well as accumulate information on further improving the piezoelectric response.
- Piezoelectric properties of both PVDF based ferroelectrics and ferroelectrets could be investigated under various environmental conditions such as humid air, salt water and under irradiation to find their possible applications and limitations.

REFERENCES

[1] J. Harrison and Z. Ounaies, *Piezoelectric polymers*: John Wiley & Sons, Inc., 2002.

[2] K. S. Ramadan, D. Sameoto, and S. Evoy, "A review of piezoelectric polymers as functional materials for electromechanical transducers," *Smart Materials and Structures,* vol. 23, p. 033001, 2014.

[3] S. A. Wilson, R. P. Jourdain, Q. Zhang, R. A. Dorey, C. R. Bowen, M. Willander*, et al.*, "New materials for micro-scale sensors and actuators: An engineering review," *Materials Science and Engineering: R: Reports,* vol. 56, pp. 1-129, 2007.

[4] H. Kawai, "Piezoelectricity of poly(vinylidene fluoride)," *Japan J. Appl. Phys.,* vol. 8, pp. 975-976, 1969.

[5] S. D. Vacche, F. Oliveira, Y. Leterrier, V. Michaud, D. Damjanovic, and J.-A. E. Månson, "The effect of processing conditions on the morphology, thermomechanical, dielectric, and piezoelectric properties of P(VDF-TrFE)/$BaTiO_3$ composites," *J. Mater. Sci.,* vol. 47, pp. 4763-4774, 2012.

[6] J. Chang, Y. Shen, X. Chu, X. Zhang, Y. Song, Y. Lin*, et al.*, "Large d33 and enhanced ferroelectric/dielectric properties of poly(vinylidene fluoride)-based composites filled with Pb(Zr0.52Ti0.48)O3 nanofibers," *RSC Adv.,* vol. 5, pp. 51302-51307, 2015.

[7] Y. J. Choi, M.-J. Yoo, H.-W. Kang, H.-G. Lee, S. H. Han, and S. Nahm, "Dielectric and piezoelectric properties of ceramic-polymer composites with 0-3 connectivity type," *J. Electroceram.,* vol. 30, pp. 30-35, 2013.

[8] L. Priya and J. Jog, "Intercalated poly (vinylidene fluoride)/clay nanocomposites: structure and properties," *J. Polym. Sci., Part B: Polym. Phys.,* vol. 41, pp. 31-38, 2003.

[9] N. Renukappa, R. Chikkakuntappa, and N. S. Kunigal, "Montmorillonite nanoclay filler effects on electrical conductivity, thermal and mechanical properties of epoxy based nanocomposites," *Polym. Eng. Sci*., vol. 51, pp. 1827-1836, 2011.

[10] L. Priya and J. Jog, "Poly (vinylidene fluoride)/clay nanocomposites prepared by melt intercalation: Crystallization and dynamic mechanical behavior studies," *J. Polym. Sci., Part B: Polym. Phys.,* vol. 40, pp. 1682-1689, 2002.

[11] T. U. Patro, M. V. Mhalgi, D. Khakhar, and A. Misra, "Studies on poly (vinylidene fluoride)-clay nanocomposites: effect of different clay modifiers," *Polymer,* vol. 49, pp. 3486-3499, 2008.

[12] J. Buckley, P. Cebe, D. Cherdack, J. Crawford, B. S. Ince, M. Jenkins*, et al.*, "Nanocomposites of poly (vinylidene fluoride) with organically modified silicate," *Polymer,* vol. 47, pp. 2411-2422, 2006.

[13] F.-A. He, K. Lin, D.-L. Shi, H.-J. Wu, H.-K. Huang, J.-J. Chen*, et al.*, "Preparation of organosilicate/PVDF composites with enhanced piezoelectricity and pyroelectricity by stretching," *Compos. Sci. Technol.,* vol. 137, pp. 138-147, 12/12/ 2016.

[14] Y. Zhang, S. Jiang, Y. Yu, G. Xiong, Q. Zhang, and G. Guang, "Phase transformation mechanisms and piezoelectric properties of poly (vinylidene fluoride)/montmorillonite composite," *J. Appl. Polym. Sci.,* vol. 123, pp. 2595-2600, 2012.

[15] S. Bauer and F. Bauer, "Piezoelectric polymers and their applications," in *Piezoelectricity*, ed: Springer, 2008, pp. 157-177.

[16] M. Paajanen, M. Wegener, and R. Gerhard-Multhaupt, "Understanding the role of the gas in the voids during corona charging of cellular electret films-a way to enhance their piezoelectricity," *Journal of Physics D: Applied Physics,* vol. 34, p. 2482, 2001.

[17] M. Sborikas and M. Wegener, "Cellular-foam polypropylene ferroelectrets with increased film thickness and reduced resonance frequency," *Applied Physics Letters,* vol. 103, p. 252901, 2013.

[18] M. Wegener, W. Wirges, J. Fohlmeister, B. Tiersch, and R. Gerhard-Multhaupt, "Two-step inflation of cellular polypropylene films: void-thickness increase and enhanced electromechanical properties," *Journal of Physics D: Applied Physics,* vol. 37, p. 623, 2004.

[19] M. Wegener, W. Wirges, R. Gerhard-Multhaupt, M. Dansachmüller, R. Schwödiauer, S. Bauer-Gogonea*, et al.*, "Controlled inflation of voids in cellular polymer ferroelectrets: Optimizing electromechanical transducer properties," *Applied Physics Letters,* vol. 84, pp. 392-394, 2004.

[20] M. Wegener, W. Wirges, R. Gerhard-Multhaupt, M. Paajanen, H. Minkkinen, and J. Raukola, "Enhancing the cellular structure and the electromechanical response of ferroelectrets-gas diffusion expansion of voided polypropylene films," in *Electrical Insulation and Dielectric Phenomena, 2003. Annual Report. Conference on*, 2003, pp. 36-39.

[21] J. Raukola, N. Kuusinen, and M. Paajanen, "Cellular electrets-from polymer granules to electromechanically active films," in *Electrets, 2002. ISE 11. Proceedings. 11th International Symposium on*, 2002, pp. 195-198.

[22] J. I. Raukola, A new technology to manufacture polypropylene foam sheet and biaxially oriented foam film: Technical Research Centre of Finland, 1998.

[23] M. Wegener and S. Bauer, "Microstorms in cellular polymers: A route to soft piezoelectric transducer materials with engineered macroscopic dipoles," *ChemPhysChem,* vol. 6, pp. 1014-1025, 2005.

[24] M. Wegener, M. Paajanen, O. Voronina, R. Schulze, W. Wirges, and R. Gerhard-Multhaupt, "Voided cyclo-olefin polymer films: Ferroelectrets with high thermal stability," in *Electrets, 2005. ISE-12. 2005 12th International Symposium on*, 2005, pp. 47-50.

[25] M. Wegener, W. Wirges, J. Dietrich, and R. Gerhard-Multhaupt, "Polyethylene terephthalate (PETP) foams as ferroelectrets," in *Electrets, 2005. ISE-12. 2005 12th International Symposium on*, 2005, pp. 28-30.

[26] M. Wegener, W. Wirges, and R. Gerhard-Multhaupt, "Piezoelectric Polyethylene Terephthalate (PETP) foams-specifically designed and prepared ferroelectret films," *Advanced Engineering Materials,* vol. 7, pp. 1128-1131, 2005.

[27] W. Wirges, M. Wegener, O. Voronina, L. Zirkel, and R. Gerhard-Multhaupt, "Optimized preparation of elastically soft, highly piezoelectric, cellular ferroelectrets from nonvoided poly (ethylene terephthalate) films," *Advanced Functional Materials,* vol. 17, pp. 324-329, 2007.

[28] O. Voronina, M. Wegener, W. Wirges, R. Gerhard, L. Zirkel, and H. Münstedt, "Physical foaming of fluorinated ethylene-propylene (FEP) copolymers in supercritical carbon dioxide: single-film fluoropolymer piezoelectrets," *Applied Physics A: Materials Science & Processing,* vol. 90, pp. 615-618, 2008.

[29] Z. L. Sun, X. Q. Zhang, G. X. Cao, K. X. Lou, and Z. F. Xia, "Performance of Piezoelectrets Made of Non-Porous Polytetrafluoroethylene and Fluoroethylenepropylene Layers," in *Materials Science Forum*, 2011, pp. 343-347.

[30] P. Fang, "Preparation and investigation of polymer-foam films and polymer-layer systems for ferroelectrets," PhD Doctoral dissertaion, University of Potsdam, 2010.

[31] Q. Qin, Advanced mechanics of piezoelectricity: Springer Science & Business Media, 2012.

[32] D. Damjanovic, "Ferroelectric, dielectric and piezoelectric properties of ferroelectric thin films and ceramics," *Reports on Progress in Physics,* vol. 61, p. 1267, 1998.

[33] J. A. Gonzalo and B. Jiménez, *Ferroelectricity: The Fundamentals Collection*: John Wiley & Sons, 2008.

[34] S. R. Anton and H. A. Sodano, "A review of power harvesting using piezoelectric materials (2003–2006)," *Smart materials and Structures,* vol. 16, pp. R1-R21, 2007.

[35] A. Andrusyk, "Piezoelectric effect in Rochelle salt," in *Ferroelectrics-Physical Effects*, ed: InTech, 2011, p. 195.

[36] A. d. Santos, W. Yaegashi, R. Marcon, B. Li, R. Gelamo, L. Cardoso*, et al.*, "Rochelle salt piezoelectric coefficients obtained by x-ray multiple diffraction," *Journal of Physics: Condensed Matter,* vol. 13, p. 10497, 2001.

[37] P. Martins, A. Lopes, and S. Lanceros-Mendez, "Electroactive phases of poly (vinylidene fluoride): determination, processing and applications," *Prog. Polym. Sci.,* vol. 39, pp. 683–706, 2014.

[38] H.-J. Ye, L. Yang, W.-Z. Shao, S.-B. Sun, and L. Zhen, "Effect of electroactive phase transformation on electron structure and dielectric properties of uniaxial stretching poly (vinylidene fluoride) films," *RSC Adv.,* vol. 3, pp. 23730-23736, 2013.

[39] H. M. Correia and M. M. Ramos, "Quantum modelling of poly (vinylidene fluoride)," *Comput. Mater. Sci.,* vol. 33, pp. 224-229, 2005.

[40] A. Lopes, C. M. Costa, C. Tavares, I. Neves, and S. Lanceros-Mendez, "Nucleation of the electroactive γ phase and enhancement of the optical transparency in low filler content poly (vinylidene)/clay nanocomposites," *J. Phys. Chem. C,* vol. 115, pp. 18076-18082, 2011.

[41] S. J. Kang, Y. J. Park, J. Sung, P. S. Jo, C. Park, K. J. Kim*, et al.*, "Spin cast ferroelectric beta poly (vinylidene fluoride) thin films via rapid thermal annealing," *Applied Physics Letters,* vol. 92, p. 012921, 2008.

[42] A. Salimi and A. Yousefi, "Conformational changes and phase transformation mechanisms in PVDF solution-cast films," *J. Polym. Sci., Part B: Polym. Phys.,* vol. 42, pp. 3487-3495, 2004.

[43] A. Salimi and A. Yousefi, " FTIR studies of β-phase crystal formation in stretched PVDF films," *Polym. Test.,* vol. 22, pp. 699-704, 2003.

[44] X.-Z. Chen, X. Li, X.-S. Qian, S. Wu, S.-G. Lu, H.-M. Gu*, et al.*, "A polymer blend approach to tailor the ferroelectric responses in P(VDF–TrFE) based copolymers," *Polymer,* vol. 54, pp. 2373-2381, 2013.

[45] B. Neese, Y. Wang, B. Chu, K. Ren, S. Liu, Q. Zhang*, et al.*, "Piezoelectric responses in poly (vinylidene fluoride/hexafluoropropylene) copolymers," *Applied physics letters,* vol. 90, p. 242917, 2007.

[46] Z. Li, Y. Wang, and Z.-Y. Cheng, "Electromechanical properties of poly (vinylidene-fluoride-chlorotrifluoroethylene) copolymer," *Applied physics letters,* vol. 88, p. 062904, 2006.

[47] L. Yang, H. Ji, K. Zhu, J. Wang, and J. Qiu, "Dramatically improved piezoelectric properties of poly(vinylidene fluoride) composites by incorporating aligned TiO_2@MWCNTs," *Compos. Sci. Technol.,* vol. 123, pp. 259-267, 2/8/ 2016.

[48] T. U. Patro, M. V. Mhalgi, D. V. Khakhar, and A. Misra, "Studies on poly(vinylidene fluoride)–clay nanocomposites: Effect of different clay modifiers," *Polymer,* vol. 49, pp. 3486-3499, 7/28/ 2008.

[49] L. Priya and J. Jog, "Polymorphism in intercalated poly (vinylidene fluoride)/clay nanocomposites," *J. Appl. Polym. Sci.,* vol. 89, pp. 2036-2040, 2003.

[50] J.-J. Wang, T.-H. Hsu, C.-N. Yeh, J.-W. Tsai, and Y.-C. Su, "Piezoelectric polydimethylsiloxane films for MEMS transducers," *Journal of Micromechanics and Microengineering,* vol. 22, p. 015013, 2011.

[51] R. Gregorio Jr and E. Ueno, "Effect of crystalline phase, orientation and temperature on the dielectric properties of poly (vinylidene fluoride)(PVDF)," *Journal of Materials Science,* vol. 34, pp. 4489-4500, 1999.

[52] V. Sencadas, R. Gregorio Filho, and S. Lanceros-Mendez, "Processing and characterization of a novel nonporous poly(vinilidene fluoride) films in the β phase," *Journal of Non-Crystalline Solids,* vol. 352, pp. 2226-2229, 7/1/ 2006.

[53] A. Salimi and A. A. Yousefi, "Analysis Method: FTIR studies of β-phase crystal formation in stretched PVDF films," *Polymer Testing,* vol. 22, pp. 699-704, 9// 2003.

[54] V. Sencadas, R. Gregorio Jr, and S. Lanceros-Méndez, "α to β phase transformation and microestructural changes of PVDF films induced by uniaxial stretch," *J. Macromol. Sci., Part B: Phys.,* vol. 48, pp. 514-525, 2009.

[55] F. Wang, P. Frübing, and R. Gerhard, "Influence of uniaxial stretching rate and electric poling on crystalline phase transitions in poly (vinylidene fluoride) films," in *Solid Dielectrics (ICSD), 2010 10th IEEE International Conference on*, 2010, pp. 1-4.

[56] E. Fukada, "History and recent progress in piezoelectric polymers," *Ultrasonics, Ferroelectrics and Frequency Control, IEEE Transactions on,* vol. 47, pp. 1277-1290, 2000.

[57] B. Ameduri, "From Vinylidene Fluoride (VDF) to the Applications of VDF-Containing Polymers and Copolymers: Recent Developments and Future Trends†," *Chem. Rev,* vol. 109, pp. 6632-6686, 2009.

[58] J. Gomes, J. S. Nunes, V. Sencadas, and S. Lanceros-Mendez, "Influence of the β-phase content and degree of crystallinity on the piezo- and ferroelectric properties of poly(vinylidene fluoride)," *Smart Mater. Struct.,* vol. 19, 2010.

[59] R. S. Dahiya, D. Cattin, A. Adami, C. Collini, L. Barboni, M. Valle*, et al.*, "Towards tactile sensing system on chip for robotic applications," *Sensors Journal, IEEE,* vol. 11, pp. 3216-3226, 2011.

[60] Y. Wu, S. L. Hsu, C. Honeker, D. J. Bravet, and D. S. Williams, "The role of surface charge of nucleation agents on the crystallization behavior of poly (vinylidene fluoride)," *The Journal of Physical Chemistry B,* vol. 116, pp. 7379-7388, 2012.

[61] F. Sadeghi and A. Ajji, "Study of crystal structure of (polyvinylidene fluoride/clay) nanocomposite films: effect of process conditions and clay type," *Polym. Eng. Sci.,* vol. 49, pp. 200-207, 2009.

[62] H. J. Ye, W. Z. Shao, and L. Zhen, "Crystallization kinetics and phase transformation of poly (vinylidene fluoride) films incorporated with functionalized $BaTiO_3$ nanoparticles," *J. Appl. Polym. Sci.,* vol. 129, pp. 2940-2949, 2013.

[63] S. Manna, S. K. Batabyal, and A. K. Nandi, "Preparation and characterization of silver-poly (vinylidene fluoride) nanocomposites: Formation of piezoelectric polymorph of poly (vinylidene fluoride)," *J. Phys. Chem. B,* vol. 110, pp. 12318-12326, 2006.

[64] D. Mandal, K. Henkel, and D. Schmeißer, "The electroactive β-phase formation in Poly (vinylidene fluoride) by gold nanoparticles doping," *Materials Letters,* vol. 73, pp. 123-125, 2012.

[65] P. Martins, C. Caparros, R. Gonçalves, P. Martins, M. Benelmekki, G. Botelho, et al., "Role of nanoparticle surface charge on the nucleation of the electroactive β-poly (vinylidene fluoride) nanocomposites for sensor and actuator applications," *The Journal of Physical Chemistry C,* vol. 116, pp. 15790-15794, 2012.

[66] J. K. Nelson and J. C. Fothergill, "Internal charge behaviour of nanocomposites," *Nanotechnology,* vol. 15, p. 586, 2004.

[67] G. Sessler and J. West, "Self-biased condenser microphone with high capacitance," *The Journal of the Acoustical Society of America,* vol. 34, pp. 1787-1788, 1962.

[68] R. Gerhard-Multhaupt, "Less can be more. Holes in polymers lead to a new paradigm of piezoelectric materials for electret transducers," *IEEE Transactions on Dielectrics and Electrical Insulation,* vol. 9, pp. 850-859, 2002.

[69] M. Paajanen, J. Lekkala, and K. Kirjavainen, "ElectroMechanical Film (EMFi)—a new multipurpose electret material," *Sensors and Actuators A: Physical,* vol. 84, pp. 95-102, 2000.

[70] X. Zhang, J. Hillenbrand, and G. Sessler, "Improvement of piezoelectric activity of cellular polymers using a double-expansion process," *Journal of Physics D: Applied Physics,* vol. 37, p. 2146, 2004.

[71] X. Qiu, Z. Xia, and F. Wang, "Piezoelectricity of single-and multi-layer cellular polypropylene film electrets," *Frontiers of Materials Science in China,* vol. 1, pp. 72-75, 2007.

[72] A. Mohebbi, F. Mighri, A. Ajji, and D. Rodrigue, "Polymer ferroelectret based on polypropylene foam: Piezoelectric properties improvement using post-processing thermomechanical treatment," *Journal of Applied Polymer Science,* vol. 134, 2017.

[73] H. Gilbert-Tremblay, F. Mighri, and D. Rodrigue, "Morphology development of polypropylene cellular films for piezoelectric applications," *Journal of Cellular Plastics,* p. 0021955X12443687, 2012.

[74] E. Tuncer and M. Wegener, "Elastic properties of highly anisotropic thin poly (propylene) foams," *Materials Letters,* vol. 58, pp. 2815-2818, 2004.

[75] J. G. Leonhartsberger, H. Salhofer, R. Schwödiauer, S. Bauer-Gogonea, S. Bauer, R. Forstner, *et al.*, "Capacitance dilatometry for the in-situ controlled expansion process of cellular polymer-filler composites (ferroelectrets)," *Ferroelectrics,* vol. 331, pp. 181-187, 2006.

[76] A. Qaiss, H. Saidi, O. Fassi-Fehri, and M. Bousmina, "Cellular polypropylene based piezoelectric films," *Polymer Engineering & Science,* vol. 52, pp. 2637-2644, 2012.

[77] B. Flaconneche, J. Martin, and M. Klopffer, "Permeability, diffusion and solubility of gases in polyethylene, polyamide 11 and poly (vinylidene fluoride)," *Oil & Gas Science and Technology,* vol. 56, pp. 261-278, 2001.

[78] M. Paajanen, H. Minkkinen, and J. Raukola, "Gas diffusion expansion-increased thickness and enhanced electromechanical response of cellular polymer electret films," in *Electrets, 2002. ISE 11. Proceedings. 11th International Symposium on*, 2002, pp. 191-194.

[79] X. Zhang, J. Hillenbrand, and G. M. Sessler, "Piezoelectric d_{33} coefficient of cellular polypropylene subjected to expansion by pressure treatment," *Applied Physics Letters,* vol. 85, pp. 1226-1228, 2004.

[80] X. Zhang, J. Hillenbrand, G. Sessler, S. Haberzettl, and K. Lou, "Fluoroethylenepropylene ferroelectrets with patterned microstructure and high, thermally stable piezoelectricity," *Appl. Phys. A,* vol. 107, pp. 621-629, 2012.

[81] E. Audet, F. Mighri, D. Rodrigue, and A. Ajji, "Effect of Biaxial Stretching Temperature and Gas Diffusion Expansion on Cellular Morphology of PP/$CaCO_3$ and PP/talc Cellular Films," *Cellular Polymers,* vol. 34, p. 233, 2015.

[82] H. Gilbert-Tremblay, F. Mighri, and D. Rodrigue, "Morphology development of polypropylene cellular films for piezoelectric applications," *Journal of Cellular Plastics,* vol. 48, pp. 341-354, 2012.

[83] F. Camacho González, "Charge-Storage mechanisms in polymer electrets," Doctor in Philosophy (PhD) Doctoral dissertation, University of Postdam, 2006.

[84] G. Sessler, J. West, and G. Gerhard, "High-resolution laser-pulse method for measuring charge distributions in dielectrics," *Physical Review Letters,* vol. 48, p. 563, 1982.

[85] A. Mellinger, M. Wegener, W. Wirges, and R. Gerhard-Multhaupt, "Thermally stable dynamic piezoelectricity in sandwich films of porous and nonporous amorphous fluoropolymer," *Applied Physics Letters,* vol. 79, pp. 1852-1854, 2001.

[86] M. Paajanen, M. Karttunen, S. Kortet, O. Härkki, and I. Orko, "Thermally more durable electromechanical films by POSS nanomodification," *Key Engineering Materials,* vol. 538, pp. 65-68, 2013.

[87] Z. Xia, S. Ma, X. Qiu, and Y. Zhang, "Thermal stability of piezoelectricity for porous polytetrafluoroethylene electret film," *Journal of Electrostatics,* vol. 58, pp. 265-274, 6// 2003.

[88] G. S. Neugschwandtner, R. Schwodiauer, S. Bauer-Gogonea, S. Bauer, M. Paajanen, and J. Lekkala, "Piezo-and pyroelectricity of a polymer-foam space-charge electret," *Journal of Applied Physics,* vol. 89, pp. 4503-4511, 2001.

[89] F. Wang, Z. Xia, X. Qiu, and J. Shen, "The electret properties of two kinds of poly (vinylidene fluoride-hexafluoropropylene) copolymer films," in *Electrets, 2005. ISE-12. 2005 12th International Symposium on*, 2005, pp. 153-156.

[90] N. Mohmeyer, B. Müller, N. Behrendt, J. Hillenbrand, M. Klaiber, X. Zhang, *et al.*, "Nucleation of isotactic polypropylene by triphenylamine-based trisamide derivatives and their influence on charge-storage properties," *Polymer,* vol. 45, pp. 6655-6663, 2004.

[91] N. Mohmeyer, N. Behrendt, X. Zhang, P. Smith, V. Altstädt, G. M. Sessler*, et al.*, "Additives to improve the electret properties of isotactic polypropylene," *Polymer,* vol. 48, pp. 1612-1619, 2007.

[92] J. Hillenbrand, N. Behrendt, V. Altstädt, H. Schmidt, and G. Sessler, "Electret properties of biaxially stretched polypropylene films containing various additives," *Journal of Physics D: Applied Physics,* vol. 39, p. 535, 2006.

[93] A. Shakoor and N. L. Thomas, "Talc as a nucleating agent and reinforcing filler in poly(lactic acid) composites," *Polymer Engineering & Science,* vol. 54, pp. 64-70, 2014.

[94] A. Kilic, E. Shim, B. Y. Yeom, and B. Pourdeyhimi, "Improving electret properties of PP filaments with barium titanate," *Journal of Electrostatics,* vol. 71, pp. 41-47, 2013.

[95] N. Jahan, F. Mighri, D. Rodrigue, and A. Ajji, "Synergistic improvement of piezoelectric properties of PVDF/$CaCO_3$/montmorillonite hybrid nanocomposites," *Applied Clay Science,* vol. 152, pp. 93-100, 2018.

[96] A. Guzhova, M. Galikhanov, Y. A. Gorokhovatsky, D. Temnov, E. Fomicheva, E. Karulina*, et al.*, "Improvement of polylactic acid electret properties by addition of fine barium titanate," *Journal of Electrostatics,* vol. 79, pp. 1-6, 2016.

[97] Z. Xia, S. Ma, X. Qiu, Y. Wu, and F. Wang, "Influence of porosity on the stability of charge and piezoelectricity for porous polytetrafluoroethylene film electrets," *Journal of Electrostatics,* vol. 59, pp. 57-69, 2003.

[98] H. Kaczmarek, B. Królikowski, E. Klimiec, and J. Kowalonek, "New piezoelectric composites based on isotactic polypropylene filled with silicate," *Journal of Materials Science: Materials in Electronics,* vol. 28, pp. 6435-6447, 2017.

[99] E. Klimiec, B. Królikowski, M. Machnik, W. Zaraska, and J. Dzwonkowski, "Increase of piezoelectric constant and thermal durability of polypropylene electret by introducing SiO_2 and kaolin filler and creating a cellular structure," *Journal of Electronic Materials,* vol. 44, p. 2283, 2015.

[100] Z. An, M. Mao, J. Cang, Y. Zhang, and F. Zheng, "Significantly improved piezoelectric thermal stability of cellular polypropylene films by high pressure fluorination and post-treatments," *Journal of Applied Physics,* vol. 111, p. 024111, 2012.

[101] Z. Xia, A. Wedel, and R. Danz, "Charge storage and its dynamics in porous polytetrafluoroethylene (PTFE) film electrets," *IEEE transactions on dielectrics and electrical insulation,* vol. 10, pp. 102-108, 2003.

[102] X. Zhang, G. Cao, Z. Sun, and Z. Xia, "Fabrication of fluoropolymer piezoelectrets by using rigid template: Structure and thermal stability," *Journal of Applied Physics,* vol. 108, p. 064113, 2010.

[103] X. Zhang, J. Hillenbrand, and G. Sessler, "Ferroelectrets with improved thermal stability made from fused fluorocarbon layers," *Journal of Applied Physics,* vol. 101, p. 054114, 2007.

[104] S. Pande, D. Kelkar, and D. Peshwe, "Peizoelectric behavior of the blended system (Nylon 6/Nylon ll)," *Adv. Electroceram. Mater.: Ceram. Trans.,* vol. 204, p. 129, 2009.

[105] L. Huang, X. Zhuang, J. Hu, L. Lang, P. Zhang, Y. Wang*, et al.*, "Synthesis of biodegradable and electroactive multiblock polylactide and aniline pentamer copolymer for tissue engineering applications," *Biomacromolecules,* vol. 9, pp. 850-858, 2008.

[106] J. S. d. C. Campos, A. A. Ribeiro, and C. X. Cardoso, "Preparation and characterization of PVDF/$CaCO_3$ composites," *Mater. Sci. Eng.: B,* vol. 136, pp. 123-128, 2007.

[107] W. Ma, X. Wang, and J. Zhang, "Effect of MMT, SiO_2, $CaCO_3$, and PTFE nanoparticles on the morphology and crystallization of poly (vinylidene fluoride)," *J. Polym. Sci., Part B: Polym. Phys.,* vol. 48, pp. 2154-2164, 2010.

[108] A. Roy, B. Dutta, and S. Bhattacharya, "Electroactive phase nucleation and non-isothermal crystallization kinetics study in [DEMM][TFSI] ionic liquid incorporated P (VDF-HFP) co-polymer membranes," *J. Mater. Sci.,* vol. 51, pp. 7814-7830, 2016.

[109] S. Biswas, B. Dutta, and S. Bhattacharya, "Correlation between nucleation, phase transition and dynamic melt-crystallization kinetics in PAni/PVDF blends," *RSC Adv.,* vol. 5, pp. 74486-74498, 2015.

[110] L. Yang, J. Qiu, H. Ji, K. Zhu, and J. Wang, "Enhanced electrical properties of multiwalled carbon nanotube/poly(vinylidenefluoride) films through a rolling process," *J. Mater. Sci.: Mater. Electron.,* vol. 25, pp. 2126-2137, 2014.

[111] T. Hattori, M. Hikosaka, and H. Ohigashi, "The crystallization behaviour and phase diagram of extended-chain crystals of poly(vinylidene fluoride) under high pressure," *Polymer,* vol. 37, pp. 85-91, 1996.

[112] T. Hattori, M. Kanaoka, and H. Ohigashi, "Improved piezoelectricity in thick lamellar β-form crystals of poly (vinylidene fluoride) crystallized under high pressure," *J. appl. phys.,* vol. 79, pp. 2016-2022, 1996.

[113] P. Martins, C. Costa, M. Benelmekki, G. Botelho, and S. Lanceros-Méndez, "Interface characterization and thermal degradation of ferrite/poly (vinylidene fluoride) multiferroic nanocomposites," *J. Mater. Sci.,* vol. 48, pp. 2681-2689, 2013.

[114] S. Ramasundaram, S. Yoon, K. J. Kim, and C. Park, "Preferential formation of electroactive crystalline phases in poly (vinylidene fluoride)/organically modified silicate nanocomposites," *J. Polym. Sci., Part B: Polym. Phys.,* vol. 46, pp. 2173-2187, 2008.

[115] W. Wang, S. Zhang, L. O. Srisombat, T. R. Lee, and R. C. Advincula, "Gold-Nanoparticle and Gold-Nanoshell-Induced Polymorphism in Poly (vinylidene fluoride)," *Macromol. Mater. Eng.,* vol. 296, pp. 178-184, 2011.

[116] S. Biswas, B. Dutta, and S. Bhattacharya, "Isothermal crystallization kinetics as a probe of the preferential electroactive phase nucleation in silver-poly (vinylidene fluoride) nanocomposites: Dependence on nanoparticle size and concentration," *Eur. Polym. J.,* vol. 86, pp. 1-16, 2017.

[117] N. An, H. Liu, Y. Ding, M. Zhang, and Y. Tang, "Preparation and electroactive properties of a PVDF/nano-TiO2 composite film," *Appl. Surf. Sci.,* vol. 257, pp. 3831-3835, 2/15/ 2011.

[118] W. Zhang, Z. Zhou, Q. Li, and G.-X. Chen, "Controlled dielectric properties of polymer composites from coating multiwalled carbon nanotubes with octa-acrylate silsesquioxane through Diels–Alder cycloaddition and atom transfer radical polymerization," *Ind. Eng. Chem. Res.,* vol. 53, pp. 6699-6707, 2014.

[119] M. Sharma, G. Madras, and S. Bose, "Process induced electroactive β-polymorph in PVDF: effect on dielectric and ferroelectric properties," *Phys. Chem. Chem. Phys.,* vol. 16, pp. 14792-14799, 2014.

[120] K. Matsushige, K. Nagata, S. Imada, and T. Takemura, "The II-I crystal transformation of poly (vinylidene fluoride) under tensile and compressional stresses," *Polymer,* vol. 21, pp. 1391-1397, 1980.

[121] Y. Sui, W.-T. Chen, J.-J. Ma, R.-H. Hu, and D.-S. Liu, "Enhanced dielectric and ferroelectric properties in PVDF composite flexible films through doping with diisopropylammonium bromide," *RSC Adv.,* vol. 6, pp. 7364-7369, 2016.

[122] Fangxiao Guan, Jing Wang, Jilin Pan, Qing Wang, and L. Zhu, "Effects of Polymorphism and Crystallite Size on Dipole Reorientation in Poly(vinylidene fluoride) and Its Random Copolymers," *Macromolecules* vol. 43, pp. 6739-6748, 2010.

[123] P. Khodaparast and Z. Ounaies, "Influence of dispersion states on the performance of polymer-based nanocomposites," *Smart Mater. Struct.,* vol. 23, p. 104004, 2014.

[124] N. Jahan, A. Narteh, M. Hosur, M. Rahman, and S. Jeelani, "Effect of Carboxyl Functionalized MWCNTs on the Cure Behavior of Epoxy Resin," *Open J. Compos. Mater.,* vol. 3, pp. 40-47, 2013.

[125] V. K. Tiwari, A. K. Prasad, V. Singh, K. K. Jana, M. Misra, C. D. Prasad, *et al.*, "Nanoparticle and process induced super toughened piezoelectric hybrid materials: the effect of stretching on filled system," *Macromolecules,* vol. 46, pp. 5595-5603, 2013.

[126] X. Li and X. Lu, "Morphology of polyvinylidene fluoride and its blend in thermally induced phase separation process," *J. Appl. Polym. Sci.,* vol. 101, pp. 2944-2952, 2006.

[127] C.-W. Tang, B. Li, L. Sun, B. Lively, and W.-H. Zhong, "The effects of nanofillers, stretching and recrystallization on microstructure, phase transformation and dielectric properties in PVDF nanocomposites," *Eur. Polym. J.,* vol. 48, pp. 1062-1072, 2012.

[128] M. Dietze, J. Krause, C.-H. Solterbeck, and M. Es-Souni, "Thick film polymer-ceramic composites for pyroelectric applications," *J. Polym. Phys.,* vol. 101, p. 054113, 2007.

[129] D. Mandal, S. Yoon, and K. J. Kim, "Origin of Piezoelectricity in an Electrospun Poly (vinylidene fluoride-trifluoroethylene) Nanofiber Web-Based Nanogenerator and Nano Pressure Sensor," *Macromol. Rapid Commun.,* vol. 32, pp. 831-837, 2011.

[130] N. Jahan, F. Mighri, D. Rodrigue, and A. Ajji, "Enhanced electroactive β phase in three phase PVDF/CaCO3/nanoclay composites: Effect of micro-$CaCO_3$ and uniaxial stretching," *J. Appl. Polym. Sci.,* vol. 134, 2017.

[131] Y.-L. Hou, P. Zhang, and M.-M. Xie, "Thermally induced double positive temperature coefficients of electrical resistivity in combined conductive filler doped polymer composites," *J. Appl. Polym. Sci.,* vol. 134, 2017.

[132] Y. Huan, Y. Liu, Y. Yang, and Y. Wu, "Influence of extrusion, stretching and poling on the structural and piezoelectric properties of poly (vinylidene fluoride-hexafluoropropylene) copolymer films," *J. Appl. Polym. Sci.,* vol. 104, pp. 858-862, 2007.

[133] S. Singha and M. J. Thomas, "Dielectric properties of epoxy nanocomposites," *IEEE Trans. Dielectr. Electr. Insul.,* vol. 15, 2008.

[134] J.-K. Tseng, S. Tang, Z. Zhou, M. Mackey, J. M. Carr, R. Mu, *et al.*, "Interfacial polarization and layer thickness effect on electrical insulation in multilayered polysulfone/poly (vinylidene fluoride) films," *Polymer,* vol. 55, pp. 8-14, 2014.

[135] O. Jayakumar, E. H. Abdelhamid, V. Kotari, B. P. Mandal, R. Rao, V. Naik, *et al.*, "Fabrication of flexible and self-standing inorganic–organic three phase magneto-dielectric PVDF based multiferroic nanocomposite films through a small loading of graphene oxide (GO) and Fe3O4 nanoparticles," *Dalton Trans.,* vol. 44, pp. 15872-15881, 2015.

[136] P. Barber, S. Balasubramanian, Y. Anguchamy, S. Gong, A. Wibowo, H. Gao, *et al.*, "Polymer composite and nanocomposite dielectric materials for pulse power energy storage," *Materials,* vol. 2, pp. 1697-1733, 2009.

[137] M. Roy, J. K. Nelson, R. MacCrone, and L. Schadler, "Candidate mechanisms controlling the electrical characteristics of silica/XLPE nanodielectrics," *J. Mater. Sci.,* vol. 42, pp. 3789-3799, 2007.

[138] P. Khanchaitit, K. Han, M. R. Gadinski, Q. Li, and Q. Wang, "Ferroelectric polymer networks with high energy density and improved discharged efficiency for dielectric energy storage," *Nat. Commun.,* vol. 4, p. 2845, 2013.

[139] S. Yu-Chen, "Development and Characterization of Next Generation Flexible Dielectric and Thermoelectric Energy Harvesting Materials," Master's thesis, Department of Mechanical and Industrial Engineering, University of Toronto, 2015.

[140] G. Tsagaropoulos and A. Eisenberg, "Dynamic Mechanical Study of the Factors Affecting the Two Glass Transition Behavior of Filled Polymers. Similarities and Differences with Random Ionomers," *Macromolecules,* vol. 28, pp. 6067-6077, 1995/08/01 1995.

[141] K. Han, Q. Li, C. Chanthad, M. R. Gadinski, G. Zhang, and Q. Wang, "A Hybrid Material Approach Toward Solution-Processable Dielectrics Exhibiting Enhanced Breakdown Strength and High Energy Density," *Adv. Funct. Mater.,* vol. 25, pp. 3505-3513, 2015.

[142] H.-D. Bao, Z.-X. Guo, and J. Yu, "Electrical resistivity, crystallization and mechenical properties of polypropylene/multi-walled carbon nanotube/calcium carbonate composites prepared by melt mixing," *Chin. J. Polym. Sci.,* vol. 27, pp. 393-398, 2009.

[143] R. Liao, G. Bai, L. Yang, H. Cheng, Y. Yuan, and J. Guan, "Improved Electric Strength and Space Charge Characterization in LDPE Composites with Montmorillonite Fillers," *J. Nanomater.,* vol. 2013, p. 7, 2013.

[144] L. Yang, J. Ho, E. Allahyarov, R. Mu, and L. Zhu, "Semicrystalline Structure–Dielectric Property Relationship and Electrical Conduction in a Biaxially Oriented Poly (vinylidene fluoride) Film under High Electric Fields and High Temperatures," *ACS Appl. Mater. Interfaces,* vol. 7, pp. 19894-19905, 2015.

[145] B. Mohammadi, A. A. Yousefi, and S. M. Bellah, "Effect of tensile strain rate and elongation on crystalline structure and piezoelectric properties of PVDF thin films," *Polym. Test.,* vol. 26, pp. 42-50, 2// 2007.

[146] C. Baur, J. R. DiMaio, E. McAllister, R. Hossini, E. Wagener, J. Ballato*, et al.*, "Enhanced piezoelectric performance from carbon fluoropolymer nanocomposites," *J. Appl. Phys.,* vol. 112, p. 124104, 2012.

[147] R. Gerhard-Multhaupt, W. Kunstler, T. Gome, A. Pucher, T. Weinhold, M. Seiß*, et al.*, "Porous PTFE space-charge electrets for piezoelectric applications," *Dielectrics and Electrical Insulation, IEEE Transactions on,* vol. 7, pp. 480-488, 2000.

[148] W. Künstler, Z. Xia, T. Weinhold, A. Pucher, and R. Gerhard-Multhaupt, "Piezoelectricity of porous polytetrafluoroethylene single-and multiple-film electrets containing high charge densities of both polarities," *Applied Physics A: Materials Science & Processing,* vol. 70, pp. 5-8, 2000.

[149] Z. Cui, E. Drioli, and Y. M. Lee, "Recent progress in fluoropolymers for membranes," *Progress in Polymer Science,* vol. 39, pp. 164-198, 2014.

[150] G. Montanari, G. Mazzanti, F. Ciani, and M. Paajanen, "Effect of gas expansion on charging behavior of quasi-piezoelectric cellular PP," in *Electrical Insulation and Dielectric Phenomena, 2004. CEIDP'04. 2004 Annual Report Conference on*, 2004, pp. 153-157.

[151] S. Harris and A. Mellinger, "Pressure dependence of space charge deposition in piezoelectric polymer foams: simulations and experimental verification," *Applied Physics A,* vol. 107, pp. 553-558, June 01 2012.

[152] G. Neugschwandtner, R. Schwödiauer, S. Bauer-Gogonea, and S. Bauer, "Large piezoelectric effects in charged, heterogeneous fluoropolymer electrets," *Applied Physics A,* vol. 70, pp. 1-4, 2000.

[153] Z. Hu and H. Von Seggern, "Breakdown-induced polarization buildup in porous fluoropolymer sandwiches: a thermally stable piezoelectret," *Journal of applied physics,* vol. 99, p. 024102, 2006.

[154] S. A. Boyer, M. H. Klopffer, J. Martin, and J. P. E. Grolier, "Supercritical gas–polymer interactions with applications in the petroleum industry. Determination of thermophysical properties," *Journal of applied polymer science,* vol. 103, pp. 1706-1722, 2007.

[155] X. Qiu, M. Wegener, W. Wirges, X. Zhang, J. Hillenbrand, Z. Xia*, et al.*, "Penetration of sulfur hexafluoride into cellular polypropylene films and its effect on the electric charging and electromechanical response of ferroelectrets," *Journal of Physics D: Applied Physics,* vol. 38, p. 649, 2005.

[156] S. C. George and S. Thomas, "Transport phenomena through polymeric systems," *Progress in Polymer Science,* vol. 26, pp. 985-1017, 2001/08/01/ 2001.

[157] M. J. El-Hibri and D. R. Paul, "Gas transport in poly(vinylidene fluoride): Effects of uniaxial drawing and processing temperature," *Journal of Applied Polymer Science,* vol. 31, pp. 2533-2560, 1986.

[158] N. Jahan, F. Mighri, D. Rodrigue, and A. Ajji, "Effect of the inflation strategy on the piezoelectric response of cellular PVDF ferroelectret," *Manuscript submitted for publication,* 2018.

[159] S. K. Mahadeva, J. Berring, K. Walus, and B. Stoeber, "Effect of poling time and grid voltage on phase transition and piezoelectricity of poly (vinyledene fluoride) thin films using corona poling," *Journal of Physics D: Applied Physics,* vol. 46, p. 285305, 2013.

[160] V. Siracusa, "Food packaging permeability behaviour: a report," *International Journal of Polymer Science,* vol. 2012, 2012.

[161] X. Zhang, J. Hillenbrand, and G. Sessler, "Piezoelectric d33 coefficient of cellular polypropylene subjected to expansion by pressure treatment," *Applied physics letters,* vol. 85, pp. 1226-1228, 2004.

[162] P. Fang, M. Wegener, W. Wirges, R. Gerhard, and L. Zirkel, "Cellular polyethylene-naphthalate ferroelectrets: Foaming in supercritical carbon dioxide, structural and electrical preparation, and resulting piezoelectricity," *Applied physics letters,* vol. 90, p. 192908, 2007.

[163] P. Fang, L. Holländer, W. Wirges, and R. Gerhard, "Piezoelectric d33 coefficients in foamed and layered polymer piezoelectrets from dynamic mechano-electrical experiments, electro-mechanical resonance spectroscopy and acoustic-transducer measurements," *Measurement Science and Technology,* vol. 23, p. 035604, 2012.

[164] V. Shah, B. Hardy, and S. Stern, "Solubility of carbon dioxide, methane, and propane in silicone polymers. Effect of polymer backbone chains," *Journal of Polymer Science Part B: Polymer Physics,* vol. 31, pp. 313-317, 1993.

[165] A. Kasturirangan, *Specific interactions in carbon dioxide+ polymer systems*: Georgia Institute of Technology, 2008.

[166] Y. Shen and A. C. Lua, "Preparation and characterization of mixed matrix membranes based on PVDF and three inorganic fillers (fumed nonporous silica, zeolite 4A and mesoporous MCM-41) for gas separation," *Chemical engineering journal,* vol. 192, pp. 201-210, 2012.

[167] L. Z. Zhang, X. R. Zhang, Q. Z. Miao, and L. X. Pei, "Selective permeation of moisture and VOCs through polymer membranes used in total heat exchangers for indoor air ventilation," *Indoor Air,* vol. 22, pp. 321-330, 2012.